Title	Studies on the Effect of Degradation/Crosslinking Degrees of Hyaluronic Acid Derivative in Hydrogels on Vascular Endothelial Cell Behavior In Vitro
Author(s)	Elvitigala Chamara Manoj Lakmal, Kelum
Citation	大阪大学, 2024, 博士論文
Version Type	VoR
URL	https://doi.org/10.18910/98677
rights	
Note	

Studies on the Effect of Degradation/Crosslinking Degrees of Hyaluronic Acid Derivative in Hydrogels on Vascular Endothelial Cell Behavior In Vitro

ELVITIGALA KELUM CHAMARA MANOJ LAKMAL

SEPTEMBER 2024

Studies on the Effect of Degradation/Crosslinking Degrees of Hyaluronic Acid Derivative in Hydrogels on Vascular Endothelial Cell Behavior In Vitro

A dissertation submitted to

THE GRADUATE SCHOOL OF ENGINEERING SCIENCE

OSAKA UNIVERSITY

in partial fulfillment of the requirements for the degree of

DOCTOR OF PHILOSOPHY IN ENGINEERING

BY

ELVITIGALA KELUM CHAMARA MANOJ LAKMAL

SEPTEMBER 2024

Preface

This dissertation was conducted under the supervision of Professor Shinji Sakai at the Division of Chemical Engineering, Graduate School of Engineering Science, Osaka University, from 2021 to 2024.

The objective of this thesis is to explore the intricate relationship between hyaluronic acid degradation and crosslinking in hydrogel and its subsequent effects on vascular endothelial cell behavior. This study examines the different methods of hyaluronic acid degradation such as hydrogen peroxide-mediated, light irradiation-mediated, and sonication methods. Through the preparation of hyaluronic acid-based hydrogels, this research seeks to elucidate the mechanisms by which the degradation/crosslinking of hyaluronic acid, as it is degraded from high to low molecular weight, influences the formation of vascular networks. Such knowledge is essential to advance the development of in vitro models of angiogenesis, which hold great promise for applications in tissue engineering and regenerative medicine.

ELVITIGALA Kelum Chamara Manoj Lakmal

Division of Chemical Engineering

Graduate School of Engineering Science

Osaka University

Toyonaka, Osaka, 560-8531, Japan

Abstract

The formation of capillary networks by vascular endothelial cells (VECs) is essential for various physiological processes, including nutrient exchange and tumor growth. The aim of this study is to investigate how the degradation and crosslinking degrees of hyaluronic acid (HA) derivatives in hydrogels affect the behavior of VECs, with a focus on understanding the mechanochemical properties that influence vascular network formation. Specifically, this study investigates the modulation of human umbilical vein endothelial cell (HUVEC) behavior using mechanochemical properties-tuned hydrogels based on hyaluronic acid (HA) modified with phenol moieties (HA-Ph). Hydrogels were prepared through horseradish peroxidase (HRP)-mediated crosslinking and photocrosslinking, providing a platform for studying the effects of hydrogel stiffness and HA-Ph degradation on HUVECs functions.

Chapter I provides a general explanation of the critical role of HA in VECs behavior and emphasizes the need to study its degradation. This chapter presents methodologies for HA degradation and hydrogel formation, demonstrating their potential applications in tissue engineering.

Chapter II describes hydrogen peroxide (H_2O_2)-mediated degradation and its key role in enabling HUVEC network formation. Using HRP and H_2O_2 to crosslink phenolated polymers, HA-based hydrogels with controlled physicochemical properties were produced. Key observations include the need for low molecular weight HA-Ph (LMWHA-Ph) and the importance of hydrogel stiffness, which can be fine-tuned by adjusting the H_2O_2 exposure time for optimal network formation.

Chapter III examines the photocrosslinking method, where control of polymer degradation and hydrogel stiffness was achieved by varying the light irradiation time, using ruthenium dye and sodium persulfate, but not H_2O_2. This approach reveals a critical balance where increasing

light exposure initially increased both polymer degradation and hydrogel stiffness up to a threshold beyond which both parameters began to decrease. The optimal conditions identified for network formation also highlighted the critical role of LMWHA-Ph in influencing F-actin fiber formation and the interaction of LMWHA-Ph with CD44 receptors, which is fundamental to HUVEC network formation.

Chapter IV continues with a detailed exploration of sonication-mediated degradation, focusing on elucidating the mechanisms by which LMWHA-Ph initiates HUVEC network formation. Before hydrogel formation, HA-Ph was degraded to its low molecular weight form by sonication of HA-Ph solution, which was subsequently used to form hydrogels by HRP-mediated crosslinking. This setup was designed to investigate the direct influence of LMWHA-Ph on HUVEC network formation, highlighting its interaction with CD44 receptors as a critical element in initiating network structure. This study not only confirms the pivotal role of LMWHA-Ph in vascular network formation, but also reveals the signaling pathways involved in this biological process.

Chapter V extends the application of this HA-Ph hydrogel system by using an additional cell line, mouse myoblast cells (C2C12), to investigate the potential of LMWHA-Ph hydrogels for muscle tissue engineering. This chapter highlights the broader applicability of HA-Ph hydrogels beyond angiogenesis.

Overall, this work provides a detailed understanding of how HA-Ph degradation in the hydrogel environment and the mechanical properties of hydrogels influence VECs and muscle cells functions. The findings underscore the potential of HA-Ph hydrogels obtained via enzymatic and photocrosslinking as versatile biomaterials for various tissue engineering applications, offering new avenues for regenerative medicine and therapeutic interventions.

Table of Contents

Chapter I

General Introduction

Vascular endothelial cells (VECs) are integral to the vascular system, forming the inner lining of blood vessels and playing a significant role in maintaining vascular homeostasis by regulating barrier integrity, blood flow, and angiogenesis [1]. Angiogenesis, forming new blood vessels from pre-existing ones, is essential for ensuring adequate tissue perfusion, nutrient delivery, and waste removal. This process is critical for various biological events, including embryonic development, wound healing, and the menstrual cycle [2]. Moreover, angiogenesis is pivotal in pathological conditions such as cancer, where it facilitates tumor growth and metastasis by supplying oxygen and nutrients to proliferating cancer cells.

The regulation of angiogenesis involves a delicate balance between pro-angiogenic and anti-angiogenic factors [3]. Vascular endothelial growth factor (VEGF) is one of the most critical pro-angiogenic signals that promote VECs proliferation and migration, leading to the formation of new blood vessels. VEGF binds to receptors on the VECs surface, initiating a cascade of signaling events that promote angiogenesis. Conversely, anti-angiogenic factors such as angiostatin and endostatin inhibit blood vessel formation, ensuring that angiogenesis does not proceed uncontrollably, essential for maintaining vascular homeostasis. Despite significant advancements in understanding the mechanisms of angiogenesis, critical research gaps remain. One major gap is the comprehensive understanding of the interplay between VECs behavior and the mechanical and biochemical properties of the extracellular matrix (ECM). Research in tissue engineering highlights the importance of ECM properties such as stiffness, composition, and degradation in regulating VECs functions [4]. However, the precise mechanisms by which these ECM properties influence VEC behavior need further exploration. Additionally, the role

of bioactive fragments generated from ECM degradation, particularly hyaluronic acid (HA), and their interactions with VEC receptors remain underexplored.

The study of VEC behavior is not only important for understanding physiological and pathological angiogenesis but also for advancing tissue engineering applications. By mimicking the natural environment of VECs, researchers can develop better biomaterials and scaffolds that promote desired cellular responses. This leads to improved therapeutic outcomes in regenerative medicine and other clinical applications.

In the subsequent sections, different types of VECs and their specific responses in the in vitro assays are explored. This exploration highlights the importance of selecting appropriate cell types for specific research objectives and provides a foundation for understanding their varied behaviors in angiogenesis studies.

1. Types of vascular endothelial cells and their response in the in vitro assays

VECs used in tissue engineering applications can be sourced from various tissues and species, each exhibiting distinct properties and behaviors. Human umbilical vein endothelial cells (HUVECs) are commonly used due to their ease of isolation and well-characterized behavior. HUVECs are known for their high responsiveness to angiogenic stimuli, making them ideal for initial studies on VEC behavior and drug screening [5]. However, they may not fully represent the behavior of microvascular endothelial cells (MVECs), which are found in the capillaries and small blood vessels and have different physiological properties [6].

Human dermal microvascular endothelial cells (HDMECs) are more representative of the microvascular environment and are crucial for studying skin-related angiogenesis and wound healing [7]. However, these cells can be more challenging to isolate, and culture compared to HUVECs. Endothelial progenitor cells (EPCs), derived from circulating progenitor cells in the

blood, offer the advantage of studying VEC differentiation and repair mechanisms, making them valuable for regenerative medicine applications [8].

Additionally, VECs can be derived from specific organs, such as the heart or lungs, providing insights into organ-specific vascular functions. For instance, cardiac endothelial cells play a pivotal role in heart tissue repair and regeneration, while pulmonary endothelial cells are essential for studying lung-related diseases and responses to hypoxia.

The response of these VECs in the in vitro assays can differ significantly based on their origin. For example, while HUVECs are highly responsive to angiogenic stimuli, they may not fully capture the behavior of MVECs or HDMECs in certain conditions. Understanding these differences is essential for selecting the appropriate cell type for specific research questions, as the choice of VECs can significantly impact the outcomes of studies on angiogenesis, vascular function, and therapeutic interventions.

2. Recent in vitro models for studying angiogenesis and vascular endothelial cells behavior

The in vitro models are indispensable for better understanding the mechanisms of angiogenesis. Various in vitro models have been utilized in different in vitro assays **(Table 1)**. These models provide controlled environments to manipulate cellular conditions, facilitating detailed studies of VECs behavior and vessel formation. Among the key in vitro assays is the tube formation assay, where VECs are seeded on a gel matrix, such as Matrigel, and align to form capillary-like structures [9]. This assay is widely used due to its simplicity and rapid results; however, it lacks the complexity of in vivo angiogenesis and does not fully replicate the intricate interactions found in living tissues.

Another commonly used model is the spheroid sprouting assay [10]. In this assay, endothelial cell spheroids are embedded in a collagen matrix, and the formation of sprouts is observed.

This model is particularly useful for studying the early stages of angiogenesis, providing insights into cell-cell and cell-matrix interactions. The three-dimensional nature of this assay offers a more physiologically relevant environment than traditional two-dimensional cultures.

Microfluidic devices represent a more advanced approach to studying VEC behavior [11]. These devices create controlled microenvironments that can simulate dynamic conditions, including shear stress and flow, which are critical factors in vascular biology. Microfluidic models provide a three-dimensional structure that mimics aspects of tissue architecture, offering valuable insights into the effects of mechanical forces on VECs.

Despite their utility, in vitro models have inherent limitations. Many in vitro models, such as the tube formation assay, are overly simplistic and do not capture the full complexity of the tissue microenvironment. In vivo, VECs interact dynamically with various cell types and extracellular matrix components, interactions that are often not replicated in vitro. Additionally, models like Matrigel, which are derived from tumor extracts, can have batch-to-batch variability, affecting reproducibility.

Furthermore, the mechanical properties of the ECM, such as stiffness and viscoelasticity, significantly influence angiogenesis [12]. Many in vitro models do not adequately mimic these mechanical cues, which are crucial for accurately studying VECs behavior. Addressing these limitations is essential for improving the predictive in vitro models and developing more effective therapies for angiogenesis related diseases.

Table 1. Summary of in vitro models used for studying angiogenesis and VEC behavior, with their advantages and disadvantages.

Model	Description	Advantages	Disadvantages	Reference
Tube formation assay	VECs are seeded on a gel matrix (e.g., Matrigel) and align to form capillary-like structures.	Simple, rapid results.	Overly simplistic, lacks complexity.	13
Spheroid sprouting assay	VEC spheroids are embedded in a collagen matrix to observe sprout formation.	Mimics early stages of angiogenesis.	Limited to early-stage observations.	10
Microfluidic devices	Devices create controlled microenvironments to simulate dynamic conditions, including shear stress and flow.	Controlled dynamic conditions	Technical complexity, cost.	11
Proliferation assays	Assess VEC proliferation using methods like MTT assay and thymidine incorporation.	Easy to perform, reproducible.	May not reflect in vivo angiogenesis.	14
Migration assays	Measure VEC movement in response to angiogenic stimuli (e.g., Boyden chamber, wound healing assay).	Assess cell migration.	Technically challenging, not fully replicative of in vivo conditions.	15

3. Hydrogels as in vitro angiogenesis model

Hydrogels are three-dimensional, polymer networks capable of holding large amounts of water while maintaining structural integrity. Hydrogels are largely utilized in biomedical applications, including tissue engineering and regenerative medicine, due to their biocompatibility, controllable mechanochemical properties, and capability to mimic the natural

ECM [14,15]. The mechanical properties of hydrogels, such as stiffness, viscoelasticity, and porosity, play a crucial role in influencing cellular behavior as shown in **Table 2**, including proliferation, migration, and differentiation.

The stiffness of hydrogels, often quantified by their elastic modulus, is a critical factor in determining cell fate [16]. Studies have shown that substrate stiffness can direct various cell differentiation. For example, softer hydrogels with lower stiffness values (1-10 kPa) tend to promote neural differentiation [17], while intermediate stiffness favors myogenic differentiation [18], and higher stiffness (>50 kPa) supports osteogenic differentiation [19]. These findings underscore the importance of tuning the mechanical properties of hydrogels to create specific microenvironments conducive to desired cellular responses.

Viscoelasticity, the property of materials that exhibit viscous and elastic characteristics when undergoing deformation, also significantly impacts cellular behavior. Hydrogels with higher viscoelastic properties can better mimic the dynamic nature of the native ECM, providing cues that influence cell morphology, motility, and function. For instance, viscoelastic hydrogels can promote the formation of focal adhesions, which are essential for cell migration and signal transduction [20].

Porosity and the degree of crosslinking within hydrogels affect the diffusion of nutrients, waste products, and signaling molecules, thereby influencing cell viability and function [21]. Highly porous hydrogels with interconnected networks facilitate better nutrient and oxygen transport, supporting cell survival and proliferation. The degree of crosslinking, which determines the density of the polymer network, can be modulated to control the release of bioactive molecules and the degradation rate of the hydrogel [22], providing temporal control over the cellular microenvironment.

The degradation of hydrogels is another crucial aspect that affects cellular functions. As hydrogels degrade, they release bioactive fragments that can influence cell behavior. For

example, the degradation of HA-based hydrogels can release low molecular weight HA (LMWHA) fragments, which have been shown to promote angiogenesis, inflammation, and cell migration [23,24]. Controlled degradation of hydrogels ensures a dynamic environment that can adapt to the changing needs of the tissue regeneration process.

The mechanical properties of hydrogels are particularly important in the context of VECs. VECs respond to the stiffness and viscoelasticity of their substrate, which affects their ability to form capillary-like structures, migrate, and proliferate [4]. By tuning the mechanochemical properties of HA-based hydrogels, researchers can create optimal conditions for promoting angiogenesis and VECs function.

Table 2. Summary of the mechanochemical properties of hydrogels and their influence on cellular functions.

Mechanical property	Description	Impact on cellular functions	Reference
Stiffness	Elastic modulus of the hydrogel.	Directs cell differentiation and influences cell morphology and adhesion.	21
Viscoelasticity	Combination of viscous and elastic properties.	Affects cell motility, morphology, and focal adhesion formation.	22
Porosity	Degree of interconnected pores within the hydrogel.	Enhances nutrient and oxygen transport, supports cell survival and proliferation.	23
Crosslinking density	Degree of crosslinking within the polymer network.	Controls release of bioactive molecules and modulates degradation rate.	24
Degradation	Breakdown of hydrogel structure over time.	Releases bioactive fragments, influences angiogenesis and cell migration.	26

4. Hyaluronic acid as a potential material for in vitro angiogenesis

4.1 Chemical properties of HA that affects cell behavior

HA is a major component of the ECM and plays a significant role in modulating cellular activities such as migration, proliferation, and differentiation. Structurally, HA is a negatively charged, non-sulfated, linear glycosaminoglycan (GAG) composed of repeating units of (β,1-4)-D-glucuronic acid-(β,1-3)-N-acetyl-D-glucosamine. Unlike other GAGs, HA is not linked to a core protein and is synthesized at the cytoplasmic surface of the plasma membrane rather than the endoplasmic reticulum and Golgi apparatus. In its native state, HA is a high molecular weight polymer (MW > 1,000 kDa) found in significant quantities in the skin, synovial fluid, brain, and vitreous body of the eye. HA is synthesized by a family of enzymes known as HA synthases (HAS1, HAS2, and HAS3), each producing HA of different molecular weights and at different catalytic rates.

The molecular weight of HA is a critical factor affecting its biological functions. High molecular weight HA (HMWHA) generally provides structural support and maintains tissue hydration, while LMWHA fragments can act as signaling molecules, promoting angiogenesis and inflammatory responses [25]. The degradation of HMWHA into LMWHA can occur enzymatically via hyaluronidases (HYALs) or non-enzymatically through reactive oxygen species (ROS) and other mechanisms at injury sites.

In VECs, HA interacts with cell surface receptors such as CD44 and RHAMM (CD168) (Receptor for Hyaluronan-Mediated Motility), influencing processes like cell adhesion, motility, and angiogenesis [26]. CD44 is a cell surface glycoprotein that binds to HA, mediating cell adhesion, migration, and signal transduction. This interaction is essential for various cellular processes, including the regulation of cell proliferation and the formation of cell-cell junctions. CD44-HA binding triggers intracellular signaling pathways that influence the cytoskeletal organization and cell motility, which is crucial for the migration and alignment of VECs during angiogenesis.

The interaction mechanisms between HA and VECs also involve RHAMM, which interacts with HA to modulate cytoskeletal dynamics and enhance cell motility, contributing to ECM remodeling and new blood vessel formation [27]. RHAMM-HA interactions are particularly important in the context of wound healing and tissue repair, where rapid VEC migration is necessary for the re-establishment of vascular integrity.

HA and its receptors CD44 and RHAMM initiate several signaling pathways critical for VEC functions. The binding of HA to CD44 can activate pathways such as Rho GTPases, which regulate cytoskeletal reorganization, and MAPK/ERK, which promotes cell proliferation [28]. RHAMM, on the other hand, is known to interact with PDGF receptors and activate signaling cascades involving SRC and RAS, further influencing cell motility and proliferation [29].

Understanding the specific interactions between HA of different molecular weights and VEC receptors is crucial for developing therapeutic strategies to modulate angiogenesis. This knowledge can inform the design of HA-based hydrogels and other biomaterials that mimic the natural ECM, providing controlled environments for studying VEC behavior and developing treatments for vascular diseases.

4.2 Degradation

The degradation of HA in vivo is a complex process influenced by various factors, including enzymatic activity, mechanical stress [30], reactive oxygen species (ROS), and other biochemical interactions. Understanding the mechanisms and kinetics of HA degradation is essential for developing HA-based biomaterials with tailored degradation profiles for specific biomedical applications. Recent studies have shown various HA degradation methods which are summarized in the following sections and **Table 3.**

In vivo, HA is primarily degraded by a family of enzymes known as hyaluronidases (HYALs). These enzymes cleave the β-1,4 glycosidic bonds between N-acetyl-D-glucosamine

and D-glucuronic acid residues, resulting in the breakdown of HA into smaller fragments [31]. The activity of hyaluronidases varies among different tissues and physiological conditions. For example, HYAL1 and HYAL2 are predominantly found in lysosomes, where they degrade HA into oligosaccharides, while HYAL3 is believed to play a regulatory role in HA turnover. The half-life of HA in various tissues can range from less than a day to several days, depending on the local concentration of hyaluronidases and other degradative factors.

ROS generated during inflammatory responses or exposure to UV radiation can also contribute to HA degradation [32]. ROS, such as hydroxyl radicals and hydrogen peroxide (H_2O_2), can non-enzymatically cleave HA chains, resulting in the formation of LMWHA fragments. These fragments can have distinct biological activities compared to their high molecular weight counterparts, often promoting angiogenesis, inflammation, and cell migration [33].

HA can be degraded in vitro using various physical, chemical, and enzymatic methods to mimic the degradation processes observed in vivo. These methods allow researchers to study the effects of HA degradation on cellular behavior and to develop HA-based hydrogels with controlled degradation. Enzymatic degradation of HA in vitro typically involves using hyaluronidases, such as bovine testicular hyaluronidase or recombinant human hyaluronidases [34]. These enzymes are added to HA solutions or hydrogels to study the kinetics of HA breakdown and the resultant biological effects. The enzymatic degradation rate can be modulated by adjusting enzyme concentration, temperature, and pH.

Oxidative degradation of HA can be induced using ROS-generating systems. For example, visible light irradiation in the presence of a photosensitizer, such as riboflavin, can produce ROS that degrades HA. This method mimics oxidative stress conditions in vivo and allows for studying ROS-mediated HA degradation and its impact on cellular behavior [35,36]. Mechanical forces, such as shear stress or ultrasonic stimulation, can also degrade HA [30]. The in vitro studies often use sonication to apply mechanical energy to HA solutions, resulting in the

breakdown of HA chains [37]. This method is useful for studying the effects of mechanical stress on HA degradation and the resultant changes in the viscoelastic properties of HA-based hydrogels.

Chemical agents, such as acids or bases, can degrade HA by cleaving its glycosidic bonds [38]. This method allows for rapid and controlled degradation of HA and is often used with other techniques to study the effects of HA fragmentation on cellular responses.

Table 3. Description of various methods for degrading HA and their applications.

Degradation method	Mechanism	Application	Reference
Enzymatic degradation	Cleavage by hyaluronidases.	Studying HA turnover and developing degradable hydrogels.	36
Oxidative degradation	ROS-mediated cleavage.	Mimicking oxidative stress, studying inflammation.	41
Mechanical degradation	Shear stress or ultrasonic stimulation.	Investigating mechanical effects on HA, modifying viscoelastic properties.	32
Chemical degradation	Acidic or basic hydrolysis.	Rapid degradation for studying the effects of HA fragments.	40

4.3 Crosslinking methods

Crosslinking is a crucial process in fabricating HA hydrogels and determining their structural integrity, mechanical properties, and degradation behavior. Various crosslinking methods can be employed to create HA hydrogels **(Table 4)**, each with its unique advantages and applications. The choice of crosslinking method significantly influences the hydrogel's performance and suitability for specific biomedical applications, such as tissue engineering and drug delivery.

HA is often chemically modified to enable specific crosslinking methods. For example, HA can be functionalized with methacrylate, acrylate, phenol or thiol groups, which allow for

subsequent crosslinking through various mechanisms [39,40]. These modifications do not alter the fundamental properties of HA but provide reactive sites that facilitate the formation of crosslinked networks.

Chemical crosslinking involves the formation of covalent bonds between HA chains, resulting in a stable and robust hydrogel network [41]. This method often utilizes crosslinking agents, such as glutaraldehyde, genipin, or carbodiimides, to create permanent links between HA molecules. For instance, aldehyde-based crosslinkers can react with amine groups on HA to form Schiff base linkages [42]. Chemical crosslinking offers the advantage of creating HA hydrogels with high mechanical strength and stability. However, the potential cytotoxicity of residual crosslinking agents necessitates thorough purification steps to ensure biocompatibility.

Physical crosslinking relies on non-covalent interactions, such as hydrogen bonding, ionic interactions, and hydrophobic interactions, to form HA hydrogel networks. These methods are generally considered more biocompatible than chemical crosslinking because they do not require potentially toxic reagents [43].

Enzymatic crosslinking utilizes natural enzymes to catalyze the formation of crosslinks between HA chains [44]. This method is highly specific and can be performed under mild physiological conditions, making it suitable for cell encapsulation and tissue engineering applications. For instance, horseradish peroxidase (HRP) in the presence of (H_2O_2) can catalyze the crosslinking of phenol-functionalized HA (HA-Ph), forming hydrogels with controlled degradation rates [45]. Enzymatic crosslinking offers the advantage of biocompatibility and the potential for in situ gelation.

Photocrosslinking involves using light to initiate crosslinking reactions, typically through photoinitiators that generate free radicals upon exposure to specific wavelengths of light. This method allows for precise spatial and temporal control over the gelation process, enabling the creation of complex hydrogel structures. Photocrosslinking is commonly used with HA

derivatives functionalized with acrylate or methacrylate groups. For example, visible light in the presence of riboflavin can crosslink HA methacrylate (HAMA), forming hydrogels suitable for tissue engineering applications [46].

Dual crosslinking combines two different crosslinking methods to enhance the mechanical properties and stability of HA hydrogels [43]. For instance, combining chemical and physical crosslinking can produce hydrogels with improved mechanical strength and tunable degradation. This approach is particularly useful for creating HA hydrogels that need to maintain structural integrity under physiological conditions while gradually degrading over time.

Table 4. Various crosslinking methods used to fabricate HA-based hydrogels, highlighting their mechanisms and typical applications.

Crosslinking method	Mechanism	Advantages	Typical applications	Reference
Chemical crosslinking	Covalent bond formation using crosslinking agents.	High mechanical strength, stability.	Tissue engineering, drug delivery.	44
Physical crosslinking	Non-covalent interactions (e.g., hydrogen bonding).	Biocompatible, reversible.	Injectable hydrogels, wound healing.	46
Enzymatic crosslinking	Enzyme-catalyzed reactions.	Specificity, mild conditions, biocompatibility.	Tissue engineering, cell sheet fabrication.	50
Photocrosslinking	Light-induced free radical generation.	Spatial and temporal control, complex structures.	Tissue engineering, angiogenesis.	48
Dual crosslinking	Combination of two crosslinking methods.	Enhanced mechanical properties, tunable degradation.	Biomedical applications, scaffolds.	46

5. Overview

HA-based hydrogels with tunable degradation and mechanical properties offer promising strategies for in vitro VECs behavior analysis. This thesis investigates the role of phenolated HA derivatives in modulating cellular behavior, focusing on VECs and muscle cells through an HA-based hydrogel system.

Chapter II utilizes H_2O_2-mediated crosslinking and degradation of HA-based hydrogels to explore how hydrogel stiffness and HA-Ph degradation affect HUVECs adhesion, elongation, and network formation **(Fig. 1-1)** [47].

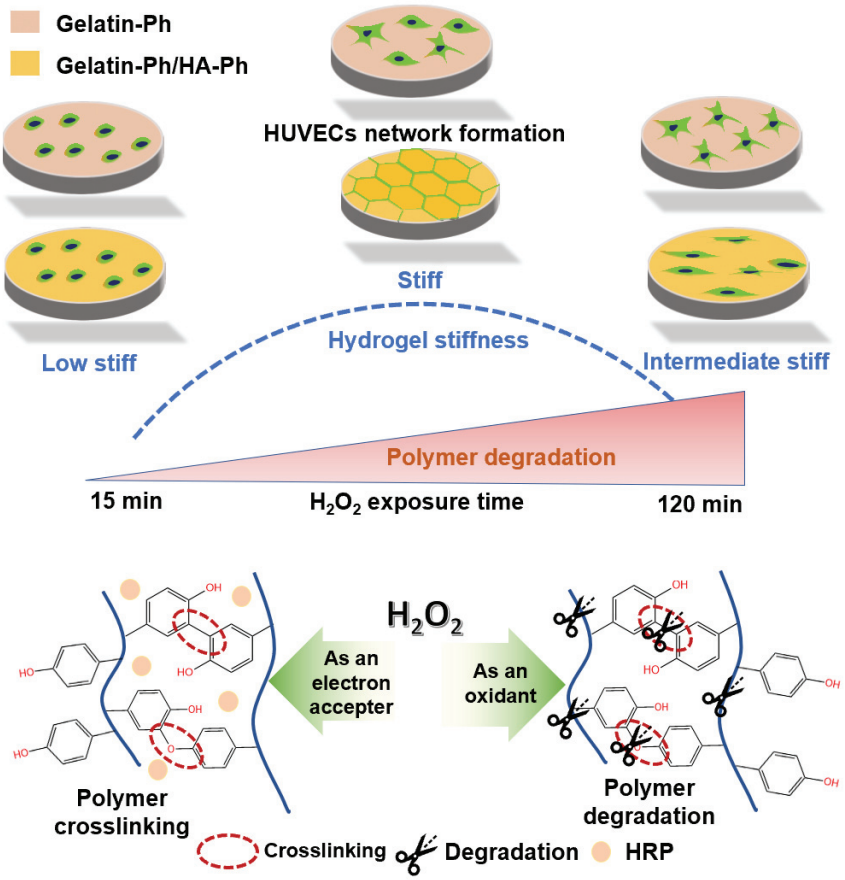

Fig. 1-1 Schematic illustrations of H_2O_2-mediated crosslinking of phenolic groups on polymer chains catalyzed by HRP and the simultaneous degradation of the polymer chains. This process is utilized in Chapter II to explore how hydrogel stiffness and HA-Ph degradation affect HUVEC behavior. Reprinted from (Elvitigala et al. 2022) [47] with permission from MDPI.

Chapter III employs visible-light-mediated photocrosslinking using ruthenium dye and sodium persulfate (SPS) to control polymer degradation and hydrogel stiffness through varying light irradiation times. This chapter emphasizes the role of LMWHA-Ph in influencing F-actin fiber formation and interactions with CD44 receptors, promoting HUVEC network formation **(Fig. 1-2)** [48].

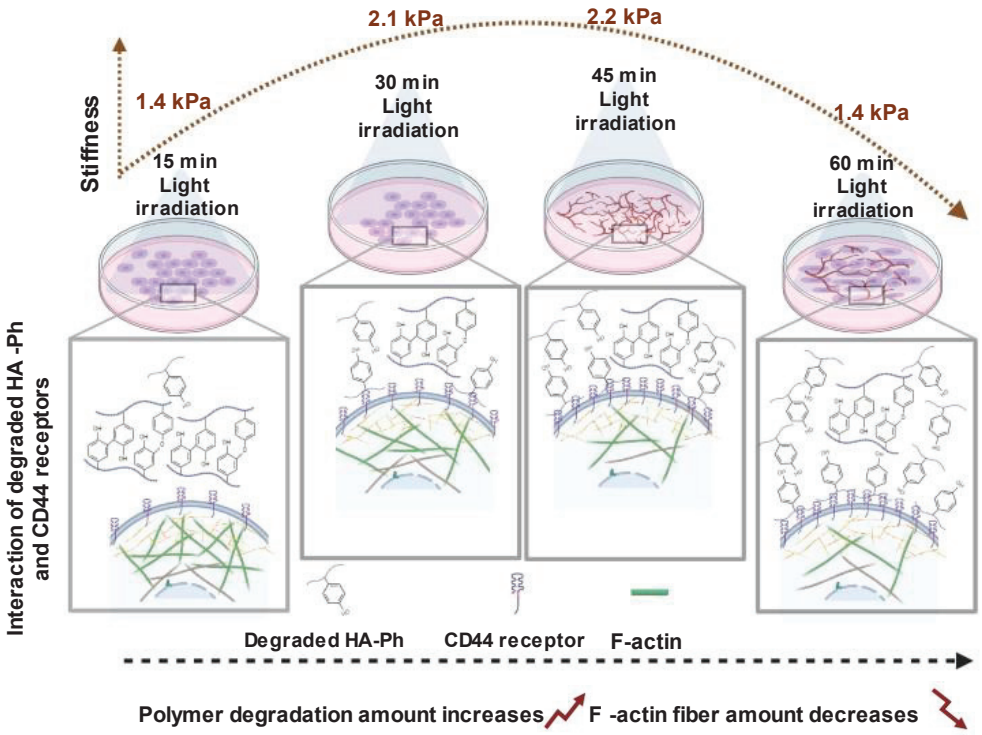

Fig. 1-2 Schematic illustration of the impact of varying light irradiation times on hydrogel stiffness, polymer degradation, and the interaction of degraded HA-Ph with CD44 receptors. This figure, discussed in Chapter III, highlights the relationship between light exposure duration, hydrogel mechanical properties, and HUVEC network formation, emphasizing the formation of F-actin fibers. This illustration was created with BioRender.com.

Chapter IV focuses on sonication-mediated degradation of HA-Ph to generate low-molecular-weight HA fragments, investigating their influence on VECs behavior and network formation **(Fig. 1-3)** [49].

Chapter IV underscores the importance of interactions between HA fragments and CD44 receptors in promoting angiogenesis. It also illustrates the effectiveness of physical degradation methods in producing bioactive materials that enhance vascularization.

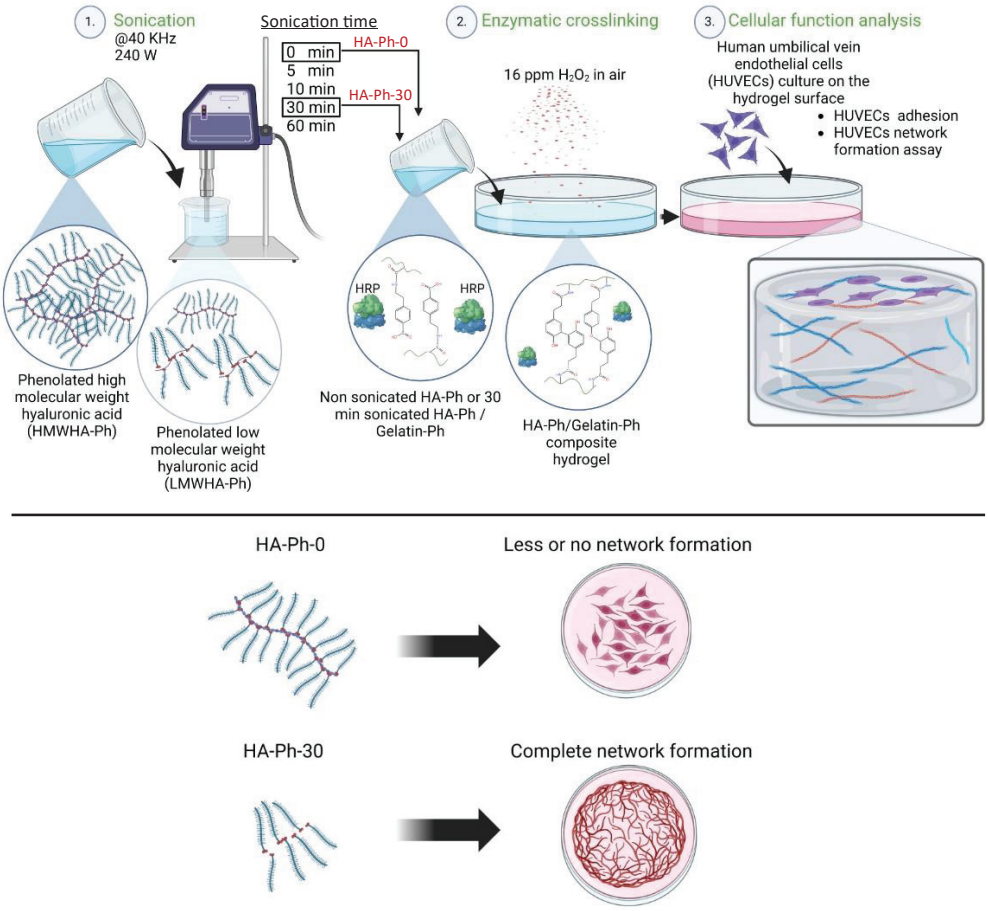

Fig. 1-3 Schematic illustration of the sonication-mediated degradation of HA-Ph to produce low molecular weight HA fragments. This figure illustrates the process and the interaction between these fragments and CD44 receptors, as explored in Chapter IV, which is crucial for enhancing the angiogenic potential of VECs. This illustration was created with BioRender.com.

Chapter V extends the application of HA-Ph hydrogels to muscle tissue engineering using mouse myoblast cells (C2C12) **(Fig. 1-4)** [50]. It demonstrates the ability of HA-Ph-based hydrogels to support C2C12 cell adhesion, proliferation, differentiation, and the fabrication of

muscle cell sheets, showcasing the broader applicability of HA-Ph hydrogels beyond angiogenesis.

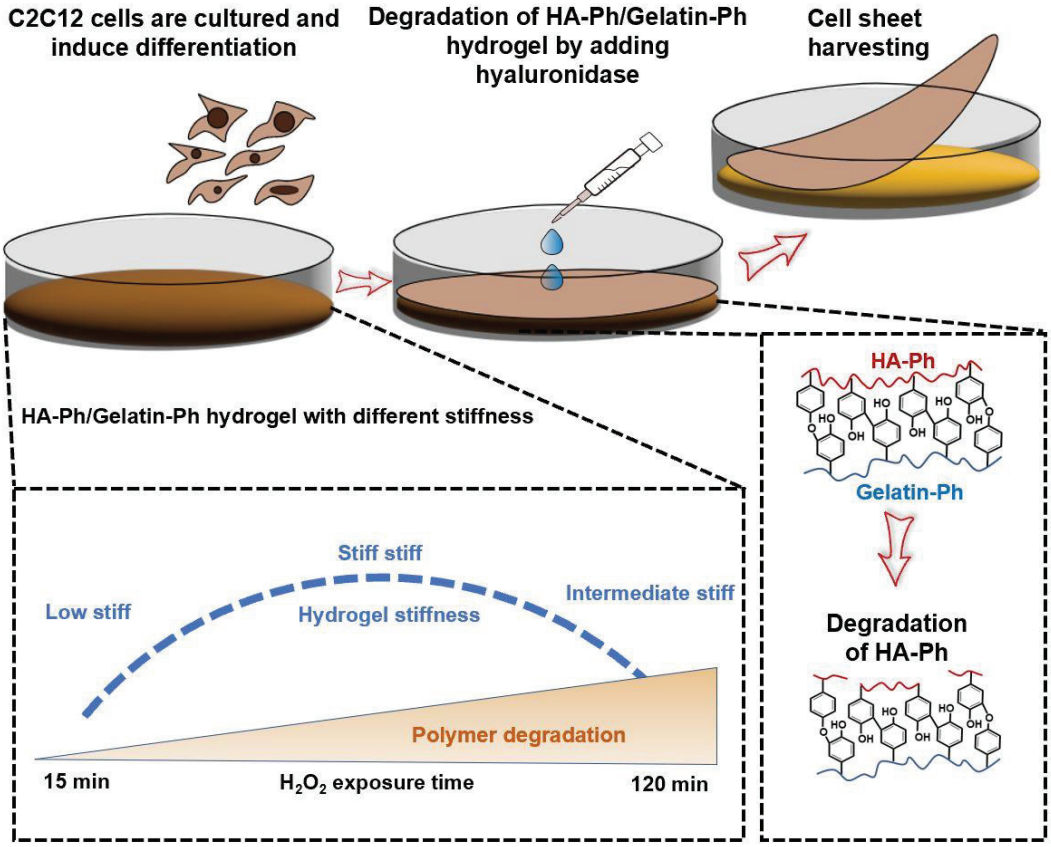

Fig. 1-4 Schematic illustration of HA-Ph hydrogels for muscle tissue engineering applications beyond angiogenesis, as discussed in Chapter V.

Chapter II

Human Umbilical Vein Endothelial Cells Form a Network on a Hyaluronic Acid/Gelatin Composite Hydrogel Moderately Crosslinked and Degraded by Hydrogen Peroxide

1. Introduction

The capillary network, composed of vascular endothelial cells (VECs), is essential for nutrient and gas exchanges between blood and tissue. In addition, capillary network formation is essential for tumor growth [51,52]. Therefore, studies dealing the capillary network formation have been intensively conducted both in vivo and in vitro [53–55]. Various hydrogels which enable to induce of the network formation of VECs have been developed for studies in vitro [56,57]. Hydrogels are water-swollen three-dimensional networks of polymers. To provide mechanical support as well as the chemical environment for cell adhesion sites, cell remodeling, nutrient support, and cell responsive remodeling, hydrogels are widely used in tissue engineering technologies as transient artificial extracellular matrix substitutes [58,59].

The physicochemical properties of the extracellular matrix (ECM) are known to modulate the cell functions such as adhesion and proliferation [60,61]. Numerous reports have been published on the effect of chemical modifications of the ECM to control VECs behavior. Rumiana et al. have reported the angiogenic potential of the VEC on gelatin-based hydrogel by controlling the growth factor release by electrical stimulation [62]. The report by Ying et al. showed that the co-delivery of growth factor by gelatin hydrogel promotes angiogenesis compared with growth factors applied alone [63]. Derek et al have reported that stimulation of hyaluronidase expression in endothelial colony-forming cells through hyaluronic acid-specific receptors for cord-like structures on hyaluronic acid hydrogels [64].

In addition, ECM stiffness also plays a vital role in cell functions. For example, Nelson et al. demonstrated that gelatin methacryloyl hydrogel stiffness was controlled by enzymatic degradation to analyze the stiffness-dependent vascular formation [65]. However, the effect of chemical and physical properties together on the behavior of VECs has been paid less attention. Thus, here, this study present a novel method to control VECs behavior, by using both physical and chemical properties of artificial ECM, in gelatin and hyaluronic acid (HA) based hydrogel.

Gelatin and hyaluronic acid-based hydrogels have been widely utilized as artificial ECM in vitro to mimic the characteristics, properties, and good biocompatibility. Gelatin is a well-known biodegradable and low immunogenic polymer that allows cell adhesion through RGD peptides. In addition, gelatin-based hydrogels can deliver growth factors like basic fibroblast growth factors (bFGF), which are vital in angiogenesis [63]. In general, HA is a widely utilized non-sulfated glycosaminoglycan found abundantly in the human body with specific activities such as high molecular weight HA (HMWHA) is crucial for wound healing [66]. HA can interact with different receptors on the cell surface and activate distinct cellular signalling. Among them, CD44 and RHAMM are identified as the most relevant for inflammation and cancer [67].

The molecular weight of HA can differently influence the activation of the cell surface receptors. The enzymatic degradation of HA produces fragments of molecules called hyaluronan oligosaccharides to promote angiogenesis [68]. The interaction between the HA and CD44 receptors stimulates angiogenesis [69]. In contrast, gelatin and HA are important materials for VEC functions, including angiogenesis. When designing an artificial ECM for tissue engineering applications, it should allow cell adhesion, proliferation, and differentiation with the same characteristic properties as the native. Only HA is not a promising cell adhesive scaffold for designing artificial ECM and combined with integrin-binding adhesive peptides promotes cell adhesion and proliferation. Therefore, in this study, gelatin and HA was mixed to make cell adhesive composite hydrogel with modification of both polymers with phenol

groups through tyramine substitution (Gelatin-Ph/HA-Ph) for the in vitro study of VECs behavior.

In the present study, gelatin and HA derivatives possessing phenol groups were used which allow enzymatically catalyzed oxidation of phenolic hydroxyl groups resulting in polyphenolic crosslinking at the aromatic ring through C-C and C-O coupling. To obtain polymer crosslinking for hydrogel preparation, a variety of methods have been reported, such as electron beam [70], or ultraviolet light [71], and chemical crosslinking with glutaraldehyde [72]. Due to the limitation of the above methods, such as low mechanical stability in irradiation crosslinking and cytotoxicity in chemical crosslinking, in this study, horseradish peroxidase (HRP)-mediated crosslinking was utilized to obtain Gelatin-Ph/HA-Ph composite hydrogel. HRP is a well-known biocompatible heme protein that catalyzes the conjunction of phenolic derivatives in the presence of hydrogen peroxide (H_2O_2).

Apart from the action of H_2O_2 as an electron acceptor during the crosslinking reaction, it has the potential to oxidize the polymer molecules **(Fig. 2-1)**. H_2O_2 is generally utilized for degrading various polymers, including HA and gelatin, through oxidative cleavage of the bond [38,73,74]. By considering these functions of H_2O_2, the physical and chemical properties of the hydrogel can be controlled by adjusting the reaction time with H_2O_2. Previously, we have reported that the stiffness of the Gelatin-Ph and HA-Ph based hydrogels can be controlled by tuning air containing H_2O_2 exposure time [18,75,76]. In this study, the behavior of human umbilical vein endothelial cells (HUVECs) on the Gelatin-Ph/HA-Ph hydrogels obtained by tuning the exposure time to H_2O_2 was explored.

In this chapter, I explored the contradictory functions of H_2O_2 in increasing hydrogel stiffness by inducing HRP-catalysed crosslinking; while also reducing hydrogel stiffness as an oxidant that induces the degradation of HA-Ph molecules were demonstrated. Moreover, the

behaviours of HUVECs on the hydrogels obtained through the H_2O_2-mediated crosslinking and degradation were reported.

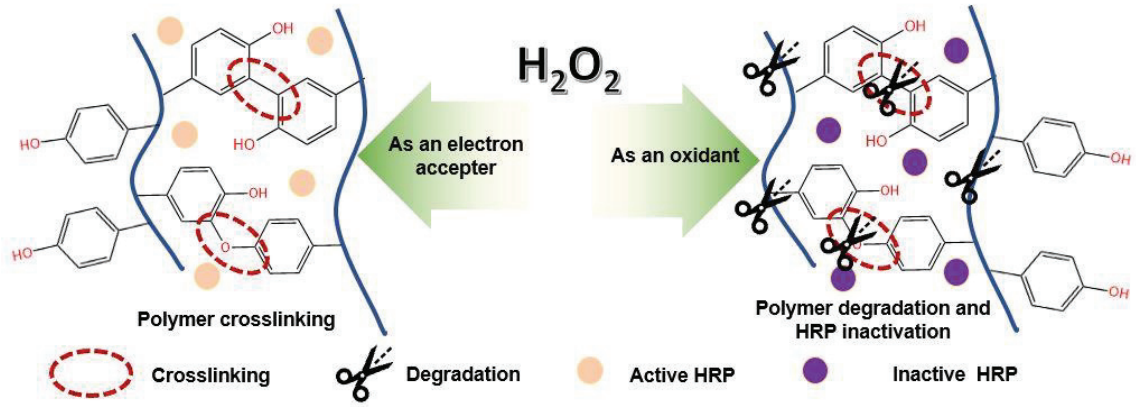

Fig. 2-1 Schematic illustration of the H_2O_2-mediated crosslinking of phenolic groups on polymer chains catalyzed by HRP and degradation of the polymer chains. Reprinted from (Elvitigala et al. 2022) [47] with permission from MDPI.

2. Materials and methods

2.1 Materials

Gelatin (type B from bovine skin, 226 g Bloom), basic fibroblast growth factor (bFGF), and endothelial growth factor (EGF) were purchased from Sigma-Aldrich (St. Louis, MO, USA). HA-Ph and Alginate-Ph containing 8 Ph groups per 100 repeat units were gifted from Nagase ChemteX (Osaka, Japan). Aqueous H_2O_2 (31 w/w%), *N*-hydroxysuccinimide, Dimethylformamide, 3-(4-hydroxyphenyl) propionic acid, 4% w/v paraformaldehyde in PBS, catalase (bovine liver), collagenase, hyaluronidase, and horseradish peroxidase (HRP) were purchased from FUJIFILM Wako Pure Chemical (Osaka, Japan). The Calcein-AM and Propidium Iodide were obtained from Nacalai Tesque Inc. (Kyoto, Japan) and Dojindo (Kumamoto, Japan) respectively. 1-Ethyl-3-(3-dimethylaminopropyl)carbodiimide and Endothelial Basal Medium MCDB107 were obtained from Peptide Institute (Osaka, Japan). Gelatin type B possessing phenol groups was synthesized based on the previously developed

protocol [77]. Briefly, dimethylformamide, 3-(4-hydroxyphenyl) propionic acid was activated using 1-ethyl-3-(3-dimethylaminopropyl)carbodiimide and *N*-hydroxysuccinimide. Then, gelatin was added and stirred for 20 h in DMF buffer solution (pH 4.2). After reacting for 20 h, unreacted 3-(4-hydroxyphenyl) propionic acid was removed from the reaction mixture by dialyzing the solution in dH_2O. Using a UV-Vis spectrometer (UV-2600, Shimadzu, Kyoto, Japan) and NMR spectroscopy (JNM ECS400, JEOL, Tokyo, Japan), indicated that the Phenolic group had been introduced to the Gelatin-Ph.

2.2 Mechanical property measurement

The stiffness of the synthesized hydrogels was determined in terms of Young's modulus using a material tester (EZ-SX, Shimadzu, Kyoto, Japan). First, composite hydrogel (HA-Ph/Gelatin-Ph) was obtained by exposing the solution of 3.0 wt% Gelatin-Ph, 0.5 wt% HA-Ph dissolved in PBS, and HRP (1 U/mL) to 16 ppm air containing H_2O_2 for 15, 60, and 120 min. Then each composite hydrogel was compressed at 6 mm/s using an 8 mm probe. Young's modulus was calculated in order to determine the stiffness of prepared hydrogel using the linear compression strain of 1 – 10% of stress-strain curve. The same experimental steps were followed for the preparation and mechanical property measurements for 3.0 wt% Gelatin-Ph/0.5 wt% Alginate-Ph, 3 wt% Gelatin-Ph, and 3.25 wt% Gelatin-Ph hydrogels.

2.3 Molecular weight measurement

PBS solutions containing 3.0 wt% Gelatin-Ph and 0.5 wt% HA-Ph were separately reacted to air containing 16 ppm H_2O_2 for 15 min, 60 min, and 120 min, respectively. The resultant molecular weights of both polymers in the solutions were analyzed using high performance liquid chromatography (HPLC) (LC-20AD, Shimadzu, Kyoto, Japan) based on an intensity-time curve. The unexposed stock solutions of both polymers were used as the control, and the

molecular weight of each sample was calculated from the calibration curve of polyethylene glycol standards.

2.4 Enzymatic degradation

An equilibrium state was reached after immersing composite hydrogel (Gelatin-Ph/HA-Ph) in PBS solution for one day. Then, the PBS solution was replaced by a mixture of hyaluronidase (1 mg/mL) and collagenase (1 mg/mL). Next, the time required for the total decomposition of hydrogel were then evaluated.

2.5 Cell culture

Human Umbilical Vein Endothelial Cells (HUVECs) were obtained from RIKEN Cell Bank (Ibaraki, Japan). The HUVECs were cultured in MDCB107 medium consisting fetal bovine serum (10 v/v%) and supplemented with the 10 ng/mL of basic fibroblast growth factor (bFGF) and 10 ng/mL of endothelial growth factor (EGF) through passage 6. Cell culture was conducted at a humidified incubator supplied with 5% CO_2 at 37 °C.

2.6 Cell adhesion and viability analysis

The composite hydrogel (Gelatin-Ph/HA-Ph) was prepared in a 6 well-plate by exposing the air containing H_2O_2 for 15 to 120 min to 1 mL of 3.0 wt% Gelatin-Ph, 0.5 wt% HA-Ph dissolved in PBS and HRP (1 U/mL) solution. The unreacted H_2O_2 was removed from the hydrogel using the growth medium containing catalase (1 mg/mL). Following overnight incubation in catalase, hydrogels were washed thoroughly several times using both PBS and MDCB107 medium. HUVECs were then cultured on the polystyrene cell culture plate or hydrogel at 4.0×10^3 cells/cm^2. HUVECs viability was analyzed based on our previously reported method [18]. HUVECs adhesion on to the substrates was analyzed based on the cell

morphological parameters including aspect ratio (ratio between cell length and width) and area were calculated for the morphology analysis using ImageJ. Previous reports in the literature mentioned Calcein-AM, which stained the cell cytoplasm, could be used to analyze the morphological parameters. Therefore, in this study, Calcein-AM staining for the morphological analysis [78,79] was used.

2.7 Human umbilical vein endothelial cell network formation

HUVECs network formation analysis was conducted on the hydrogels according to the previously reported protocol [13]. First, 3 wt% Gelatin-Ph, 0.5 wt% HA-Ph in PBS, and HRP (1 U/mL) was mixed and put into a 6-well plate (1 mL/well). Then the polymer solution was exposed to the air containing H_2O_2 (16 ppm) for 15-120 min. Subsequently, 1 mL of catalase dissolved in MCDB107 medium was added to fabricated hydrogel and incubated overnight at 37 °C in humidified incubator supplied with 5% CO_2. After incubation overnight, the cells with 70% confluent were trypsinized and seeded on the Gelatin-Ph/HA-Ph hydrogel at 4.0×10^4 cells/cm^2 [13]. HUVECs were cultured in an MCDB107 medium containing 10 ng/mL bFGF, 10 ng/mL EGF and 2 v/v% FBS. The HUVECs network formation was analyzed using an optical microscope (OLYMPUS IX71, Tokyo, Japan) at 20 h of post-culture. Parallel experiments were conducted on the 3 wt% Gelatin-Ph/0.5 wt% Alginate-Ph, 3 wt% Gelatin-Ph, 3.25 wt% Gelatin-Ph hydrogel, and cell culture dish following the same experimental procedure.

2.8 Statistical analysis

Microsoft® Excel® (Microsoft Corp., Redmond, WA, USA) 2019 version 1808 was used for all data analysis. Statistical analyses were performed using One-way analysis of variance (ANOVA). A post hoc t-test was conducted using Tukey HSD, with a p-value of <0.05 was considered significantly different.

Table 5. The abbreviation of hydrogels and the H_2O_2 exposure time applied to fabricate the hydrogels from the solutions containing 1 U/mL HRP.

Abbreviation	Hydrogel composition	H_2O_2 exposure time (min)
G3-15	3 wt% Gelatin-Ph	15
G3-60	3 wt% Gelatin-Ph	60
G3-120	3 wt% Gelatin-Ph	120
G3/HA0.5-15	3 wt% Gelatin-Ph/0.5 wt% HA-Ph	15
G3/HA0.5-60	3 wt% Gelatin-Ph/0.5 wt% HA-Ph	60
G3/HA0.5-120	3 wt% Gelatin-Ph/0.5 wt% HA-Ph	120
G3.25-60	3.25 wt% Gelatin-Ph	60
G3/Alg0.5-60	3 wt% Gelatin-Ph/0.5 wt% Alginate-Ph	60

3. Results and discussion

3.1 Hydrogel characterization

Firstly, air containing H_2O_2 exposure time (15, 60, and 120 min) on the stiffness of the hydrogels was analyzed after confirming the hydrogelation within 1 min of the exposure for all the compositions shown in **Table 5**. As shown in **Fig. 2-2a**, Young's modulus increases with H_2O_2 exposure time from 15 to 60 min, and the values decreased with a further increase of the time to 120 min both in G3 and G3/HA0.5 hydrogels. The values detected for G3-60 and G3/HA0.5-60 after exposure to the air containing H_2O_2 for 60 min were 1.90 kPa and 2.40 kPa, respectively. These values were about 8- and 2-times larger than those detected for the specimens obtained through 15 and 120 min of exposure, respectively, at the same composition. The air containing H_2O_2 exposure time-dependent change of the hydrogel mechanical properties is consistent with the results in the literature [18,75].

The hydrogel stiffness increase with an increase in the exposure time to the H_2O_2 from 15 to 60 min was explained by the increase of the crosslinking between Ph groups through the progression of the HRP-catalyzed reaction [76]. The hydrogel stiffness decrease with an increase

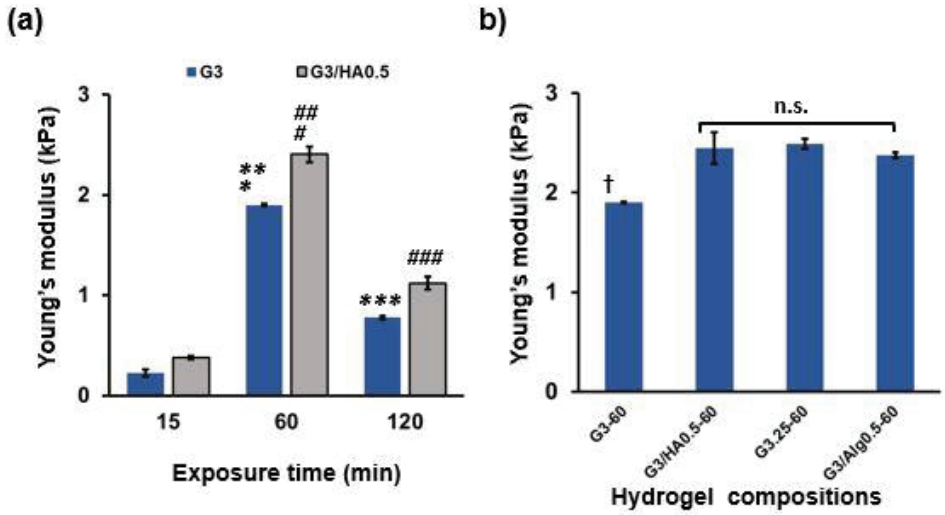

Fig. 2-2 Effect of the air containing 16 ppm H_2O_2 exposure time on the stiffness of G3 and G3/HA0.5 hydrogels. (b) Effect of the composition of polymers on the stiffness of hydrogels obtained by applying air containing H_2O_2 for 60 min. (G3-60, G3/HA0.5-60, G3.25-60, and G3/Alg0.5-60). Bars: S. E. (n = 3). $^{*}p<0.005$, $^{\#}p<0.005$, 15min compared to 60 min; $^{**}p<0.005$, $^{\#\#}p<0.005$, 60 min compared to 120 min; $^{***}p<0.005$, $^{\#\#\#}p<0.005$, 15 min compared to 120 min; $^{\dagger}p<0.005$, G30-60 compared to G3/HA0.5-60, G3.25-60, and G3/Alg0.5-60; n.s.: $p>0.05$. Tukey HSD. Reprinted from (Elvitigala et al. 2022) [47] with permission from MDPI.

in the exposure time from 60 to 120 min was explained by the HRP inactivation and polymer degradation by H_2O_2 [75].

Furthermore, the effect of the air containing H_2O_2 exposure time on the mechanical property was analyzed by measuring the time required for total degradation of the G3/HA0.5 hydrogel using hyaluronidase and collagenase as shown in **Fig. 2-3.** The stiff hydrogel (G3/HA0.5-60) required long time (92 s), due to the high crosslinking formation, compared to the soft and intermediate stiff hydrogels (G3/HA0.5-15 and G3/HA0.5-120, respectively). As shown in **Fig. 2-4**, the molecular weights of both polymers were decreased with increasing the H_2O_2 exposure time.

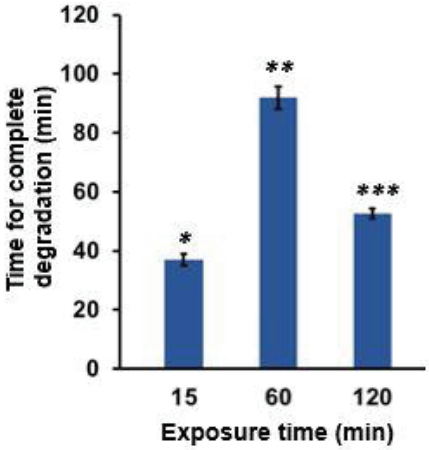

Fig. 2-3 Effect Enzymatic degradation of Gelatin-Ph/HA-Ph hydrogel by a mixture of hyaluronidase (1 mg/mL) and collagenase (1 mg/mL). The composite hydrogel was prepared by exposing air containing H_2O_2 for 15 – 120 min into PBS solution containing 3 w/v% Gelatin-Ph/0.5 w/v% HA-Ph and 1 U/mL HRP. Bar. S. E. (n = 3). $^{*}p<0.005$, 15min compared to 60 min; $^{**}p<0.005$, 60 min compared to 120 min; $^{***}p<0.05$, 15 min compared to 120 min. Tukey HSD. Reprinted from (Elvitigala et al. 2022) [47] with permission from MDPI.

The higher stiffness of G3/HA0.5 hydrogels than G3 hydrogels at each exposure time was caused by the denser polymer network due to the higher concentration of polymer. The stiffness of the hydrogels prepared from 3.25 wt% Gelatin-Ph solution (G3.25-60) and 3 wt% Gelatin/0.5 wt% Alginate-Ph solution after 60 min of exposure to the air containing H_2O_2 (G3.25-60 and G3.25/A0.5-60, respectively) were comparable to that of G3/HA0.5-60 **(Fig. 2-**

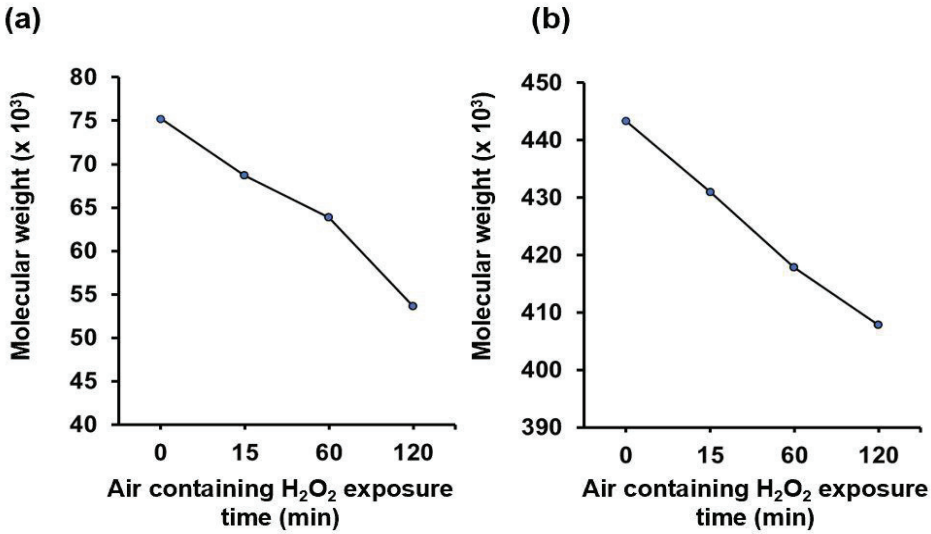

Fig. 2-4 Effect of the exposure time to the air containing 16 ppm H_2O_2 on the molecular weights of (a) Gelatin-Ph and (b) HA-Ph. Reprinted from (Elvitigala et al. 2022) [47] with permission from MDPI.

2b). G3.25-60 and G3.25/A0.5-60 hydrogels were prepared for evaluating the effect of the hydrogel stiffness and composition on HUVECs behavior shown in Section 3.2.

3.2 Cell behavior on hydrogel

The influence of the physicochemical property changes on the behavior of the HUVECs were examined. Initially, the viability of the HUVECs on G3 and G3/HA0.5 hydrogels prepared by exposing air containing H_2O_2 for 15 – 120 min were analyzed. The hydrogels were used after soaking overnight in a medium containing catalase for the removal of H_2O_2. HUVECs showed >90% viability on all the hydrogels independent of the composition and the exposure time. This result indicates that the hydrogels prepared through exposure to the air containing H_2O_2 have no cytotoxicity on HUVECs.

Cell area analysis showed that HUVECs cultured on both G3 and G3/HA0.5 hydrogels had a stiffness-dependent alteration of the cell area. The cells on the G3-60 and G3/HA0.5-60 had the largest area (Figure 2-5a-b). Interestingly, cell elongation analysis based on the aspect ratio of the cells showed a different elongation trend of HUVECs cells on G3 and G3/HA0.5 hydrogels. While cells on G3 showed a stiffness-dependent elongation, in which cells cultured on G3-120 had a lower aspect ratio than those on G3-60 hydrogel, those on G3/HA0.5-120 hydrogel showed a higher aspect ratio on 120 min hydrogels **(Fig. 2-5c)**.

This result is possibly mediated by the HA-Ph degradation in the 120 min-exposed hydrogels. In fact, the cells on G3.25-60 hydrogel with a com-parable stiffness with G3/HA0.5-60 **(Fig 2-2b)** showed a similar aspect ratio with those on G3-60 ($p = 0.906$, Tukey HSD) but a different aspect ratio with those on G3/HA0.5-60 ($p = 0.020$, Tukey HSD). Previous report by Pang et al. have reported that the LMWHA could induce cell elongation and epithelial to mesenchymal transition.

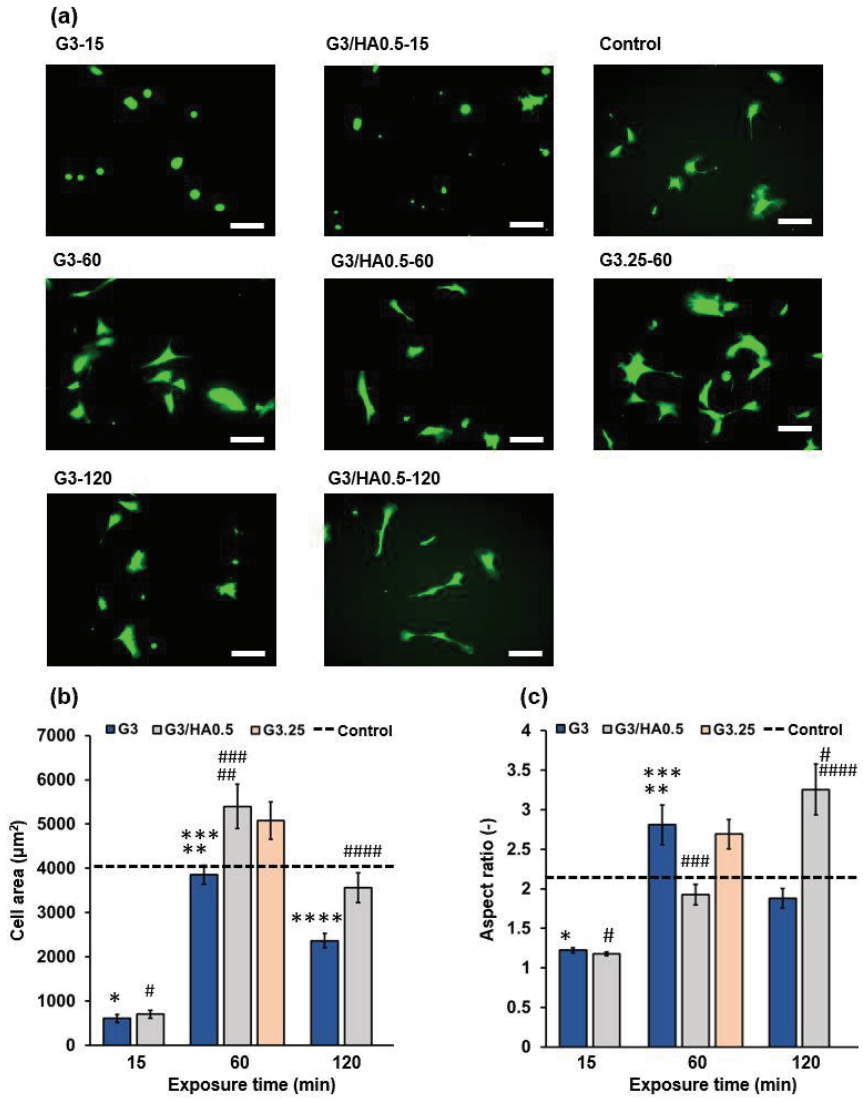

Fig. 2-5 Fluorescence micrographs of HUVECs stained with Calcein-AM after 2 days of post-culture on the G3, G3/HA0.5, and G3.25 hydrogels. Effect of the exposure time to the air containing 16 ppm H_2O_2 on the (b) cell area and (c) aspect ratio of HUVECs on G3, G3/HA0.5, and G3.25 hydrogels. Scale bar:100 μm. Bars: S. E. ($n \geq 35$ cells). $^{*}p<0.05$, $^{\#}p<0.005$, $^{\dagger}p<0.05$ 15min, 60 min and 120 min exposure time compared to control (dashed line); $^{**}p<0.05$, $^{\#\#}p<0.005$, 15 min compared to 60 min; $^{***}p<0.05$, $^{\#\#\#}p<0.005$, 60 min compared to 120 min; $^{****}p<0.05$, $^{\#\#\#\#}p<0.005$, 15 min compared to 120 min. Tukey HSD. Reprinted from (Elvitigala et al. 2022) [47] with permission from MDPI.

This epithelial to mesenchymal transition process involves the physiological transition of cells from eukaryotic cells to mesenchymal cells, which exhibit morphological changes such as spindle-like morphologies. As shown in **Fig. 2-4**, prolonged exposure to air containing H_2O_2 could degrade the HA-Ph. The degraded fragments of HA-Ph might interact with cell receptors that induce cell elongation. A similar result was also observed in our previous study using

NMuMG/Fucci2 cells cultured on composite hydrogel (Gelatin-Ph/HA-Ph) obtained through 120 min of the air containing H_2O_2 exposure. In general, this result shows that HUVECs adhesion depends on the biomaterials component and the mechanical property of the hydrogel.

3.3 Human umbilical vein endothelial cell network formation

Finally, we investigated the HUVECs network formation on each hydrogel with seeding HUVECs at 4.0 x 10^4 cells/cm^2. This seeding density was selected considering the successful network formation by previous studies [13].

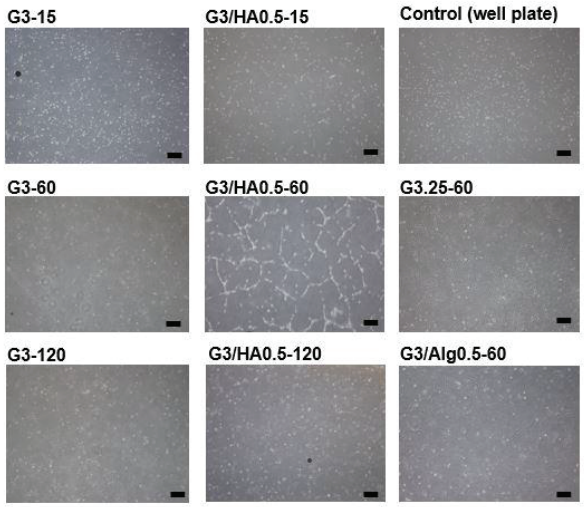

Fig. 2-6 The effect of hydrogel composition and air containing H_2O_2 exposure time on HUVECs capillary-like network formation. HUVECs were seeded at 4.0 x 10^4 cells/cm^2 on G3-15, G3-60, G3-120, G3/HA0.5-15, G3/HA0.5-60, G3/HA0.5-120, G3.25-60, G3/Alg0.5-60, and culture well plate. Scale bar:100 μm. Reprinted from (Elvitigala et al. 2022) [47] with permission from MDPI.

As shown in **Fig. 2-6**, HUVECs formed a visible network only on G3/HA0.5-60 hydrogel. The different behavior of the cells on G3/HA0.5-15, -60, and -120 hydrogels suggests the possible effect of hydrogel stiffness on the network formation. The different behavior of the cells on G3-60 and G3/HA0.5-60 also suggests the possible effect of the stiffness. G3/HA0.5-60 had the highest stiffness in G3 and G3/HA0.5 hydrogels **(Fig. 2-2a)**. However, the sole effect of the hydrogel stiffness on the network formation of HUVECs was denied by the non-network formations of the cells on G3.25-60 and G3/A0.5-60 hydrogels having similar stiffnesses with G3/HA0.5-60 **(Fig. 2-2a).**

These results demonstrate that the combined effects of hydrogel stiffness and the low molecular weight HA-Ph generated through the degradation of HA-Ph by H_2O_2 caused the network formation of HUVECs on G3/HA0.5-60 hydrogel. Currently, the detailed mechanism of how the HA molecular weight and stiffness of the hydrogel affect the HUVECs behavior is unknown and will be a subject of our future study. However, there are several possible mechanisms. The presence of small fragments of HA, such as those as a product of HA-Ph degradation by air containing H_2O_2 exposure **(Fig. 2-4)**, was reported to induce HUVECs capillary-like network formation by interacting with CD44 and RHAMM [80,81]. HA-CD44 interaction could activate γ-adducin which plays a role in tube formation [82]. Meanwhile, the interaction between HA and RHAMM induces AP-1 binding to the RHAMM promoter which promotes the capillary-like network formation of HUVECs [82,83].

In addition to the chemical signalling of ECM components, ECM stiffness plays an essential role in the capillary-like network formation of HUVECs through mechanical signalling. Joseph et al. reported the effect of substrate mechanics and matrix chemistry on endothelial cell network assembly using polyacrylamide substrates derivatized with type I collagen [84]. They investigated that stiff hydrogel (2.5 – 10 kPa) with low cell-substrate adhesiveness could form a capillary-like network while soft substrate (0.2 – 1 kPa) retained a round morphology without network formation [85]. Therefore, the combination of both substrate stiffness and ECM components is vital for the capillary-like network formation of HUVECs. Taken together, our studies demonstrate that the effect of H_2O_2 on inducing polymer crosslinking and degradation could modulate the behavior of HUVECs. From the translational perspective view, these investigations are useful in different tissue engineering applications. Several studies have reported that the alteration in HA molecular weight and amount are characteristic of pathological conditions. The accumulation of HA in cancer stroma is a marker of malignancy for different kinds of tumors. In addition, angiogenesis is essential for invasive tumor growth

and constitutes a crucial point in the control of tumor progression. In cancer therapy, inhibition of angiogenesis may be a valuable new approach. Therefore, our findings could be used as a tool for the in vitro study of cancer therapy through factors affecting inhibition and stimulation of angiogenesis.

4. Conclusion

In this chapter, the influence of the composition and mechanical properties of the hydrogels on the behavior of HUVECs was investigated, setting the stage for the next chapters, which will delve into different aspects of HA-Ph hydrogel applications, including varying crosslinking methods, the effects of HA-Ph degradation on other cell types, and broader tissue engineering applications. The degree of polymer degradation and hydrogel stiffness were tuned by simply controlling the exposure time to air containing H_2O_2 during the hydrogel preparation. HUVECs showed different responses depending on the degree of polymer degradation and the stiffness of the hydrogel. HUVECs cultured on Gelatin-Ph/HA-Ph hydrogel showed higher elongation on prolonged exposure to air containing H_2O_2, a phenomenon that was not observed in the absence of HA-Ph. More importantly, HUVECs network formation was observed only on stiff Gelatin-Ph/HA-Ph hydrogels, while cells on hydrogels composed of Gelatin-Ph alone or mixed with Alginate-Ph instead of HA-Ph showed no network formation regardless of the stiffness.

Some portion of this thesis, including text and figures, have been previously published in the journal article “Human Umbilical Vein Endothelial Cells Form a Network on a Hyaluronic Acid/Gelatin Composite Hydrogel Moderately Crosslinked and Degraded by Hydrogen Peroxide” by Elvitigala et al., published in *Polymers*, 2022, 14, 5034 (Reference No. 47). These sections are reproduced here with permission from MDPI (Basel, Switzerland).

Chapter III

Photo-Tuning of Hyaluronic Acid-Based Hydrogel Properties to Control Network Formation in Human Vascular Endothelial Cells

1. Introduction

The study in Chapter II has demonstrated the intricate balance between crosslinking and degradation of HA-based hydrogels using H_2O_2. By adjusting the exposure time to H_2O_2, we were able to control the stiffness and degradation rate of the hydrogels, which significantly influenced the behavior of human umbilical vein endothelial cells (HUVECs). As discussed in Chapter II, the interplay between HA-Ph degradation and hydrogel stiffness was shown to be crucial for optimizing the conditions for in vitro angiogenesis studies. Building on these insights, Chapter III delves into the effects of photocrosslinking on the properties of HA-based hydrogels and their subsequent impact on HUVEC network formation. While enzymatic crosslinking methods provide valuable control over hydrogel properties, photocrosslinking offers a unique advantage of spatial and temporal control, allowing for precise tuning of hydrogel characteristics. This chapter explores how visible-light-mediated photocrosslinking, combined with the oxidative degradation of HA, can be used to modulate the mechanical properties of the hydrogels and enhance the formation of network-like structures by HUVECs.

As discussed in Chapter I, understanding the formation of network-like structures of HUVECs is crucial for advancing the knowledge of angiogenesis and its role in various physiological and pathological conditions. This process is necessary for the formation of complex networks of blood vessels and capillaries and plays a crucial role in wound healing, tissue regeneration, and embryonic development. Therefore, exploring the mechanisms of network-like structure formation in vivo and in vitro has become an important area of research

in tissue engineering. Kubota et al. first demonstrated in vitro network-like structure formation using a collagen-based gel infused with basement membrane components to determine the role of signals responsible for the morphological differentiation of VECs and network-like structure formation [86]. As mentioned in Chapter I, hydrogels have emerged as the preferred platform for in vitro angiogenesis, where the polymers used to prepare them are chemically modified to govern both in vitro and in vivo angiogenesis.

This study focused on modulating the physicochemical properties of hydrogels, such as their stiffness and polymer degradation as same as Chapter II, to elicit their effects on the network-like structure formation of HUVECs. Natural polymers, such as hyaluronic acid (HA), gelatin, and alginate, [87–89] are widely used to design hydrogels by photocrosslinking as promising biomimetic materials [90–92]. Alginate is widely utilized owing to its biocompatibility and gelation properties, which are ideal for 3D bioprinting and tissue engineering[88]. Meanwhile, HA and gelatin, the major elements of the basement membrane as discussed in Chapter I in detail, have been increasingly employed to fabricate biomaterials because of their biocompatibility, [93] biodegradability, and ability to influence cell behavior, including angiogenesis [94,95]. However, HA alone does not promote cellular adhesion; therefore, it must be combined with materials such as gelatin to promote cellular adhesion through the arginine–glycine–aspartic acids (RGD) sequence, and various studies have shown the usefulness of combining HA and gelatin to fabricate biomaterials. In particular, RGD enhances vascular endothelial growth factor (VEGF)-mediated angiogenesis in HA hydrogels by promoting RAS activation, a key step for vascular endothelial cells (VECs) proliferation, migration, and morphogenesis [96,97]. Moreover, the enzymatic responsiveness to matrix metalloproteinases (MMPs) is pivotal, allowing HA-based hydrogels to mimic the dynamic ECM, facilitating cell migration essential for vascular morphogenesis [98–100].

In addition, the molecular weight of HA, which can be modified by external conditions such as the physical properties of the surrounding biomaterials, can substantially dictate cell response [4]. HMWHA affects cell adhesion and proliferation, [101] whereas LMWHA, typically found in degraded ECM, tends to inhibit these processes [102] and instead enhances the network-like structure formation of HUVECs. These effects are primarily mediated by cell surface receptors for HA, such as CD44[102,103]. The interaction between CD44 receptors and HA of different molecular weights results in distinct cellular functions. Specifically, LMWHA fragments play a crucial role in F-actin formation by activating specific signaling pathways [4]. Consequently, F-actin formation induced by LMWHA is a critical factor in regulating the formation of network-like HUVEC structures. Therefore, the controlled degradation of HA during hydrogel preparation, particularly into low molecular weight fragments, is important for optimizing the hydrogel properties for vascular tissue engineering.

In our previous studies, phenolated HA and gelatin molecules (i.e., HA-Ph and Gelatin-Ph, respectively) were crosslinked with the aid of horseradish peroxidase/hydrogen peroxide (HRP/H_2O_2) to control the physicochemical properties of the resultant hydrogel [18,47,104]. In HRP-catalyzed gelation, H_2O_2 is used as an electron donor to crosslink phenol (-Ph) groups. Apart from inducing gelation, H_2O_2 is known to cleave the glycosidic bonds of HA through oxidative degradation, which enhances the network-like structure formation of HUVECs on the hydrogel [18,47,104]. In this study, a photocrosslinking process was employed to investigate the correlation between the oxidative degradation of HA and the mechanical properties of the hydrogel by evaluating the formation of network-like structure of HUVECs. Typically, the photopolymerization process involves grafting photolabile functional moieties, such as methacryloyl, phenol, or styrene, onto the polymer backbone. Among various photolabile candidates, polymer chains modified with phenol are promising as biomaterials, because their physical properties can be tuned for diverse tissue engineering applications. Therefore, in this

study, HA modified with tyramine and gelatin modified with 3-(4-hydroxyphenyl)propionic acid were used to prepare composite hydrogels.

To date, various photoinitiators have been used to crosslink chemically modified polymers. Previously, our group reported the visible-light-mediated crosslinking of various biomaterials, including sugar beet pectin that naturally possessed phenol, [105] as well as Alginate-Ph, HA-Ph and Gelatin-Ph in which tris(2,2'-bipyridyl)ruthenium(II) chloride hexahydrate ($[Ru(bpy)_3]^{2+}$) was employed as the photoinitiator because of its biocompatibility with living tissues and its ability to initiate crosslinking in a controlled manner without requiring UV light, which can be harmful to cells. When exposed to visible light, HA-Ph and Gelatin-Ph crosslink via radical polymerization in the presence of $[Ru(bpy)_3]^{2+}$ and sodium persulfate (SPS). The crosslinking mechanism of the phenolic moieties can be summarized as follows: $[Ru(bpy)_3]^{2+}$ molecules absorb photons and dissociate SPS into radicals, which then propagate through the phenolic groups, thereby crosslinking the polymer chains by covalently bonding the phenolic moieties in different polymer chains. The novelty of this study lies in the development of an HA-Ph-based hydrogel system by harnessing the power of photocrosslinking to precisely control the stiffness and oxidative degradation rates of the HA-Ph units. SPS and $[Ru(bpy)_3]^{2+}$ are typically used not only to initiate the crosslinking of polymeric chains by forming SPS radicals but also to contribute to the breakdown of the HA-Ph chains via the oxidative cleavage of glycosidic bonds, leading to a delicate balance between crosslinking and HA-Ph degradation, as illustrated in **Fig. 3-1**. This balance dictates the overall properties of the hydrogel and subsequently influences the HUVECs behavior. Previous work by Rumiana et al. demonstrated the angiogenic potential of VECs in gelatin-based hydrogels through the controlled release of growth factors [62], while Ying et al. highlighted the benefits of co-delivering growth factors in gelatin hydrogels for enhanced angiogenesis [81]. Derek et al. further explored the stimulation of hyaluronidase in VECs colony-forming cells via HA-specific receptors, underscoring the

importance of HA in vascular network formation [64]. Our study expands on these foundational discoveries by focusing on the generation of LMWHA during hydrogel fabrication, which I have identified as a critical factor in inducing network formation and providing mechanical support for angiogenesis. By offering a substrate that combines both biochemical cues and mechanical properties, our work not only bridges existing gaps but also introduces a comprehensive approach to facilitating angiogenesis, setting a new benchmark for research in tissue engineering and regenerative medicine.

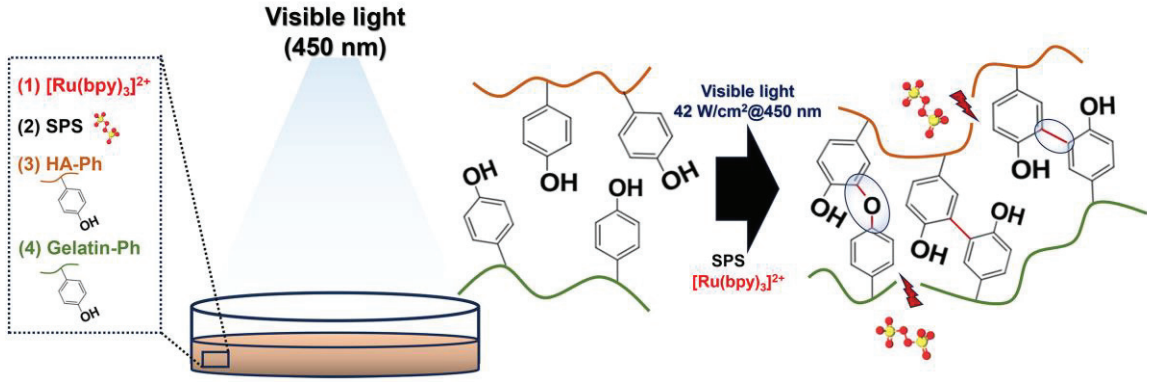

Fig. 3-1 (a) The Schematic illustration of the contradictory impact of SPS on the formation of HA-Ph/Gelatin-Ph hydrogels and the degradation of the crosslinked polymer under visible-light irradiation (450 nm) in the presence of a photoinitiator, $[Ru(bpy)_3]^{2+}$. Reprinted from (Elvitigala et al., 2024) [48] with permission from Wiley-VCH.

2. Materials and methods

2.1 Materials

Gelatin HA-Ph with four phenyl groups per 100 repeating units of HA and Gelatin-Ph with a phenyl content of 4.1×10^{-4} mol g^{-1} were synthesized according to previously reported methods [77,106]. In brief, tyramine hydrochloride (Chem-Impex, Wood Dale, IL, USA) was reacted with Na-HA (Kewpie, Tokyo, Japan) to obtain HA-Ph. In addition, type B gelatin from bovine skin (Sigma-Aldrich, St. Louis, MO, USA) was modified with 3-(4-hydroxyphenyl)propionic acid (Tokyo Chemical Industry, Tokyo, Japan) to obtain Gelatin-Ph.

The introduction of phenolic groups into HA and gelatin was confirmed through ^{1}H NMR spectroscopy. SPS, phosphate-buffered saline (PBS) containing 4 w/w% paraformaldehyde, and hyaluronidase from ovine testes (1110 U/mL) were purchased from FUJIFILM Wako Pure Chemical (Osaka, Japan). $[Ru(bpy)_3]^{2+}$ was purchased from Tokyo Chemical Industry (Tokyo, Japan). Phalloidin-iFluor 647 (ab176759) was procured from Abcam (Cambridge, UK).

2.2 Cell culture

HUVECs immortalized by the electroporation of pIRES-hTERT-hygr (HUEhT-1) cell line was purchased from RIKEN Cell Bank (Ibaraki, Japan). Cell culture medium, MCDB107 (Nissui, Tokyo, Japan), supplemented with 10 ng mL^{-1} endothelial growth factor, basic fibroblast growth factor (Sigma-Aldrich, St. Louis, MO, USA), and 10 v/v% fetal bovine serum (FBS) was used to maintain the culture. The cell culture environment was maintained at 37 °C in a humidified incubator with 5% CO_2.

2.3 Rheological and molecular weight measurement

Sodium salt of HA (Na-HA, 2 w/v%) was dissolved in PBS containing SPS and $[Ru(bpy)_3]^{2+}$ at a final concentration of 2 mM each and then exposed to 450 nm light for 15, 30, 45, or 60 min at an intensity of 42 W cm^{-2}. The viscoelastic properties of the polymer solutions were determined using a parallel plate rheometer (HAAKE MARS III, Thermo Fisher Scientific, MA, USA) at 1% constant shear strain and a 1 mm gap between plates at 25°C. The molecular weight of Na-HA was analyzed by high-performance liquid chromatography (Shimadzu, Kyoto, Japan). Pullulan standards were used to prepare a calibration curve for determining the molecular weight of each sample.

2.4 Hydrogel preparation

Composite hydrogels were prepared by photocrosslinking HA-Ph and Gelatin-Ph. Gelatin-Ph was used to enhance cellular adhesion because of the poor cell adhesion properties of HA-Ph. A mixed solution of HA-Ph (2 w/v%), Gelatin-Ph (0.1 w/v%), SPS (2 mM), and $[Ru(bpy)_3]^{2+}$ (2 mM) was prepared in PBS and exposed to 450 nm light (42 W cm^{-2}) for 15, 30, 45, or 60 min. The SPS and concentrations were chosen according to our previous studies [105,107].

2.5 Hydrogel stiffness

Hydrogel sheets with a diameter of 35 mm and thickness of 2 mm were prepared in a 35 mm dish, as described in the hydrogel preparation section. Specifically, 1 mL of the polymer solution was used per dish. The Young's moduli of the hydrogels were measured using a material tester (EZ-SX; Shimadzu, Kyoto, Japan). The hydrogel sheets were compressed at the rate of 6.0 mm min^{-1} using a 5 mm diameter probe at 37 °C. The stress–strain curves obtained at 1–10% compression were used to calculate the Young's moduli.

2.6 Hydrogel degradation

Hydrogel pellets with a diameter of 8 mm and thickness of 2 mm were prepared, as described in the hydrogel preparation section. Unreacted materials in the hydrogels were removed by washing several times with PBS. Then, the hydrogel pellets were soaked in a mixture of collagenase and hyaluronidase (both at a final concentration of 0.1 w/v%) in an MCDB107 medium at 37 °C. Next, changes in the hydrogel morphology over time and the time required for the hydrogel to degrade were evaluated from photographs taken at appropriate time intervals.

2.7 Fluorescence-based evaluation of phenol crosslinking

The hydrogel was prepared as described in the hydrogel preparation section in a 96-well plate by pouring 200 μL of the polymer and photo-crosslinker solution into each well. The influence of light irradiation time (15–60 min) on the coupling of the phenol groups attached to the polymer backbone was determined using a fluorescence plate reader (Gemini XPS; Molecular Devices, San Jose, CA, USA). The fluorescence intensity between 350 and 500 nm was measured under 310 nm excitation.

2.8 Cell Adhesion and morphology

The hydrogel was fabricated in a 6-well plate by adding 1 mL of the polymer and photo-crosslinker solution into each well. Before cell seeding, unreacted materials in the hydrogels were removed by washing several times with PBS. The viability of the HUEhT-1 cells cultured on this hydrogel was determined using a previously reported method [50]. At the concentrations used in this study, SPS and $[Ru(bpy)_3]^{2+}$ showed no toxic effects in cells consistent with previous report [105]. Subsequently, the hydrogels were replenished with fresh MCDB107 medium, and then, HUEhT-1 cells were seeded onto the hydrogels (5.0×10^3 cells cm^{-2}). After two days of culture, the cell adhesion area and cell shape changes (quantified as the aspect ratio, i.e., the major axis to the minor axis of the fitted ellipse representing each cell) were analyzed by staining with Calcein-AM (Dojindo, Kumamoto, Japan). The fluorescently stained cells were imaged using a fluorescence microscope (BZ-9000; Keyence, Osaka, Japan). The cell adhesion area and aspect ratio were measured using ImageJ software (version 2.1.0/1.53c, NIH, Bethesda, MO, USA).

2.9 Network-like structure formation

The HA-Ph/Gelatin-Ph hydrogels were prepared in a 6-well plate and washed several times with PBS to remove the unreacted materials. Thereafter, HUEhT-1 cells with 70% confluence (through passage number 18) were trypsinized and seeded onto the hydrogel in each well at 4.0 × 10^4 cells cm^{-2} in low serum (2 v/v% FBS) MCDB107 medium. The network-like structure formation of the cells was analyzed using an inverted light microscope (CKX41; Olympus, Tokyo, Japan) and Provi CM20 incubation monitoring system (Olympus, Tokyo, Japan) at 16 h post culture.

2.10 Flow cytometry

After 48 h of culture, the cells were carefully detached from the hydrogel by treatment with hyaluronidase (0.1 w/v%) for 10 min. They were then incubated with the BD FC block reagent (BD Biosciences, San Jose, CA, USA) to block nonspecific binding sites. Subsequently, the cells were washed with PBS and incubated with an APC-conjugated mouse CD44 antibody (EXBIO Praha, a.s., Nad Safinou, Czech Republic) for 30 min at 4 °C. Thereafter, the cells were washed twice with PBS and analyzed using a BD Accuri C6 flow cytometer (BD Biosciences, San Jose, CA, USA).

2.11 Real-time quantitative polymerase chain reaction (RT-PCR) analysis for β-actin and RhoA expression

The HUEhT-1 cells were collected from the hydrogel after treatment with hyaluronidase (1 mg mL^{-1}) for 10 min. The cells cultured in cell culture dishes were trypsinized and subjected to RNA extraction. The total RNA was isolated from the cultured HUEhT-1 cells using an RNA isolation kit (Takara, Shiga, Japan), following the manufacturer's protocol. Reverse transcription was performed using the PrimerScript RT Master Mix reagent kit, following the

manufacturer's protocol (Takara, Shiga, Japan). The RhoA and β-actin genes were detected by qPCR using the TB Green Master Kit (Takara, Shiga, Japan). Quantification was performed via the comparative C(t) method using GAPDH as the housekeeping gene.

2.12 Statistical analysis

Microsoft Excel 2019, version 1808 (Microsoft Corp., Redmond, WA, USA) was used for the statistical data analysis. One-way analysis of variance (ANOVA) was used to determine statistical differences between the results obtained under each experimental condition. Significant differences were determined based on post-hoc *t*-test using Tukey's HSD, in which $p < 0.05$ was considered significantly different.

3. Results and discussion

3.1 Effect of light irradiation on polymer degradation and crosslinking

First, the effect of visible-light irradiation on the molecular weight of the sodium salt of HA (Na-HA) was assessed. **Fig. 3-2a, b** reveals that HA treated with the SPS/$[Ru(bpy)_3]^{2+}$ system induced the degradation of HA, as evidenced by a decrease in its viscosity and average molecular weight. As the irradiation time increased, the HA degradation increased because more SPS radicals formed. Reactive oxygen species are known to degrade HA by cleaving the glycosidic bonds between the monomeric units of the HA backbone [74,108]. As shown in **Fig. 3-2a**, light irradiation time-dependent degradation of Na-HA indicated by decrease in the viscosity of Na-HA solution with increasing light irradiation time. After 15 min of irradiation, the molecular weight of HA decreased from 515 to 417 kDa **(Fig. 3-2b)**. The formation of low molecular weight fragments increased after 45 min, although the decrease in the average molecular weight of HA was small **(Fig. 3-2c)**. After 60 min, the average molecular weight reached the lowest value of 132 kDa, which was three times lower than that of non-irradiated

HA. Control experiments assessing HA degradation with only light irradiation or SPS treatment alone revealed no significant change in polymer degradation, confirming that the observed HA degradation was specifically mediated by the combined action of light irradiation and the SPS/$[Ru(bpy)_3]^{2+}$ system. Therefore, the SPS/$[Ru(bpy)_3]^{2+}$ system is suitable for degrading HA into fragments with a range of molecular weights simply by changing the visible light irradiation time (450 nm, 42 W cm^{-2}).

Next, the mechanical properties of the HA-Ph/Gelatin-Ph composite hydrogels prepared through 15–60 min of light irradiation were analyzed. As depicted in **Fig. 3-2d**, increasing the irradiation time of the HA-Ph/Gelatin-Ph mixture added with SPS/$[Ru(bpy)_3]^{2+}$ from 15 to 30 min significantly increased Young's modulus from 1.4 ± 0.1 to 2.1 ± 0.2 kPa. However, it

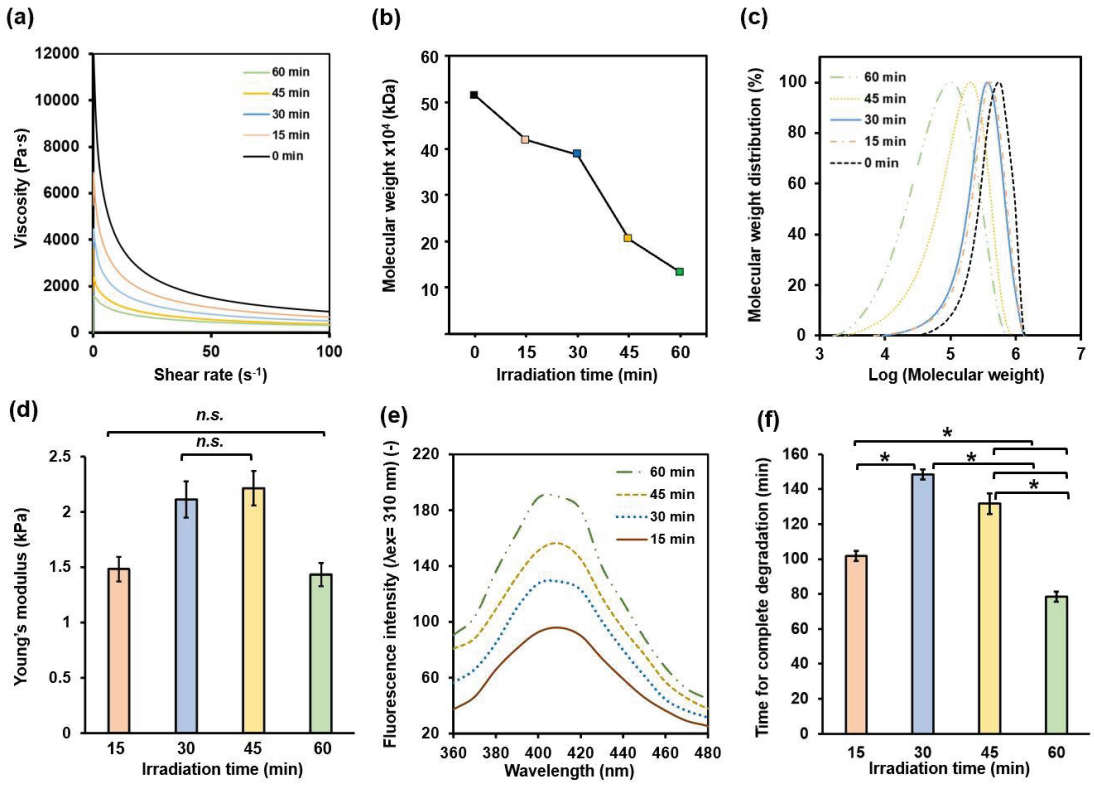

Fig. 3-2 Effect of visible-light-irradiation (42 W cm^{-2} at 450 nm) time on the (a) viscosity of PBS containing 2 mM SPS, 2 mM $[Ru(bpy)_3]^{2+}$, and Na-HA (2 w/v%) (b) average molecular weight of Na-HA, (c) molecular weight distribution of Na-HA (d) Young's modulus (n = 3) of the HA-Ph/Gelatin-Ph hydrogel, and (e) diphenol formation in the HA-Ph/Gelatin-Ph hydrogel. (f) enzymatic degradation (n = 3) Bar: standard error, *n.s.*: no significant difference ($p > 0.05$), Tukey's honestly significant difference (HSD). Reprinted from (Elvitigala et al., 2024) [48] with permission from Wiley-VCH.

decreased from 2.2 ± 0.1 to 1.4 ± 0.1 kPa upon further increasing the exposure time from 45 to 60 min. As light irradiation increases, more free radicals are produced by the reaction with SPS, leading to a more robust crosslinked polymer network and thus a stiffer hydrogel. Upon extending the irradiation time to 60 min, however, the hydrogel stiffness decreases because of the significant fragmentation of HA units in the hydrogel. In summary, the HA degradation and hydrogel stiffness analyses indicate that the polymer degradation increases with increasing irradiation time, and the hydrogel stiffness reaches a maximum value and then decreases. The hydrogel stiffness is maximized upon the optimal fragmentation of HA-Ph during the polymer degradation process. Further, the HA-Ph fragmentation increases with prolonged light-irradiation time, resulting in excessive degradation that decreased stiffness, as illustrated in **Fig. 3-2a and 2c**. To further clarify these phenomena, the change in the degree of crosslinking between HA-Ph and gelatin-Ph with the irradiation time was analyzed using a fluorescence-based method. As shown in **Fig. 3-2e**, the formation of diphenol linkages increased as irradiation was prolonged from 15 to 60 min because an increased number of $[Ru(bpy)_3]^{2+}$ molecules were photoexcited, resulting in greater crosslinking of the two polymers. Next, the degradability of the HA-Ph/Gelatin-Ph hydrogel was evaluated by measuring the time required to completely degrade the hydrogel after being treated hyaluronidase and collagenase **(Fig. 3-2f)**. Consistent with their highest stiffness, the hydrogels obtained by irradiation for 30 and 45 min required the longest times to be degraded (135 and 150 min, respectively), in contrast with the softer hydrogels obtained by 15 and 60 min of light irradiation. Meanwhile, none of the hydrogels obtained by 15–60 min of irradiation degraded after seven days of immersion in a cell culture medium that did not contain hyaluronidase or collagenase. Our preliminary studies also confirmed that adding 0.1 w/v% gelatin-Ph did not significantly impact the hydrogel mechanical properties.

3.2 Cell adhesion and cell morphology on the hydrogel

Understanding the importance of the mechanochemical property-dependent cell adhesion could reveal the correlation between cellular adhesiveness and the dynamics of the angiogenic behavior of the HUEhT-1 cells (HUVECs immortalized by the electroporation of pIRES-hTERT-hygr). Cell behaviors, such as proliferation, differentiation, and morphology, depend on the physicochemical properties of the substrate [61,109–111]. As discussed in the previous section, HA-Ph/Gelatin-Ph composite hydrogels with distinct HA-Ph degradation rates and mechanical properties were first produced by modulating visible-light exposure at 450 nm during hydrogel fabrication. Then, the HUEhT-1 cells were cultured on the hydrogels to investigate the effects of their physicochemical properties on cell morphology, which is an important factor in the promotion or inhibition of angiogenesis. Our findings revealed that the HUEhT-1 cell morphology parameters, particularly the adhesion area and aspect ratio, were significantly influenced by the physicochemical properties of the hydrogel. For the adhesion area, which is the surface area of the substrate covered by cells, significant differences were observed across the hydrogels irradiated for different durations. The hydrogels prepared by 30 and 45 min of irradiation showed the highest average adhesion areas of 4462 and 4373 μm², respectively (**Fig. 3-3a, b**), with no significant difference between them. These values are 60% and 20% larger than those of the hydrogels irradiated for 15 and 60 min, respectively; specifically, their adhesion areas were 2760 and 3626 μm², respectively. Notably, the cell adhesion areas on the hydrogels were lower than those of the cells cultured directly in the dish (4999 μm²). In terms of the aspect ratio, which is a measure of cell elongation and spread on the hydrogel, a steady increase was observed with increasing irradiation time. The lowest aspect ratio of 1.7 was observed in the hydrogel irradiated for 15 min **(Fig. 3-3c)**, and it increased to 2.1, 3.5, and 5.5 (the highest ratio) for the hydrogels irradiated for 30, 45, and 60

min, respectively. These results suggest that the cells spread to a greater extent and become more elongated on the hydrogels prepared with longer irradiation times **(Fig. 3-3)**.

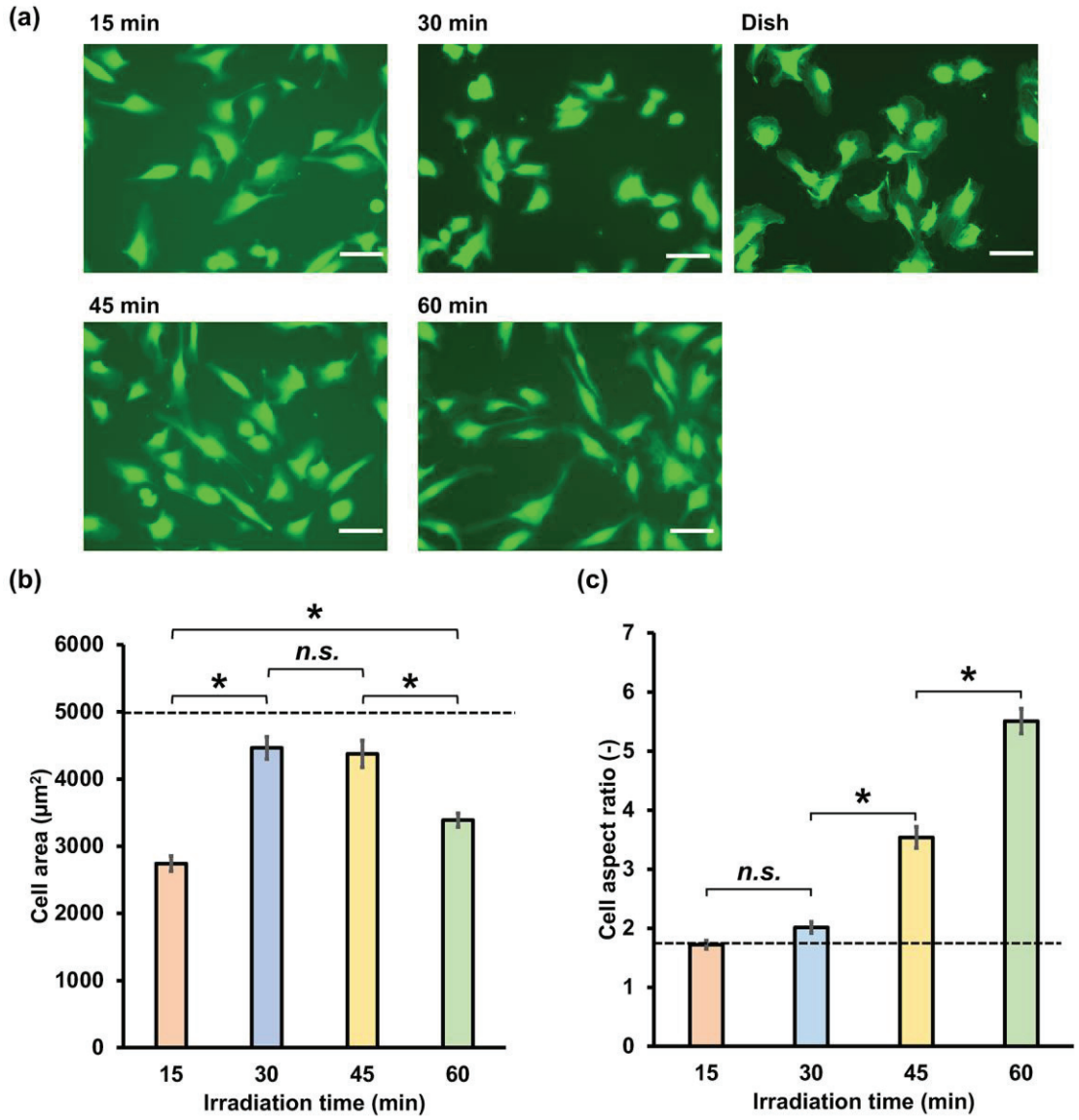

Fig. 3-3 Effect of visible light irradiation time during hydrogel preparation on the HUEhT-1 cell morphology after two days of culture. (a) Fluorescence micrographs of the HUEhT-1 cells on hydrogels stained with Calcein-AM. Scale bars: 100 μm. (b) Adhesion area and (c) aspect ratio of the cells on the hydrogels produced through light irradiation for different durations. Bar: standard error ($n \geq 50$). In (a–c), the dashed lines represent the results of cells cultured in a dish. $^{*}p < 0.05$, *n.s.*: no significant difference ($p > 0.05$), Tukey HSD. Reprinted from (Elvitigala et al., 2024) [48] with permission from Wiley-VCH.

The small adhesion areas of cells on hydrogels with low stiffness are consistent with those observed in our previous studies, wherein HUVECs were circular with a small cell adhesion

area on substrates with low stiffness [47]. In addition to the influence of the stiffness of the ECM, the relationship between the cells and ECM materials can influence the cell behavior. According to previous reports, interactions with low-molecular-weight fragments can induce cell elongation [103]. In our earlier study, the same trend with HUVECs and mouse mammary cells cultured on a composite hydrogel (HA-Ph/Gelatin-Ph) were observed, in which the cells elongated more in a hydrogel with a higher amount of the LMWHA-Ph fragments [104]. Moreover, the interaction between the LMWHA-Ph fragments and HA receptors, such as CD44 and RHAMM, causes the epithelial–mesenchymal transition (EMT), which is the reprogramming of the epithelial cells into mesenchymal ones [112]. A recent study by Jariyal et al. revealed that LMWHA induces EMT in MCF-7 and MDA-MB-231 cells [113]. Therefore, changes in the aspect ratio of the HUEhT-1 cells cultured in hydrogels prepared with increasing irradiation time can be attributed to both the changes in the substrate stiffness and interactions with the LMWHA-Ph fragments generated by SPS-mediated degradation.

Exploring cell adhesion dynamics is crucial for understanding HUEhT-1 network formation. As described above, hydrogels irradiated for 30 and 45 min showed the largest average adhesion areas, indicating increased cell spreading. However, the transition from cell spreading to network formation depends on not only the adhesion area but also the cell aspect ratio and the presence of LMWHA-Ph fragments. The aspect ratio suggests more pronounced cell elongation in hydrogels irradiated for longer times. In particular, although both the 30 and 45 min conditions promoted cell spreading, the presence of more LMWHA-Ph fragments in the 45 min irradiated hydrogels may be critical in facilitating network formation. These fragments, which are known to interact with HA receptors such as CD44, may induce signaling pathways that support not only cell elongation but also the organization of these elongated cells into network-like structures.

3.3 Network-like structure formation

The dependence of the network-like structure formation of HUEhT-1 cells on the visible-light-irradiation time of the hydrogel was investigated to further explore the VECs behavior. The HUEhT-1 cells formed a network-like structure on the HA-Ph/gelatin-Ph hydrogel prepared by 30 min of irradiation **(Fig. 3-4)**. HUEhT-1 cells formed a complete network-like structure within 16 h, as shown in **Fig. 3-4**, which became unstable and disintegrated after 24 h. According to Califano et al., [85] substrate mechanics and matrix chemistry play vital roles in VECs network assembly. The authors reported that soft substrates (0.2–1 kPa) do not promote network formation of VECs, but stiffer substrates (2.5–10 kPa) do [85]. Consistent with a previous study in which the stiffness was in the same range, the hydrogel prepared with 45 min of light irradiation presented a more robust network-like structure of HUEhT-1 cells than the soft hydrogels obtained by 15 and 60 min of light irradiation **(Fig. 3-4)**. Interestingly, the hydrogel obtained after 60 min of light irradiation also supported some network-like structure formation of the HUEhT-1 cells, although it was less distinct than that obtained in the hydrogel formed through 45 min of irradiation **(Fig. 3-4)**. These results indicate that the combined effect of the mechanical properties of the hydrogel and the amount of LMWHA-Ph fragments generated through the degradation of HA-Ph by SPS in the hydrogel irradiated for 45 min caused the formation of a network-like structure of the HUEhT-1 cells. The greater amount of HA-Ph fragments generated during 45 min of irradiation might induce the formation of a more robust network-like structure of the HUEhT-1 cells compared with that achieved with the hydrogel irradiated for 30 min, although both the hydrogels had nearly the same stiffness. In our study, network formation was optimized at a hydrogel stiffness of approximately 2.2 kPa, filling a crucial gap in the understanding of the effects of matrix stiffness, as outlined by Frye et al., [16] Alderfer et al., [34] Ingber et al., [35] and Hanjaya-Putra et al., [36]. Collectively, these studies span a range of stiffness values and highlight the importance of mechanical cues in vascular

and lymphatic morphogenesis, from promoting cell elongation and sprouting to facilitating attachment and spreading. Considering the stiffness values reported by Hanjaya-Putra et al., [36] which highlight the influence of substrate mechanics on endothelial progenitor cell tubulogenesis across a range of stiffness from soft (10 Pa) to rigid (650 Pa) matrices, our optimal stiffness of ~2.2 kPa represent an advance beyond this range.

Similarly, Alderfer et al. [35] reported that stiffness values of approximately 30 Pa were optimal for lymphatic tube formation, which would underscore the importance of this stiffness

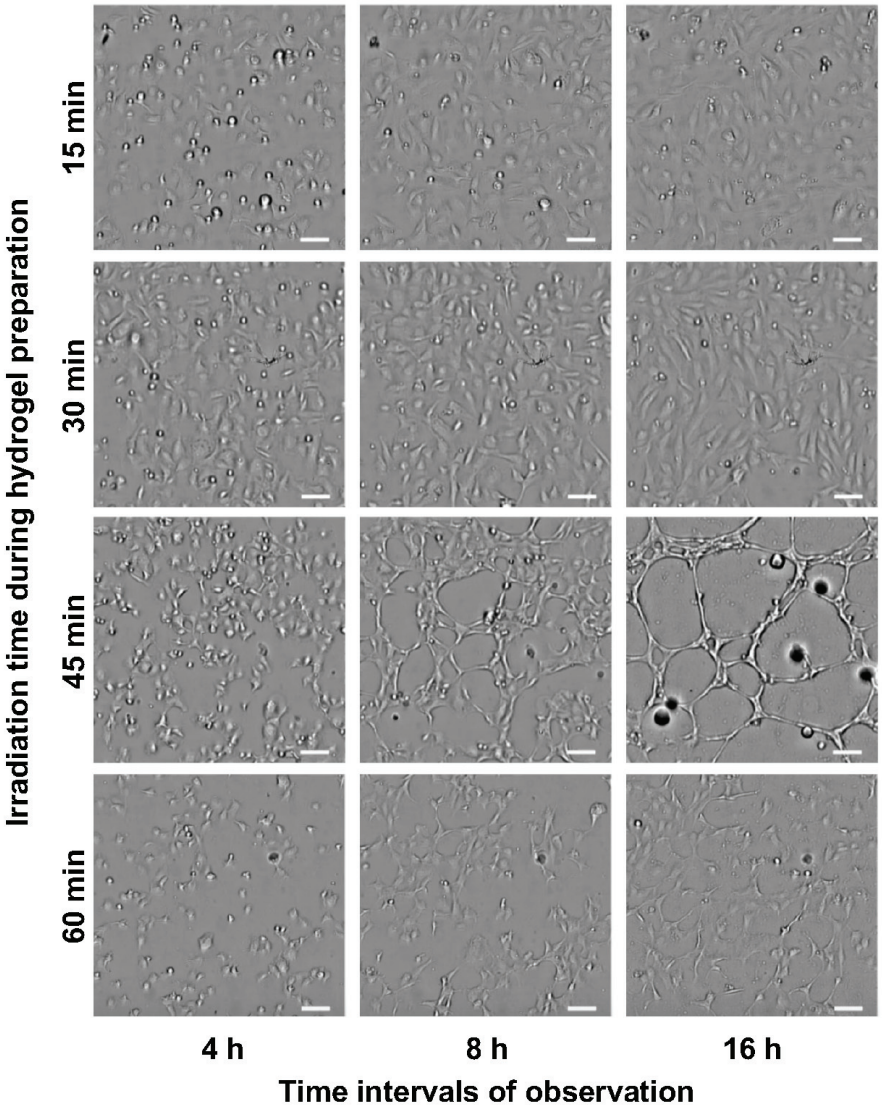

Fig. 3-4 Effect of the visible-light-irradiation time on HUEhT-1 cell network formation on HA-Ph/Gelatin-Ph hydrogels obtained through 15 to 60 min of visible-light irradiation. Timelapse images were captured at 4 h intervals. Scale bar: 100 µm. Reprinted from (Elvitigala et al., 2024) [48] with permission from Wiley-VCH.

range in both vascular and lymphatic endothelial biology and provide a comprehensive understanding of the role of the mechanical environment in both hemangiogenesis and lymph angiogenesis. A possible mechanism for the network formation of the HUEhT-1 cells on the hydrogel obtained with 45 min of light irradiation could be explained by the interactions of the LMWHA-Ph fragments in the hydrogel with CD44 and RHAMM receptors, which promote network-like structure formation, as reported earlier [80,81]. These receptors induce the formation of network-like structures of the HUEhT-1 cells through distinct pathways. The interaction between HA with CD44 could activate γ-adduct formation, while that between HA and RHAMM induces AP-1 binding to the RHAMM promoter, thereby inducing the network-like structure formation of the cells [82,83].

3.4 Role of F-actin and CD44

F-actin formation during network formation is crucial for the establishment and maintenance of the network structure. A previous study by Choi et al. reported the importance of F-actin expression and assembly in promoting VEC migration and angiogenesis [117]. Other studies have also demonstrated that cytoskeletal reorganization, which is the primary step in angiogenesis, is critical for the migration of HUVECs. Furthermore, the interaction of ECM materials with relevant cell surface receptors, such as CD44 and RHAMM, initiates intracellular signaling pathways, leading to F-actin formation,[118] and these events ultimately promote or inhibit angiogenesis. Therefore, the hydrogel-stiffness-dependent and HA-Ph-CD44 interaction-related F-actin organization in the HUEhT-1 cells was examined by staining the actin stress fibers in the cells (**Fig. 3-5 and 3-6**). The cells cultured on the hydrogel obtained with 60 min of light irradiation showed the lowest amount of stress fibers among the different hydrogels. However, the cells cultured on the hydrogel irradiated for 15 min showed the highest

integrated density of stress fibers, whereas those cultured on the hydrogels irradiated for 30 and 45 min showed no significant difference in actin fiber formation.

The cells cultured in the dish showed the highest integrated density, confirming the formation of more stress fibers. The stiffness-dependent F-actin formation could be explained based on mechanotransduction. HA is known to exert different modulatory effects on CD44

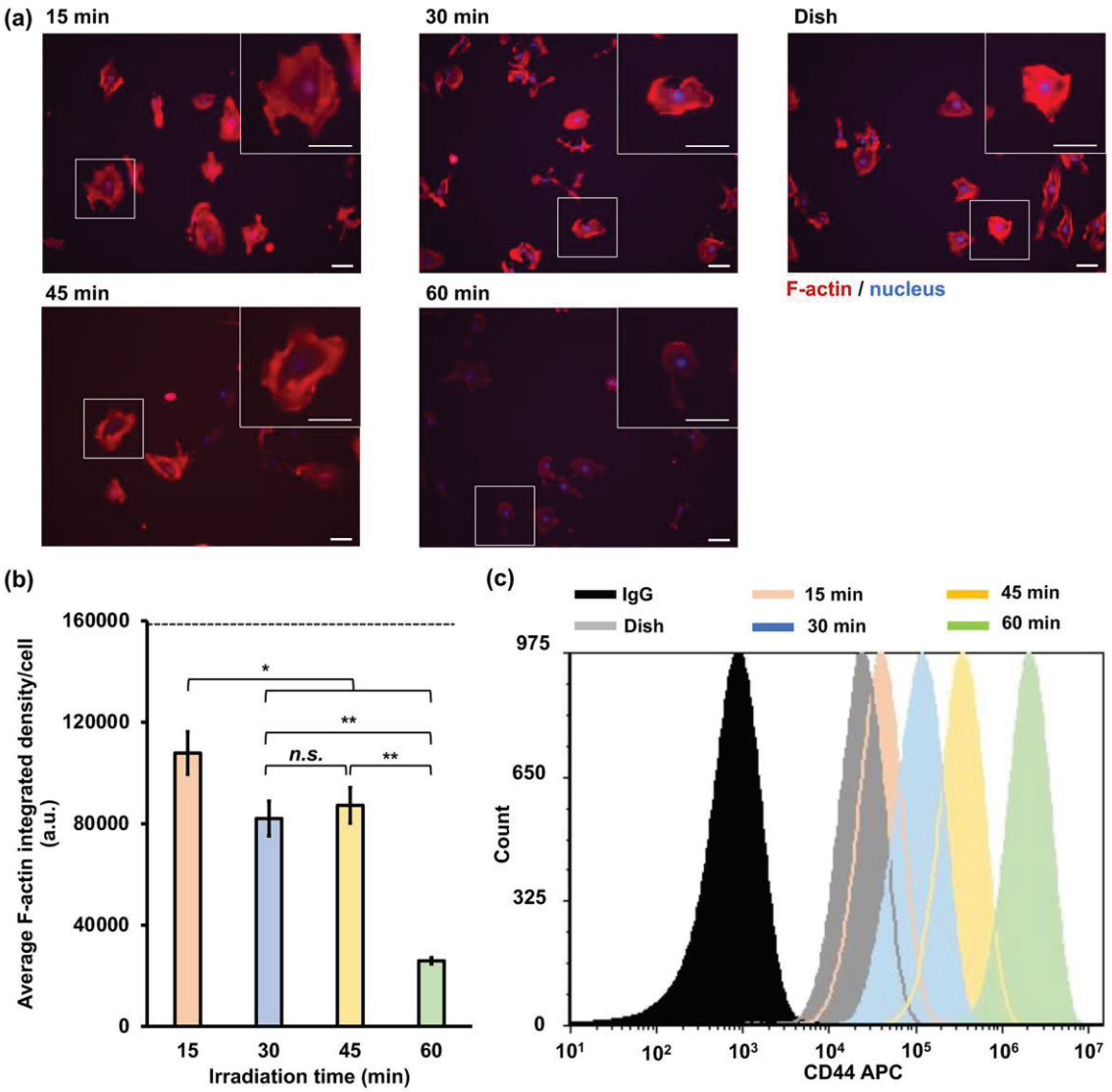

Fig. 3-5 The F-actin formation in HUEhT-1 cells cultured on HA-Ph/Gelatin-Ph hydrogels obtained through irradiation for 15, 30, 45, and 60 min. (a) Fluorescence micrographs obtained by fluorescence microscope and (b) integrated density of the F-actin in HUEhT-1 cells cultured in a dish (dashed line) and on different hydrogels. (c) Flow cytometry histogram of allophycocyanin (APC) in cells cultured on each hydrogel and well plate. Scale bars: 200 μm. Bar: standard error (n > 45 cells). *p < 0.05, **p < 0.005, *n.s.*: no significant difference (p > 0.05), Tukey HSD. Reprinted from (Elvitigala et al., 2024) [48] with permission from Wiley-VCH.

receptors according to its molecular weight. The interaction of LMWHA-Ph with CD44 receptors has been recognized to play a significant role in cell adhesion and intracellular signaling pathways. Specifically, a high F-actin content enhances cell adhesion to the hydrogel, potentially leading to a less conducive environment for network formation. On the other hand, flow cytometry results showed the opposite trend in F-actin formation with increasing irradiation time, as shown in **Fig. 3-5c**.

As mentioned above, when the irradiation time was increased, more LMWHA-Ph fragments were generated, which may have enhanced CD44 expression. This increase in CD44 expression by LMWHA-Ph fragments initiates CD44-mediated intracellular signaling pathways related to F-actin formation. Moreover, Kim et al. suggested that the interaction between LMWHA and CD44 receptors enhances the activation of CD44 receptors and eventually facilitates network formation [26]. Intriguingly, while F-actin formation was notably higher in hydrogels prepared by 15 and 30 min of irradiation, a robust cell network was formed in the hydrogel prepared by 45 min of irradiation. These contradictory results can be attributed to the intricate relationships among F-actin expression, CD44 expression, and substrate stiffness.

To further elucidate the effect of the interaction between HA-Ph and CD44 on F-actin formation and CD44 expression, additional experiments were conducted **(Fig. 3-6)**. Cells were cultured in a cell culture dish treated with HMWHA-Ph or LMWHA-Ph using the growth medium. Compared with the cells cultured in an untreated dish, the cells in the LMWHA-Ph-treated dish showed less F-actin formation, whereas the cells cultured in the dish treated with HMWHA-Ph showed more F-actin formation. This observation suggests that LMWHA-Ph may affect cell adhesion or spreading, possibly because of its smaller size and possible differences in interactions with cell surface receptors compared with HMWHA-Ph.

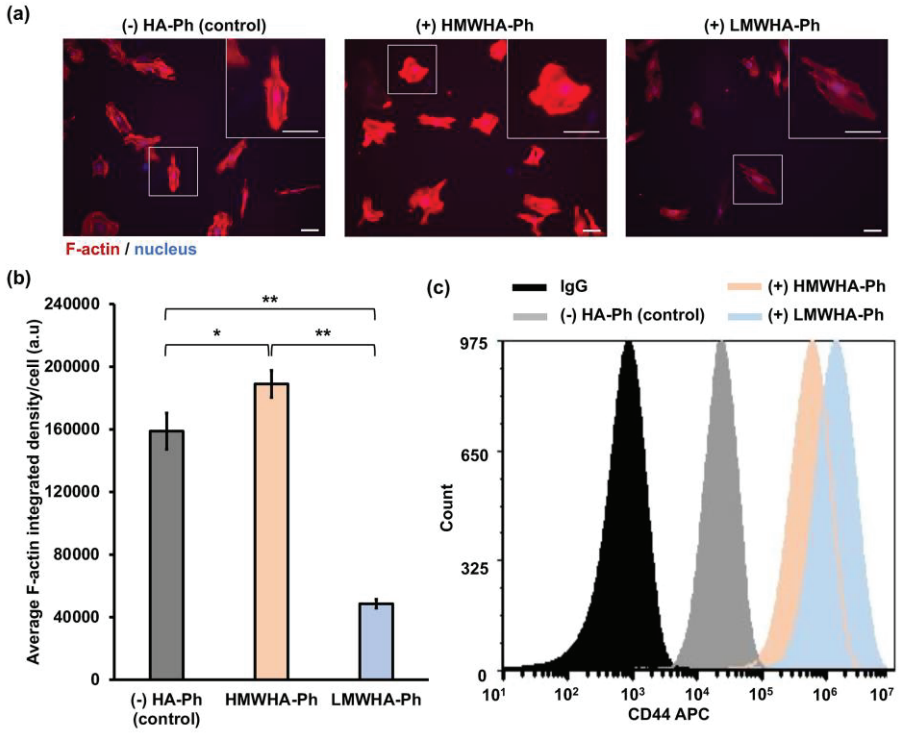

Fig. 3-6 (a) Fluorescence observation of F-actin formation in HUEhT-1 cells cultured on a well plate treated with HMWHA-Ph and LMWHA-Ph. Cells cultured in an untreated dish (without HA-Ph treatment) were used as control. Scale bar: 100 μm. (b) Integrated density of F-actin under each condition. (c) Flow cytometry histogram of the APC in cells cultured in the presence and absence of different HA-Ph fragments. Bar: standard error (n = 45 cells). *p < 0.05, **p < 0.005, Tukey HSD. Reprinted from (Elvitigala et al., 2024) [48] with permission Wiley-VCH.

Further, the higher integrated density of F-actin for the cells in the dish treated with HMWHA-Ph compared with that in the untreated dish could be the result of improved cell adhesion or spreading owing to the interaction of the larger HMWHA-Ph molecules with cell surface receptors, which may influence cell behavior and lead to a more robust F-actin cytoskeleton. Contrarily, flow cytometry results revealed a different trend. Specifically, when LMWHA-Ph interacted with the HUEhT-1 cells, CD44 expression levels increased. This interaction led lower F-actin formation, especially when compared to the effects of HMWHA-Ph.

To elucidate the mechanism by which LMWHA-Ph affects F-actin formation via CD44 receptors, additional experiments were conducted (**Fig. 3-7**). The CD44 receptor was blocked

with an anti-CD44 antibody, and the cells were cultured in a cell culture dish with an LMWHA-Ph-treated medium.

The results provided critical insights into the role of CD44 in mediating the effects of LMWHA-Ph on the cell behavior. Specifically, the cells cultured with LMWHA-Ph, under CD44-blocking conditions, showed no significant differences from the control in terms of their aspect ratio and the integrated density of F-actin. This result suggests that CD44 blockade effectively mitigated the LMWHA-Ph-induced changes in cell elongation and F-actin

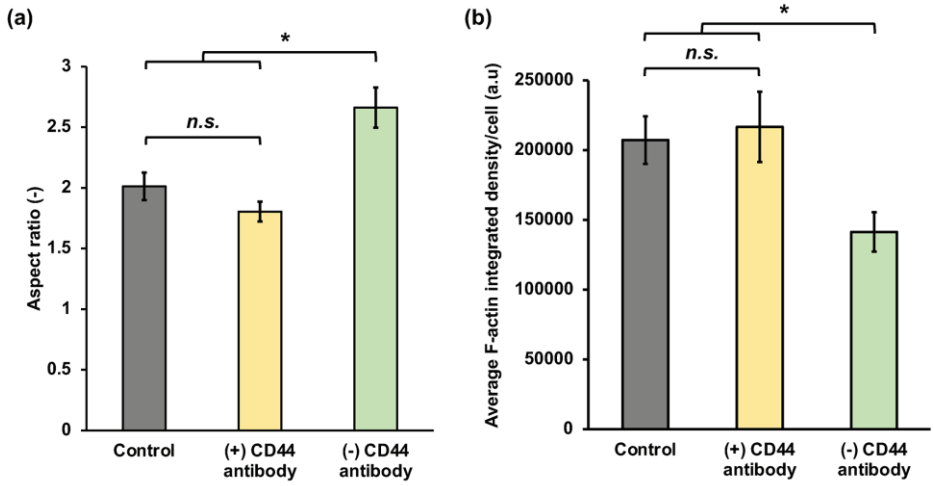

Fig. 3-7 Effect of the CD44 receptor and LMWHA-Ph interaction on the (a) aspect ratio and (b) F-actin formation in HUEhT-1 cells cultured in a dish using a medium containing LMWHA-Ph with CD44 receptors blocked and not blocked. Bar: standard error ($n > 20$ cells). *$p < 0.05$, *n.s.*: no significant difference ($p > 0.05$), Tukey HSD. Reprinted from (Elvitigala et al., 2024) [48] with permission from Wiley-VCH.

rearrangement observed in the absence of blockade. In contrast, cells cultured with LMWHA-Ph without CD44 receptor blocking exhibited a large aspect ratio and decreased integrated density of F-actin. Considered together, these results strongly suggest that CD44 plays a key role in mediating the effects of LMWHA-Ph on F-actin rearrangement and cell shape changes. The blockade of the CD44 receptors effectively negated the effect of LMWHA-Ph, providing substantial evidence that LMWHA-Ph-induced changes were regulated, at least in part, through interactions with the CD44 receptors.

3.5 Role of RhoA and β-actin on F-actin formation

The formation of F-actin fibers plays a crucial role in HUEhT-1 cell network formation, especially through interactions between LMWHA-Ph fragments and CD44 receptors. As discussed in previous sections, the interaction of LMWHA-Ph with CD44 receptors may result in the modulation of the signaling pathways that are critical for the production of F-actin fibers. RhoA stimulates the formation of stress fibers, and β-actin is one of the primary proteins involved in the regeneration of F-actin fibers. Therefore, the irradiation-time-dependent RhoA and β-actin gene expression levels are discussed in this section. According to the findings shown in **Fig. 3-8**, compared with the gene expression of the cells cultured in untreated cell culture dishes, the cells cultured on the hydrogel prepared with 30 min of light irradiation showed the highest levels of RhoA and β-actin gene expression of 1.25 and 1.36, respectively.

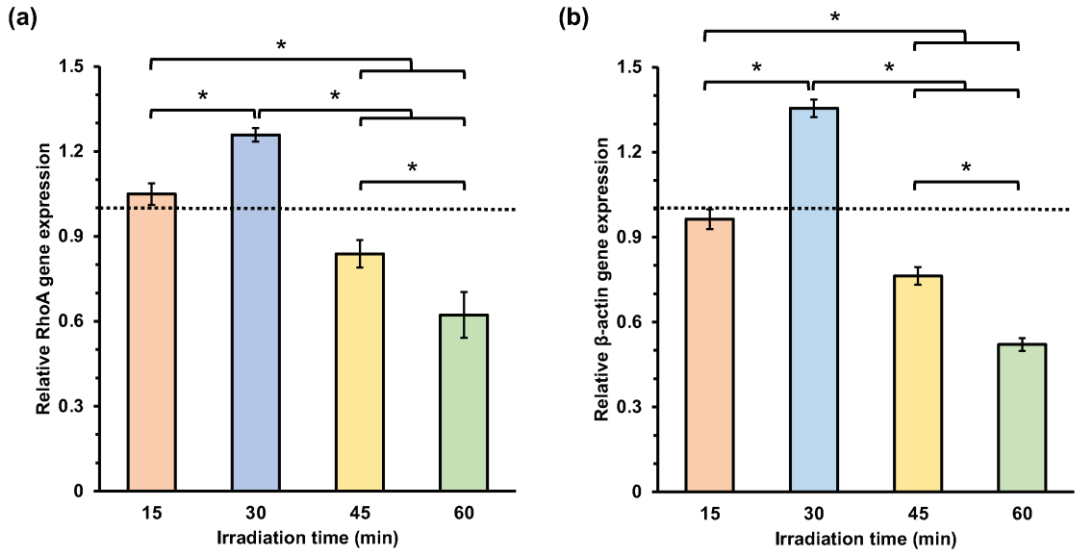

Fig. 3-8 Effect of light-irradiation time on relative (a) RhoA expression and (b) β-actin expression of HUEhT-1 cells cultured on HA-Ph/Gelatin-Ph hydrogels obtained through irradiation for 15, 30, 45, and 60 min with respect to cells cultured in a dish (dashed line). Bar: standard error ($n = 2$). *$p < 0.05$, *n.s.*: no significant difference ($p > 0.05$), Tukey HSD. Reprinted from (Elvitigala et al., 2024) [48] with permission from Wiley-VCH.

The hydrogels obtained through 45 and 60 min of irradiation showed the lowest expression of both genes, as shown in **Fig. 3-8**. Notably, different irradiation times induced changes in the expression of genes related to F-actin formation. Thus, the intricate effects of light irradiation on LMWHA-Ph fragmentation and CD44 receptor interactions play a critical role in modulating F-actin dynamics. Future research should further optimize these parameters for targeted outcomes in specific signaling pathways related to network-like structure formation of cells.

4. Conclusion

In this chapter the role of hydrogel constitution, with particular emphasis on the effect of photocrosslinking, and the effects of the mechanical and chemical properties of the hydrogel on HUEhT-1 cell behavior were investigated. Unlike the previous chapter, which utilized H_2O_2-mediated crosslinking, this chapter demonstrated the ability to achieve precise control over hydrogel properties using light irradiation. By tuning the visible-light-irradiation time during hydrogel preparation, variations in HA-Ph degradation rates and the associated hydrogel stiffness were detected. HUEhT-1 cells exhibited distinct behaviors depending on the level of HA-Ph degradation and hydrogel stiffness. The HUEhT-1 cells cultured in the hydrogel with intermediate stiffness prepared through prolonged light irradiation exhibited optimal elongation and network formation, suggesting an interplay between the degree of HA-Ph degradation and substrate stiffness.

Some portion of this thesis, including text and figures, have been previously published in the journal article “Photo-Tuning of Hyaluronic Acid-Based Hydrogel Properties to Control Network Formation in Human Vascular Endothelial Cells” by Elvitigala et al., published in *Advanced Healthcare Materials*, 2024, 13, 2303787 (Reference No. 48). These sections are reproduced here with permission from the Wiley-VCH (Weinheim, Germany).

Chapter IV

Hydrogels with Ultrasound-Treated Hyaluronic Acid Regulate CD44-Mediated Angiogenic Potential of Human Vascular Endothelial Cells In Vitro

1. Introduction

Chapters II and III revealed that the interplay between HA degradation into low molecular weight fragments and hydrogel stiffness enhances HUVEC network formation, with CD44 receptors playing a key role in modulating cell behavior. With this foundational knowledge, Chapter IV explores the application of ultrasound-treated HA-Ph to regulate the CD44-mediated angiogenic potential of HUVECs. This chapter examines how HA-Ph degradation by ultrasound affects its interaction with CD44, influencing vascular endothelial cells (VECs) behavior.

HA, an endogenous glycosaminoglycan, is a crucial component of various tissues and is present in the ECM. It plays an important role in various physiological processes, such as angiogenesis, tissue regeneration, and wound healing. In these physiological processes, the interactions of HA with the cell surface receptors CD44 and RHAMM are critical in modulating cellular functions such as adhesion, proliferation, and migration. The ability of HA to interact with cells depends on its molecular weight [119]. HA can be classified into two main groups: high-molecular-weight HA (>500 kDa, HMWHA) and low-molecular-weight HA (10–500 kDa, LMWHA) [120]. LMWHA interacts distinctively with cell surface receptors such as CD44 and RHAMM in various cell types and induces unique intracellular signaling pathways [119]. The engagement of CD44 with LMWHA triggers a cascade of intracellular signaling and upregulates the synthesis of hyaluronidase, an enzyme responsible for degrading HA, resulting in the remodeling of the ECM [121].

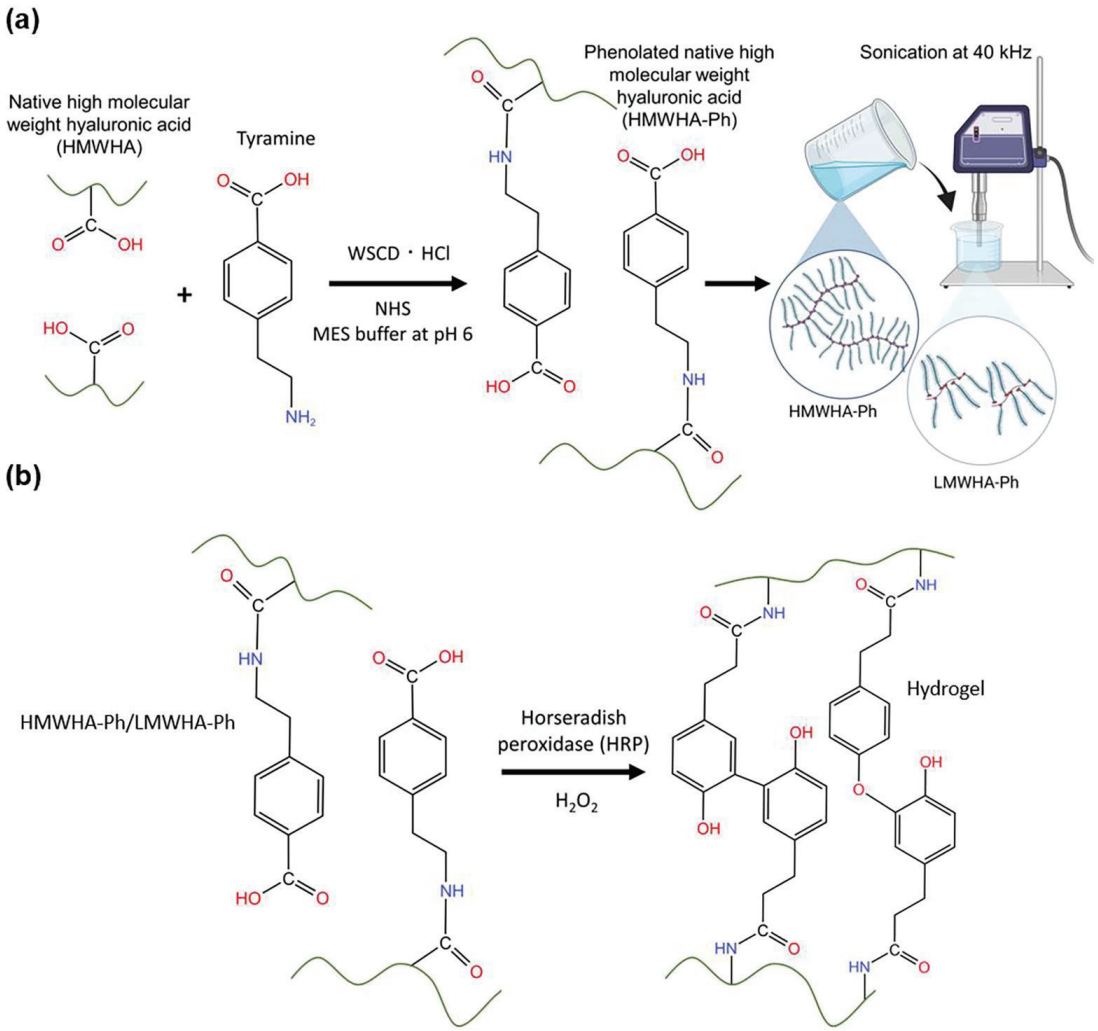

Fig. 4-1 Schematic illustrations of (a) HA-Ph synthesis and degradation by sonication of HA-Ph solution to obtain the low molecular weight HA-Ph. (b) Hydrogel preparation method using HRP-mediated crosslinking of phenolated HMWHA-Ph or LMWHA-Ph in the presence of H_2O_2. Reprinted from (Elvitigala et al. 2024) [49] with permission from MDPI.

This study aimed to develop hydrogels incorporating LMWHA-Ph obtained by controlled sonication that allow VECs to form capillary-like networks through a process similar to angiogenesis in vivo, which is related to the expression of cell surface CD44, using HUVECs in vitro. HUVECs have been widely used as model cells in angiogenesis studies to understand the behavior of VECs. Hydrogels, which provide a three-dimensional matrix, are critical for

mimicking the natural cellular environment, allowing a more accurate assessment of VECs behavior involving HA-regulated network formation.

To obtain hydrogels composed of LMWHA, HMWHA possessing phenol moieties (HMWHA-Ph) was synthesized and then degraded the polymer by sonication to obtain LMWHA-Ph (**Fig. 4-1a**). I applied sonication to degrade HMWHA-Ph instead of enzymatic degradation using hyaluronidase or thermal degradation, which have been applied for the same purpose, owing to the difficulty of precise control of molecular weight [30]. Degradation by sonication allows finer control of the molecular weight of HA by adjusting the ultrasound frequency, intensity, and duration of exposure [122].

Hydrogels were obtained through HRP-mediated crosslinking of the phenol moieties introduced into HA (**Fig. 4-1b**). Phenolated gelatin (gelatin-Ph) was also present in the hydrogels to support the adhesion and elongation of HUVECs, which was not accomplished via HA-Ph alone. The effectiveness of compositing gelatin-Ph with a less cell-adhesive Polymer-Ph to obtain hydrogels with superior cell adhesion and proliferation has been reported [50,123]. Several studies have demonstrated the potential of composite or hybrid hydrogels containing both HA and gelatin to mimic the ECM in the body [27,124,125], including their interaction with CD44 receptors [27].

The hydrogels obtained in this study will provide valuable insights into the mechanisms of angiogenesis and the role of ECM components in regulating this complex process and will advance tissue engineering and drug discovery involving VECs. I hypothesize that hydrogels composed of sonication-degraded LMWHA-Ph will enhance the formation of capillary-like networks by HUVECs in vitro, potentially through upregulation of CD44 receptor expression and subsequent PI3K-mediated signaling pathways.

2. Materials and methods

2.1 Materials

HA-Ph (3.5-Ph groups per 100 repeating units) and Gelatin-Ph (4.1×10^{-4} mol-Ph/g) were synthesized according to the previous protocols, and the phenol contents were determined based on the tyramine standard curve [77,93]. Sodium hyaluronate (average molecular weight: 550 kDa, HA-LQ) was purchased from Kewpie (Tokyo, Japan) (molecular weight was measured as per the protocol described in the molecular weight measurement section). Tyramine hydrochloride, 3-(4-hydroxyphenyl)propionic acid, gelatin type B from bovine skin, and phalloidin-iFluor 488 (ab176759) were purchased from Chem-Impex (IL, USA), Tokyo Chemical Industry (Tokyo, Japan), Sigma-Aldrich (St. Louis, MO, USA), and Abcam (Cambridge, UK), respectively. N-Hydroxysulfoccinimide, 3-ethylcarbodiimide hydrochloride, 4% paraformaldehyde, hyaluronidase, catalase from ovine, HRP, 31 w/w% hydrogen peroxide (H_2O_2) aqueous solution, and phosphate-buffered saline (PBS) containing 4 w/w% paraformaldehyde were purchased from FUJIFILM Wako Pure Chemical (Osaka, Japan).

2.2 Cell culture

The HUEhT-1 (HUVECs modified with pIRES-hTERT-hygr) cell line was purchased from the RIKEN Cell Bank (Ibaraki, Japan). Cells were cultured in a humidified incubator with 5% CO_2 at 37°C using MCDB107 (Peptide Institute, Osaka, Japan) base medium supplemented with 10 ng/mL endothelial growth factor, 10 ng/mL basic fibroblast growth factor (Sigma-Aldrich), and 10 v/v% fetal bovine serum (FBS).

2.3 HA-Ph degradation

PBS containing 2 w/v% HA-Ph (HA-Ph-0) was sonicated using an ultrasonic cleaner (RoHS, China) operating at 40 kHz and 240 W at 50°C for 5 min (HA-Ph-5), 10 min (HA-Ph-10), 30 min (HA-Ph-30), and 60 min (HA-Ph-60).

2.4 Molecular weight measurement

The polymer molecular weights were determined via high-performance liquid chromatography (HPLC) with respect to pullulan standards using an intensity–time curve. The eluent flow rate in the column (LC-20AD; Shimadzu, Kyoto, Japan) was set to 0.7 mL/min at 25°C.

2.5 Rheological measurement

The viscoelastic properties of solutions containing 2 w/v% HA-Phs obtained after different sonication times were determined using a parallel plate rheometer (HAAKE MARS III, Thermo Fisher Scientific, MA, USA) at 1% constant shear strain and 1 mm gap between plates at 25°C.

2.6 Hydrogel preparation and gelation time

Hydrogels were prepared from PBS containing 2 w/v% and 1.5 w/v% HA-Ph-0 or 2 w/v% HA-Ph-30 and 10 U/mL HRP by exposure to 16 ppm air containing H_2O_2 for 30 min. A composite hydrogel (HA-Ph/gelatin-Ph) was prepared by mixing 0.1 w/v% gelatin-Ph with this solution. The gelation time was determined by adding 1 mL of the above polymer solutions into a 12-well plate and exposing it to 16 ppm air containing H_2O_2 while stirring with a magnetic bar. The gelation time was determined based on the swelling of the polymer solution.

2.7 Mechanical property measurement

Hydrogels were prepared by exposing air containing 16 ppm H_2O_2 to PBS containing 0.1 w/v% gelatin-Ph, 2 w/v% HA-Ph-0 to HA-Ph-60, and 10 U/mL HRP in a 6-well plate (1 mL/well) for 30 min (diameter 35 mm and height 3 mm). The stiffness of these hydrogels was measured using a material tester (EZ-SX, Shimadzu, Kyoto, Japan) at a compression speed of 6 mm/s with an 8 mm probe. Young's modulus was determined using a linear compression strain.

2.8 Diphenol formation

PBS containing 2 w/v% HA-Ph-0 to HA-Ph-60 and 10 U/mL HRP was poured into a 96-well plate (200 μL/well) and exposed to air containing 16 ppm H_2O_2. Diphenol bond formation was analyzed using a fluorescence plate reader (Molecular Devices, San Jose, CA, USA). Fluorescence emission intensity at 420 nm was measured at an excitation wavelength of 310 nm.

2.9 Impact of sonicated HA-Ph solutions on cellular dynamics

***Cell migration*:** HUEhT-1 cells were cultured in 6-well plates until they reached confluence. A scratch was created using a pipette tip. After scratching, the growth medium was replenished with a growth medium containing 0.1 w/v% HA-Ph-0 to HA-Ph-60. Cell migration speed, defined as the scratch area covered by the cells over time, was monitored using a cell culture monitoring system (CM20, Olympus, Tokyo, Japan).

***Cell proliferation*:** HUEhT-1 cell proliferation was determined via cell doubling time. Cells were cultured in a 24-well plate at 5×10^2 cells/cm^2 using MCDB107 growth medium containing 0.1 w/v% HA-Ph-0 to HA-Ph-60 and monitored using the cell culture monitoring system to calculate the doubling time.

2.10 Cell adhesion and morphology on the hydrogel

Hydrogels were prepared from solutions containing 10 U/mL HRP, 0.1 w/v% Gelatin-Ph, and 1.5 or 2 w/v% HA-Ph-0 or 2 w/v% HA-Ph-30 in 6-well plates following the protocol outlined in section hydrogel preparation, and cells at 5×10^3 cells/cm^2 were seeded on the hydrogels. Before cell seeding, the residual H_2O_2 on the hydrogels was degraded by overnight incubation in MCDB107 medium containing 1 mg/mL catalase. After 48 h of culture, F-actin and nuclei were stained with the phalloidin iFluor488 reagent and CellStain DAPI (Dojindo, Kumamoto, Japan), respectively. These stains facilitated the analysis of cell morphological parameters, specifically cell area and aspect ratio (the ratio between cell length and width). The morphological parameters were analyzed based on fluorescence images captured using a fluorescence microscope (Model BZ-9000, Keyence, Osaka, Japan) and ImageJ software (Version 1.53f, NIH, Bethesda, MD, USA).

2.11 Network formation

HUEhT-1 cell network formation on the prepared hydrogels was analyzed as described in the hydrogel preparation section. Then, CD44 receptor-blocked and non-blocked HUEhT-1 cells at 4×10^4 cells/cm^2 were cultured on the hydrogels using MCDB107 medium supplemented with 2 v/v% FBS, 10 ng/mL endothelial growth factor, and 10 ng/mL basic fibroblast growth factor for 16 h. Before cell seeding, the remaining H_2O_2 was degraded according to the method described in the cell adhesion and morphology on the hydrogel section. A fluorescence microscope and cell culture monitoring system were used to analyze network formation.

2.12 Flow cytometry

Cells were carefully detached from the hydrogel via treatment with MCDB107 medium containing 0.1 w/v% hyaluronidase (FUJIFILM Wako Pure Chemicals) after culturing for 3 h. Next, the cells were incubated with FCblock (BD Bioscience, CA, USA) reagent to block non-specific binding sites. Subsequently, cells were washed with PBS and incubated with an APC-conjugated mouse CD44 antibody for 30 min at 4°C. After 30 min of incubation, the cells were washed twice with PBS and analyzed using a BD Accuri C6 flow cytometer (BD Biosciences).

2.13 Real-time quantitative polymerase chain reaction (PCR) analysis for PI3K and hypoxia-inducible factor (HIF)-1 expression

HUEhT-1 cells were collected from the hydrogel as described in the flow cytometry section. For comparison, cells cultured in the dish were trypsinized. Total RNA was isolated from cells using an RNA isolation kit (Takara, Shiga, Japan) according to the manufacturer's protocol. Reverse transcription was performed using the PrimerScript RT Master Mix reagent kit (Takara) according to the manufacturer's protocol. PI3K and HIF-1 gene expression was quantified via real-time polymerase chain reaction (RT-PCR) using the TB Green Master Kit (Takara) normalized to the expression of GAPDH gene with the delta Ct method.

2.14 Statistical analysis

Statistical analyses were performed using Microsoft Excel 2019 version 1808 (Microsoft Corp., Redmond, WA, USA). A one-way analysis of variance was used to determine statistical differences between experimental conditions. Significant differences were identified using Tukey's honestly significant difference (HSD) and the post-hoc t-test; $p < 0.05$ was considered statistically different.

3. Results and discussion

3.1 Viscoelastic properties, molecular weight, and hydrogel characterization

The possibility of HA-Ph degradation by sonication was evaluated by measuring the change in viscosity of the sonicated HA-Ph solutions and the molecular weight of HA-Ph in the solutions. As shown in **Fig. 4-2a** and **4-2b**, the time-dependent degradation of HA-Ph was indicated by the decrease in the viscosity of the solutions with increasing sonication time; 30 and 60 min of sonication resulted in a 50% and 75% reduction in viscosity, respectively, compared with that of the non-sonicated solution. The average molecular weight of HA-Ph in the sonicated solutions, determined via HPLC analysis **(Fig. 4-2b)**, decreased from 510 kDa (HA-Ph in the non-sonicated solution) to 198 and 159 kDa after 30 and 60 min of sonication, respectively. These results demonstrate that HA-Ph is degradable by sonication, similar to unmodified HA (H. Chen, Qin, & Hu, 2019). Ultrasound treatment causes HA chains to break into shorter fragments, mainly through the breakage of glycosidic bonds [122].

The phenol moieties were introduced to obtain hydrogels through HRP-mediated oxidative crosslinking. Phenols can be oxidized by sonication [37,126]. Therefore, I analyzed the remaining unoxidized phenol moieties, HA-Phs, in the sonicated solutions by measuring diphenol formation through HRP-mediated crosslinking. I found that there was no significant decrease in the fluorescence emission of diphenol at 420 nm for the HA-Ph solutions sonicated for 5–30 min, whereas 60 min of sonication showed a slight decrease in the fluorescence emission compared to that detected for the non-sonicated HA-Ph solution. This result indicates that sonication causes the oxidation of the phenolic moieties of HA-Ph, but the degree of oxidation is not as high with treatments lasting less than 60 min under the conditions applied in this study (**Fig. 4-2c)**.

Next, I evaluated the gelation time and mechanical properties of the hydrogels formed from the solutions obtained through HRP-mediated crosslinking, which are affected by the

molecular weight of the polymers [127] and density of cross-linkable phenol moieties [77,128]. These are crucial parameters for hydrogel sheet fabrication in the in vitro cell culture studies.

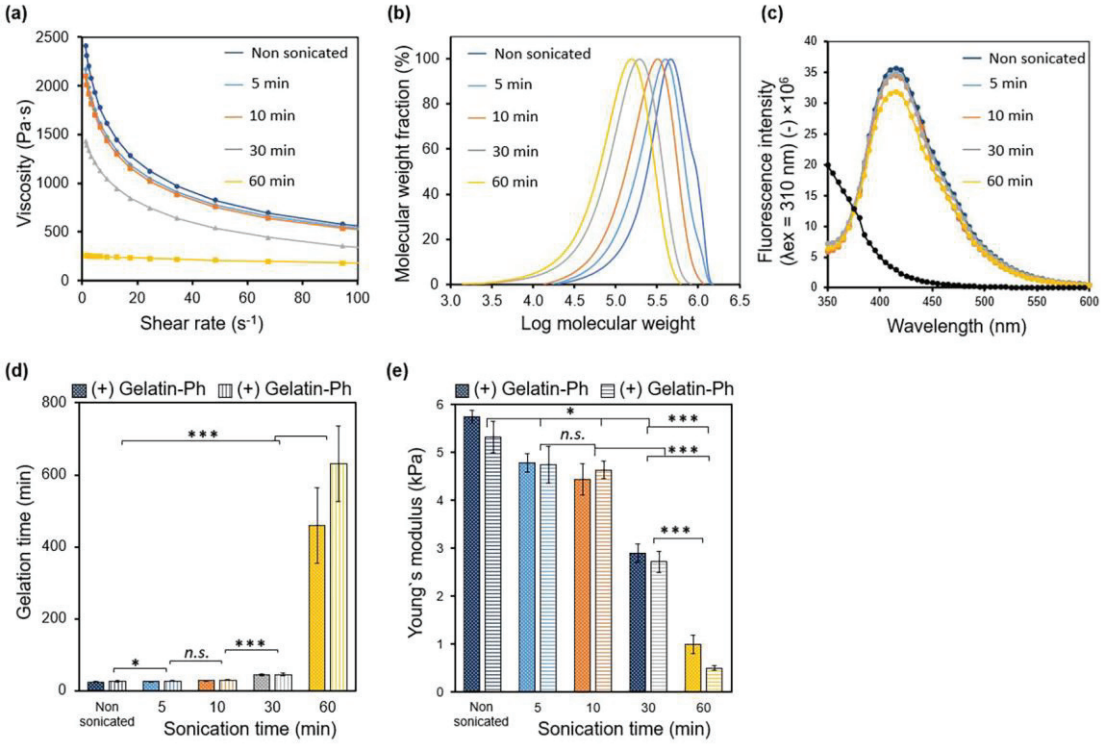

Fig. 4-2 Effect of sonication time on the (a) viscosity of HA-Ph solution and (b) molecular weight of HA-Ph. The stability of phenol groups with sonication time represents the fluorescence emission of (c) diphenol bond at excitation at 310 nm. The effect of sonication time on the mechanical properties of HA-Ph hydrogels with and without Gelatin-Ph is represented as (d) gelatin time and (e) Young's modulus calculated based on the stress–strain curve at 1% to 10% strain. Error bars represent the standard deviation (n = 5) for Young's modulus and (n = 3) for gelation time. $^{*}p < 0.05$, $^{***}p < 0.01$, *n.s.*: no significant difference ($p > 0.05$) Tukey's HSD. Reprinted from (Elvitigala et al. 2024) [49] with permission from MDPI.

The gelation time increased significantly with the sonication time. A longer average gelation time of 10 min was obtained with 60 min-sonicated HA-Ph solution, which was nearly 10 times higher than that for all the other sonication times **(Fig. 4-2d)** ($p < 0.05$). The hydrogel stiffness (as measured by Young's modulus) decreased with increasing sonication time (**Fig. 4-2e**). The hydrogels obtained from the HA-Ph solutions sonicated for 5 and 10 min exhibited a negligible change in stiffness ($p = 0.4$), whereas those from the solutions sonicated for 30 and 60 min

decreased Young's modulus to 51% and 90%, respectively, compared to that of the hydrogel obtained from the non-sonicated HA-Ph solution ($p < 0.05$). These results demonstrate that the hydrogelation time and mechanical properties of the hydrogels obtained from sonicated HA-Ph solutions can be controlled by varying the sonication time.

The effect of adding 0.1 w/v% gelatin-Ph to the HA-Ph solutions on the gelation time and mechanical properties of the hydrogels also evaluated because the incorporation of gelatin-Ph is necessary for cell adhesion and growth on HA-Ph hydrogels [129]. As shown in **Fig. 4-2d, e**, the addition had a negligible effect on the gelation time and hydrogel stiffness within 30 min of sonication. This result indicates that the hydrogelation rate and mechanical properties were mainly due to HA-Ph at 0.1 w/v% gelatin-Ph under these conditions.

3.2 Influence of sonicated HA-Ph solutions on cell migration and proliferation

Next, low molecular weight HA fragments enhance VECs migration [130,131] and proliferation [132]. Therefore, I evaluated whether HA-Ph degraded by sonication can promote VECs migration and proliferation, similar to unmodified HA. As shown in **Fig. 4-3**, HUEhT-1 cells cultured in the presence of HA-Ph-30 and HA-Ph-60 showed significantly enhanced migration speed by 32% and 31%, respectively, compared to those cultured in the presence of non-sonicated HA-Ph (HA-Ph-0) ($p < 0.05$) (**Fig. 4-3a, b)**. Proliferation was enhanced by HA-Ph-30 and HA-Ph-60, as shown in **Figure 4-3c**. The cells treated with HA-Ph-30 and HA-Ph-60 showed decreased doubling time by approximately 17.7% and 40.6%, respectively, compared to that of untreated cells ($p < 0.05$) (**Fig. 4-3c**). These results demonstrate that low-molecular-weight HA-Ph obtained by sonication-mediated degradation can enhance the migration and proliferation of VECs, similar to non-modified HA. Slevin et al. have reported that the interaction between LMWHA and VECs enhances cell migration speed via the activation of extracellular-regulated kinase 1/2 (ERK1/2) [130]. Low molecular weight HA regulates VECs

proliferation through interactions with cell receptors such as CD44. Clustering of CD44 on the cell surface was proposed to enhance the production of vascular endothelial growth factor (VEGF), promoting EC proliferation [133].

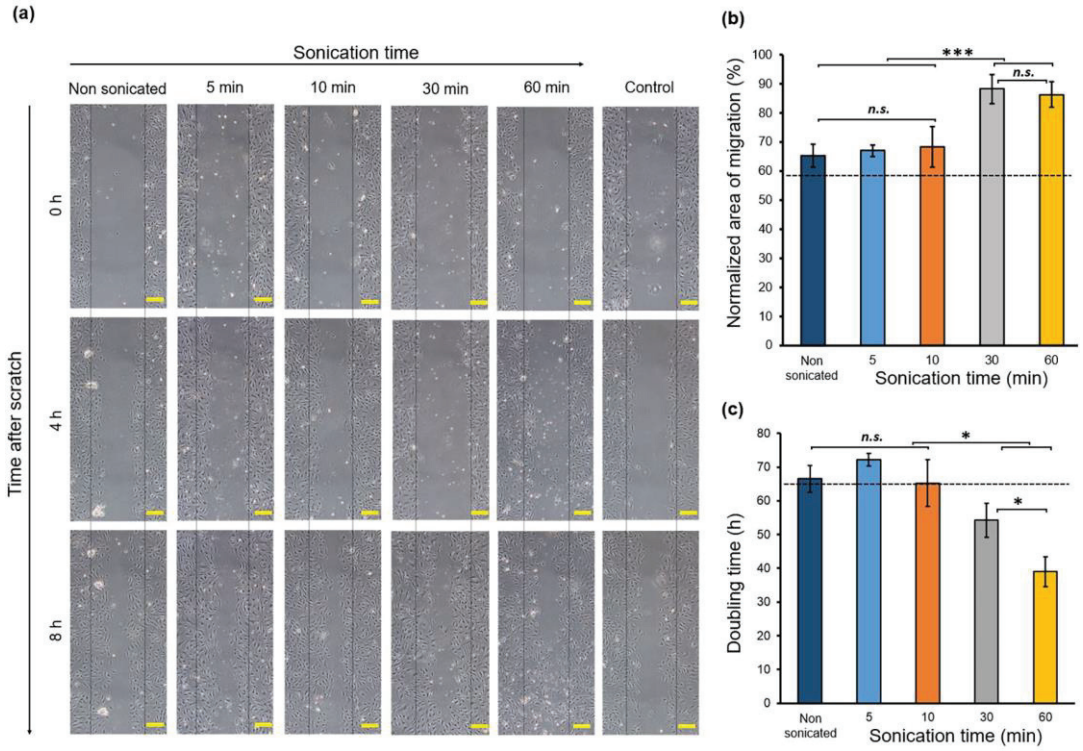

Fig. 4-3 Impact of medium containing degraded HA-Ph on HUEhT-1 cell migration and proliferation. (a) Time-lapse images captured at 0, 4, and 8 h after creating a scratch wound (scale bar 50 μm). (b) Quantitative analysis of the normalized area of cell migration as a percentage. Error bars represent standard deviation (n = 3). (c) Doubling time of HUEhT-1 cells as a function of HA-Ph solution sonication time. Error bars represent the standard deviation (n = 3). Cells cultured without adding HA-Ph into the medium were considered the control, and the values are represented as the dashed line in the graphs. *$p < 0.05$, ***$p < 0.01$, *n.s.*: no significant difference ($p > 0.05$) Tukey's HSD. Reprinted from (Elvitigala et al. 2024) [49] with permission from MDPI.

3.3 Cell adhesion and morphology on hydrogels

Next, Understanding the adhesion of HUEhT-1 cells is essential to elucidate their ability to form networks, particularly when interacting with HA of different molecular weights. Based on the above results for the formation of hydrogels in a short time (**Fig. 4-2d, e**) and the enhancement of migration with smaller decrease in cell growth (**Fig. 4-3**), hydrogels composed

of 2 w/v% HA-Ph-30 and 0.1 w/v% gelatin-Ph (HA-Ph-30 hydrogel) were used to evaluate the effect of the incorporation of degraded HA-Ph through sonication on the behavior of VECs. Cellular adhesion is governed by substrate stiffness [134].

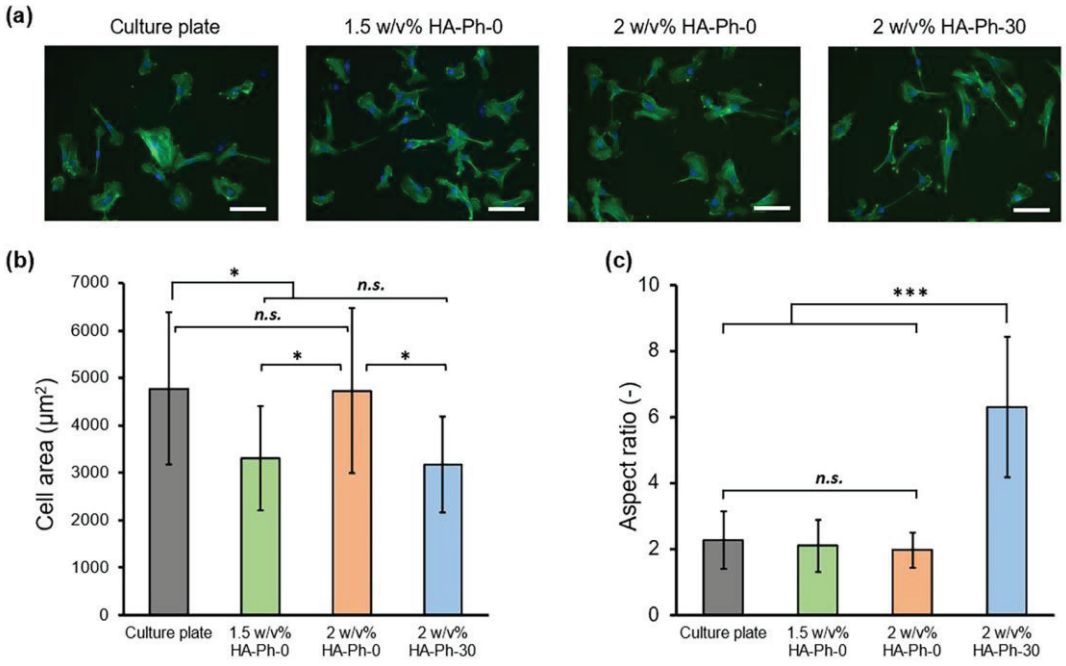

Fig. 4-4 Evaluation of HUEhT-1 cell adhesion and morphology on the hydrogels composed of 2 w/v% or 1.5 w/v% HA-Ph-0 and 2 w/v% HA-Ph-30. (a) Fluorescence micrographs of the HUEhT-1 cells on hydrogels stained with phalloidin iFluoro488 (actin fibers) and DAPI (nucleus). Scale bars: 100 μm. (b) Area and (c) aspect ratio of cells on hydrogels ($n \geq 50$). $^{*}p < 0.05$, $^{***}p < 0.01$, *n.s.*: no significant difference ($p > 0.05$), Tukey's HSD. Error bars represent standard deviation. Reprinted from (Elvitigala et al. 2024) [49] with permission from MDPI.

As shown in **Fig. 4-2e**, the 2 w/v% HA-Ph-0 and 2 w/v% HA-Ph-30 hydrogels exhibited different stiffness values. Therefore, to mitigate the impact on hydrogel stiffness and investigate the effect of the HA-Ph molecular weight on cellular adhesion, I utilized 1.5 w/v% HA-Ph-0 hydrogel (Young's modulus: 2.9 kPa), which also has nearly the same stiffness of 2 w/v% HA-Ph-30 hydrogel (Young's modulus: 2.7 kPa, **Fig. 4-2e**). As shown in **Fig. 4-4**, HUEhT-1 cells cultured on the 2 w/v% HA-Ph-0 hydrogel showed a similar shape (**a**), cell area (**b**), and aspect ratio (**c**) to those on a cell culture plate. The cells on the 1.5 w/v% HA-Ph-0 hydrogel showed a similar shape and aspect ratio as those on the 2 w/v% HA-Ph-0 hydrogel

and culture plate but with a smaller cell area ($p < 0.05$). The cells on the 2 w/v% HA-Ph-30 hydrogel showed a similar cell area to those on the 1.5 w/v% HA-Ph-0 hydrogel ($p = 0.9$) but showed an approximately 3-fold larger aspect ratio ($p < 0.01$). Consistent with our previous studies, I found that LMWHA-Ph induced significant cellular elongation [47,104]. A possible mechanism for cell elongation on the HA-Ph-30 hydrogel is the epithelial-to-mesenchymal transition [112], which involves morphological changes of cells to an elongated spindle-like morphology.

3.4 CD44-mediated HUEhT-1 cell network formation

Next, I investigated the network formation of HUEhT-1 cells on hydrogels with the same composition of HA-Phs as described in the cell adhesion and morphology analysis section.

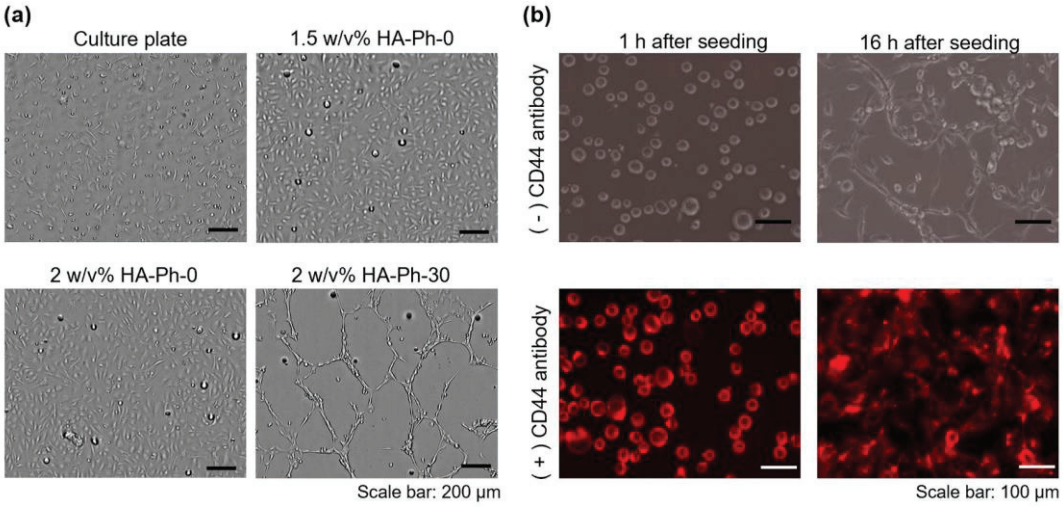

Fig. 4-5 HUEhT-1 cell network formation assay on the hydrogels composed of 2 w/v% or 1.5 w/v% HA-Ph-0 and 2 w/v% HA-Ph-30. (a) Microphotographs of HUEhT-1 cells cultured on the hydrogel after 16 h. (b) Fluorescence images of HUEhT-1 network formation on the hydrogel under CD44 block (red: APC-CD44 antibody) and non-block conditions. Reprinted from (Elvitigala et al. 2024) [49] with permission from MDPI.

HUEhT-1 cells only formed a visible network-like structure in the 2 w/v% HA-Ph-30 hydrogel **(Fig. 4-5a)**. In contrast, the cells cultured on the culture dish with 1.5 w/v% and 2 w/v% HA-Ph-0 hydrogels exhibited no discernible network formation. This difference underscores the pivotal role of the molecular weight of HA-Ph, particularly that of HA-Ph-30, in VECs network formation. A targeted approach was used to elucidate the specific interactions between the CD44 receptors and HA-Ph-30. The CD44 receptors on HUEhT-1 cells were selectively blocked using an anti-CD44 antibody before cell seeding onto the 2 w/v% HA-Ph-30 hydrogel. Cells in which the CD44 receptors were blocked showed no network formation on the 2 w/v% HA-Ph-30 hydrogel **(Fig. 4-5b),** whereas non-blocked cells exhibited robust network-like structures. HA oligomers obtained via enzymatic degradation promote network formation by activating ICAM-1 and VCAM-1 expression [133]. The interaction of HA oligomers with CD44 receptors enhanced the production of VEGF, an essential growth factor in angiogenesis [135]. Therefore, the suppression of network formation under CD44-blocked conditions may be due to the regulation of the necessary signaling pathways for the secretion of necessary growth factors.

3.5 HA-Ph molecular weight modulates the expression of CD44 receptors

Based on flow cytometry analysis, CD44 expression was notably influenced by the molecular weight of the HA-Phs, as shown in **Fig. 4-6**. CD44 expression in HUEhT-1 cells cultured on a cell culture dish and 2 w/v% and 1.5 w/v% HA-Ph-0 hydrogels decreased by 83, 71, and 71.1%, respectively, compared to those cultured on the 2 w/v% HA-Ph-30 hydrogel ($p < 0.01$). **(Fig. 4-6a, b**). These results are consistent with those of Khanmohammadi et al., who showed that LMWHA-immobilized gelatin-based hydrogels increased endothelial cell motility and CD44 expression [106].

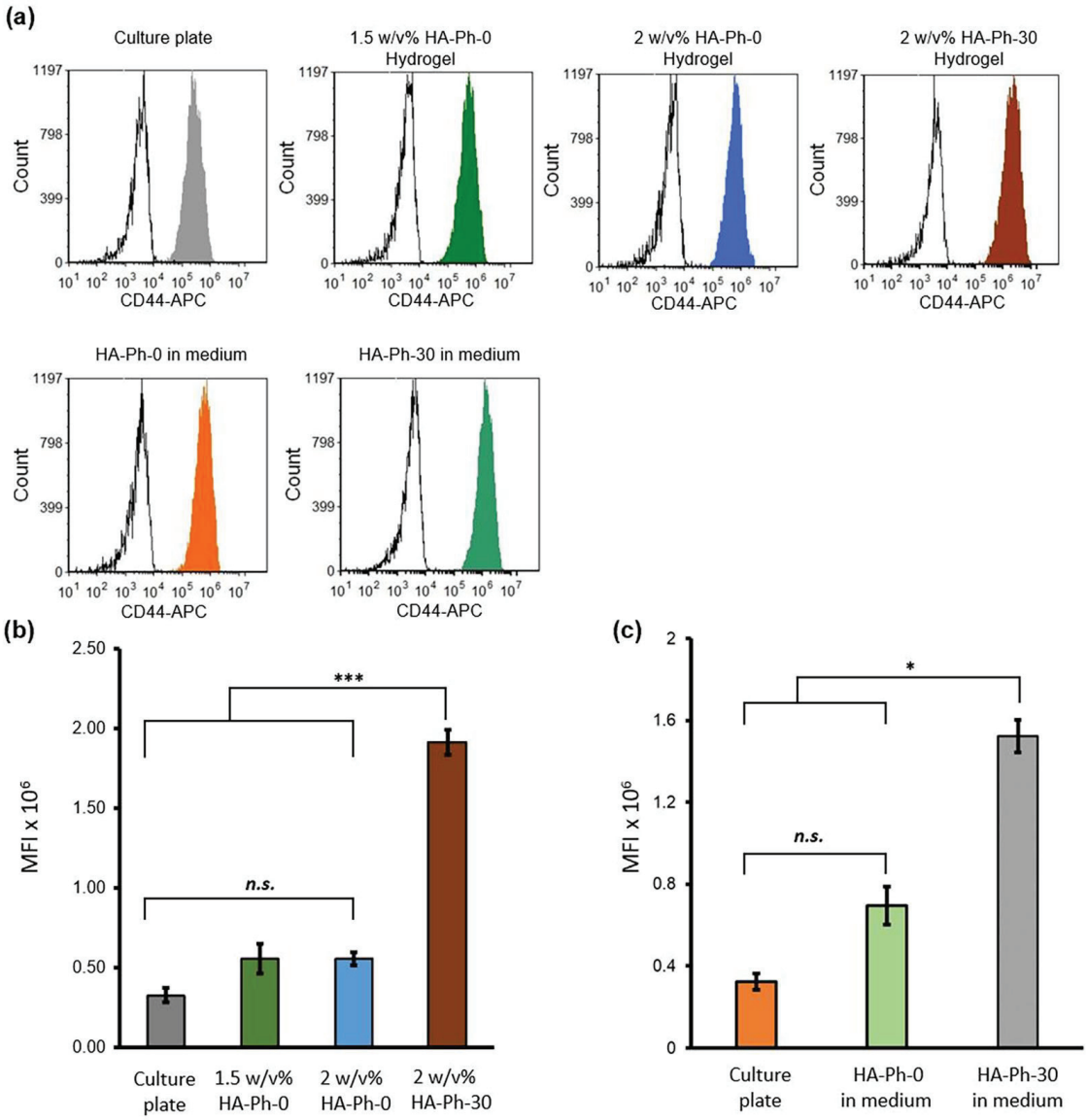

Fig. 4-6 Flow cytometry analysis of HUEhT-1 cells. (a) Representative flow cytometry histogram of HUEhT-1 cells cultured on the hydrogels and well plate (medium containing different molecular weights of HA-Ph). The quantitative mean fluorescence intensity (MFI) values of HUEhT-1 cells cultured on the (b) hydrogel composed of 2 w/v% or 1.5 w/v% HA-Ph-0 and 2 w/v% HA-Ph-30 and (c) culture plate (culture medium consisting of 0.1 w/v% HA-Ph-0 and HA-Ph-30). Error bar: standard deviation (n > 1000 cells). *p < 0.05, ***p < 0.01, *n.s.*: no significant difference (p > 0.05), Tukey's HSD. Reprinted from (Elvitigala et al. 2024) [49] with permission from MDPI.

The soluble forms of HA-Phs were also used to elucidate the effect of the molecular weight of the HA-Phs on CD44 expression **(Fig. 4-6a, c)** by incorporating HA-Ph-0 and HA-Ph-30 into the cell culture medium at a concentration of 0.1 w/v%. The mean fluorescence intensity (MFI) for the 0.1 w/v% HA-Ph-0-treated cells and untreated cells showed a decrease of

approximately 45.6% and 21.2%, respectively, compared to the 0.1 w/v% HA-Ph-30-treated cells ($p < 0.05$). These results demonstrate that both the crosslinked and soluble forms of HA-Ph-30 enhanced CD44 expression in HUEhT-1 cells.

3.6 Effect of HA-Ph-CD44 interaction on PI3K and HIF-1 gene expression

PI3K and HIF genes play a significant role in angiogenesis. The PI3K gene is associated with angiogenesis and is activated through various signaling pathways initiated by the interaction of CD44 and HA [136–138]. Therefore, I analyzed the effect of the HA-Phs obtained by sonication-mediated degradation on PI3K gene expression in HUEhT-1 cells cultured on hydrogels. The cells cultured on the 2 w/v% HA-Ph-30 hydrogel showed 10-fold higher PI3K gene expression than those cultured on the same hydrogel with CD44 blocked and the 2 w/v% HA-Ph-0 hydrogel ($p < 0.05$), indicating that the interaction of HA-Ph-30 with CD44 receptors may increase PI3K gene expression **(Fig. 4-7a)**.

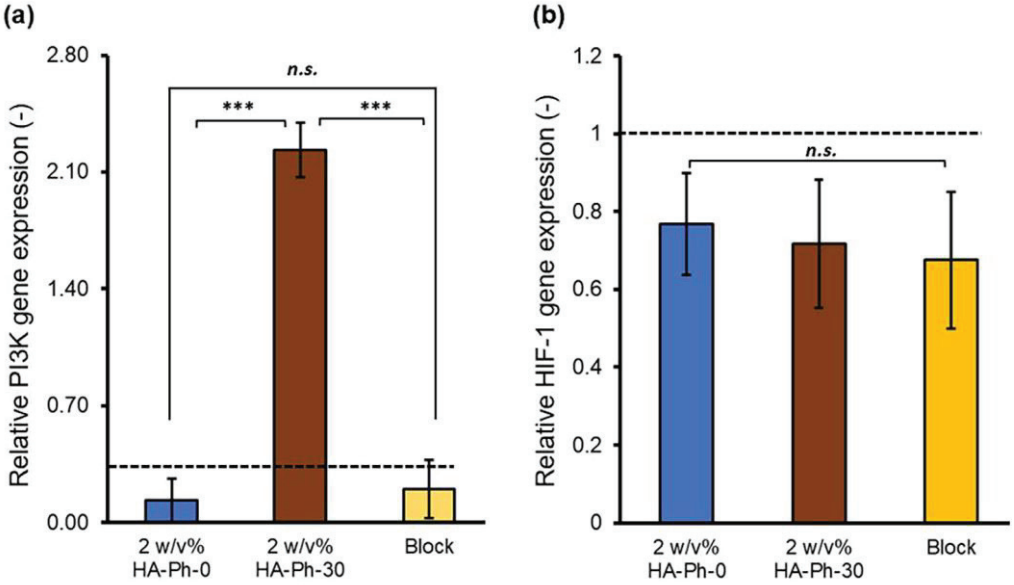

Fig. 4-7 Relative gene expression levels of (a) PI3K and (b) HIF-1 in HUEhT-1 cells cultured in 2 w/v% HA-Ph-0 and 2 w/v% HA-Ph-30 hydrogels. Relative *Ct* values were calculated with respect to the cells cultured on the culture plate, and gene expression was set to one (dashed line). Error bar: standard deviation (n = 2–3). *$p < 0.05$, *n.s.*: no significant difference ($p > 0.05$), Tukey's HSD. Reprinted from (Elvitigala et al. 2024) [49] with permission from MDPI.

The hypoxia-inducible factor 1 (HIF-1) is a key gene involved in angiogenesis under hypoxic conditions. Notably, no significant differences were observed in HIF-1 gene expression across all tested conditions ($p > 0.05$) **(Fig. 4-7b)**. These findings suggest that hypoxic conditions did not primarily govern network formation in HUEhT-1 cells but were likely due to the interaction between LMWHA and CD44, as evidenced by the significant variations observed in PI3K gene expression.

4. Conclusion

In this chapter, we investigated the role of HA-Ph molecular weight, obtained by sonication of HA-Ph solutions, in VECs network formation within a hydrogel prepared by HRP-mediated crosslinking. Unlike the previous chapters, which focused on crosslinking methods, this chapter highlighted the significance of physical degradation methods in producing bioactive materials that enhance vascularization. The degree of HA-Ph degradation by controlling the sonication time at a constant frequency was tuned. Human vascular endothelial cells exhibited distinct migration speeds and proliferation depending on the degree of degradation. The degraded HA-Ph present in the hydrogel promoted the formation of the HUEhT-1 cell network via CD44 interactions and elevated the expression of PI3K. These results indicate that the sonication-mediated degradation of HA-Ph plays a crucial role in VECs behavior. Therefore, these results provide a promising avenue for fabricating hydrogels for in vitro VEC studies.

Some portion of this thesis, including text and figures, have been previously published in the journal article “Hydrogels with Ultrasound-Treated Hyaluronic Acid Regulate CD44-Mediated Angiogenic Potential of Human Vascular Endothelial Cells In Vitro” by Elvitigala et al., published in *Biomolecules*, 2024, 14, 604 (Reference No. 49). These sections are reproduced here with permission from the MDPI (Basel, Switzerland).

Chapter V

Tuning the Crosslinking and Degradation of Hyaluronic Acid/Gelatin Hydrogels Using Hydrogen Peroxide for Muscle Cell Sheet Fabrication

1. Introduction

In this chapter, our focus shifts to the broader applicability of the HA-Ph hydrogel system. This chapter explores the potential of low molecular weight HA-Ph hydrogels to support muscle tissue engineering using C2C12 cells. By investigating how the mechanical properties and degradation of HA-Ph hydrogels influence muscle cell behavior, I aim to expand the utility of these hydrogels in various tissue engineering contexts, paving the way for new applications in regenerative medicine and therapeutic interventions. Cell sheet technology is a strategy for fabricating sheets composed of cells with cell-to-cell connections in vitro. The cell sheets can be transplanted into patients to repair damaged tissues or organs, such as the cornea,[139] myocardium, [140] cartilage, [141] and skeletal muscles, [142] and they can be used in disease models in drug testing[143]. The most common approach for fabricating cell sheets involves growing cells on temperature-responsive surfaces that are modified with poly(N-isopropyl acrylamide) (PNIPAAm). The cells are harvested by decreasing the temperature to below 32 °C, [144] which induces a phase transition between PNIPAAm's hydrophilic and hydrophobic states. These transitions occur around 32 °C; therefore, decreasing the temperature below this threshold facilitates cell harvest [144]. While temperature-responsive dishes have been widely used, they have limitations, such as cell type dependent detachment and difficulties in cell adhesion and growth [145]. Moreover, the surface properties of temperature-responsive dishes, such as stiffness, surface charge, and surface chemistry, which are critical for controlling cell behaviour including functional expression and differentiation, are difficult to tune [146,147]. Surface

properties play a significant role in determining cell behaviours, as cells interact with their surrounding substrates through physical, chemical, and biological cues [146].

The objective of this study was to address some of the limitations of commonly used temperature-responsive substrates for cell sheet fabrication. Specifically, I aimed to develop hydrogels that could influence the myogenic differentiation of myoblasts into skeletal muscle cells and allow for easy harvesting of cell sheets without temperature control. To achieve this, a hydrogel was prepared from a mixture of phenolated hyaluronic acid (HA-Ph) and type B gelatin (Gelatin-Ph) via HRP-mediated crosslinking of the phenol moieties (**Fig. 5-1a**) using H_2O_2 as an electron acceptor. H_2O_2-mediated hydrogelation has been applied to create hydrogels from various polymer solutions for diverse biomedical applications [15,148–151]. Hydrogels are water-swollen networks of polymer chains that are commonly used for in vivo and in vitro cell culture applications owing to their high biocompatibility, antibacterial properties, degradability, and similarity to the natural extracellular matrix (ECM) [152–155]. They can be designed with various physical, chemical, and biological properties, such as stiffness, porosity, and specific moieties that interact with cell surface receptors [156,157]. Previous studies have reported the successful differentiation of mouse myoblast C2C12 cells into myotubes on substrates with muscle tissue-like stiffness [158] and have effectively controlled hydrogel stiffness for the proliferation and differentiation of C2C12 cells and human myoblasts [159].

HA is a biocompatible polysaccharide abundant in the ECM and is known to regulate skeletal muscle cell functions, [160] and myogenic differentiation [161]. HA interacts with the receptors present on the cell surface, such as CD44 and receptor for HA-mediated motility (RHAMM) [162]. However, HA alone does not support cell adhesion; therefore, it must be combined with materials that promote cell adhesion. In a preliminary study, C2C12 cells did not adhere to or grow on hydrogels made of HA-Ph alone. Consequently, in this study, the composite hydrogels prepared from a mixture of HA-Ph and Gelatin-Ph were tested. Gelatin is

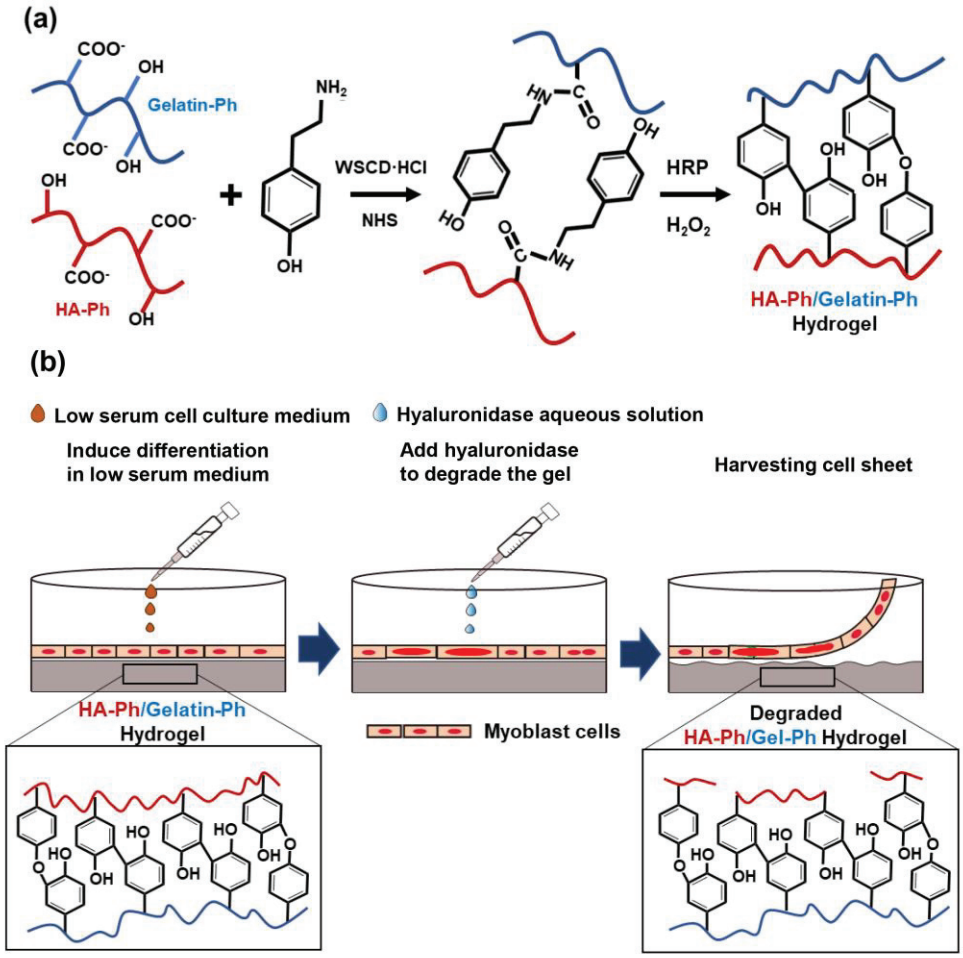

Fig. 5-1 Schematics of (a) synthesis of HA-Ph and Gelatin-Ph using WSCD·HCl and NHS, followed by HRP-mediated crosslinking of these polymers utilising hydrogen peroxide (H_2O_2) to yield the hydrogel, and (b) after inducing myogenic differentiation on the hydrogel, the cell sheet is harvested by treating the HA-Ph/Gelatin-Ph hydrogel with hyaluronidase. Reprinted from (Elvitigala et al., 2023) [50] with permission from Royal Society of Chemistry.

known to promote cell adhesion because it possesses an arginyl-glycyl-aspartic acid (RGD) peptide, which allows for cell attachment [163]. Gelatin is also an attractive choice owing to its biocompatibility, biodegradability, and ability to mimic some aspects of the ECM properties, making it a suitable component for composite hydrogels in tissue engineering applications [151].

In this study, the crosslinking density and degradation of these polymers were controlled by changing the H_2O_2 exposure time during hydrogel preparation. We have reported that H_2O_2 functions not only as an essential substrate for HRP-catalysed crosslinking of phenolic hydroxyl moieties but also degrades polymer chains in the hydrogels [18,45,47]. Our previous study demonstrated that C2C12 cell attachment and myogenic differentiation could be influenced by

adjusting the degree of crosslinking and degradation of Gelatin-Ph molecules in hydrogels prepared from a solution containing Gelatin-Ph alone via H_2O_2-mediated reactions [18].

The hypothesis for this study was that HA-Ph/Gelatin-Ph composite hydrogels with varying degrees of H_2O_2-mediated crosslinking and degradation would facilitate control over myogenic differentiation of myoblasts on the hydrogels and allow cell sheet harvesting using hyaluronidase (**Fig. 5-1b**). The enzyme hyaluronidase degrades hyaluronic acid without the need for temperature control, making it an attractive option for cell sheet preparation [164]. In this study, mouse myoblast C2C12 cells, a frequently used myoblast model, [165,166] were used to test the potential of HA-Ph/Gelatin-Ph composite hydrogels as platforms for cell sheet fabrication.

2. Materials and methods

2.1 Materials

HA-Ph, which contains 8 Ph groups per 100 repeat units of HA, was supplied by Nagase ChemteX (Osaka, Japan). Gelatin-Ph was synthesized (4.1 × 10-4 mol-Ph/g-Gelatin-Ph) following a previously reported method by conjugating type B gelatin (bovine skin, 226 g Bloom, Sigma-Aldrich, St. Louis, MO, USA) with 4-(2-hydroxyethyl)-1-piperazineethanesulfonic acid (HPPA; Tokyo Chemical Industry, Tokyo, Japan) using water-soluble carbodiimide hydrochloride (WSCD·HCl; Peptide Institute, Osaka, Japan) and N-hydroxysuccinimide (NHS FUJIFILM, Wako Pure Chemical, Osaka, Japan). Aqueous H_2O_2 (31 w/w%), catalase from bovine liver (8000 U/mg), 4 w/w% paraformaldehyde in phosphate-buffered saline (PBS, pH7.4), collagenase (203 U/mg), hyaluronidase (890 U/mg), and HRP (190 U/mg) were purchased from FUJIFILM Wako Pure Chemical. Propidium iodide (PI) and CellStain-DAPI were purchased from Dojindo (Kumamoto, Japan). Calcein-AM and phalloidin-iFluor 647 (ab176759) were purchased from Nacalai Tesque Inc. (Kyoto, Japan)

and Abcam (Cambridge, UK), respectively. DMEM from Nissui (Tokyo, Japan) was used for cell culture experiments.

2.2 Cell culture

Mouse myoblast C2C12 cells (Riken Bio-Resource Center, Ibaraki, Japan) were cultured in DMEM with 10 v/v% FBS in a humidified incubator with 95% air/5% CO_2 at 37 °C.

2.3 Molecular weight measurement

HA-Ph was dissolved in PBS at 2 w/v%, and the polymer solution was exposed to 16 ppm H_2O_2 in air for 15–120 min. The resulting HA-Ph solutions were analysed using HPLC (LC-20AD, Shimadzu, Kyoto, Japan). Unexposed polymer solutions were used as controls. A calibration curve for the molecular weight determination was prepared using the Pullulan standard.

2.4 Composite hydrogel (HA-Ph/Gelatin-Ph) preparation

Hydrogels were prepared from 2 w/v% HA-Ph, 0.75 w/v% Gelatin-Ph, and 1 U/mL HRP dissolved in PBS by varying the exposure time to 16 ppm H_2O_2 in air from 15 to 120 min.

2.5 Measurement of mechanical properties

HA-Ph/Gelatin-Ph hydrogels with a diameter of 22.1 mm and a height of 4 mm were prepared by pouring 1 mL of the polymer solution containing HA-Ph and Gelatin-Ph mixed with 1 U/mL HRP into a 12-well plate. Young's moduli of the prepared hydrogels were determined utilising a material tester (EZ-SX, Shimadzu, Kyoto, Japan) working at a compressing rate of 6.0 mm/min with a 5 mm diameter probe at 37 °C. The stress-strain curve

in the linear range of 2-8% compression was used to calculate the values. For each hydrogel, three measurements were performed, and the average value was used in the calculations.

2.6 Enzymatic degradation

The degradability of the HA-Ph/Gelatin-Ph hydrogels by hyaluronidase was evaluated by preparing three hydrogels for each condition (8 mm in diameter and 2 mm in height). The hydrogels were immersed in 1 mL DMEM containing 0.1 w/v% hyaluronidase at 37 °C, and the morphological changes of the hydrogels were observed for 2 h. The degradation time reported in the results is the average of all three hydrogels under each condition.

2.7 Cell adhesion and viability analysis

The hydrogels were poured into the wells of a 6-well plate at a density of 1 mL/well. Before cell seeding, residual H_2O_2 was removed from the hydrogels by overnight immersion in 1 mL of DMEM containing 0.1 w/v% catalase and thorough washing in PBS thrice. After replacing the medium with fresh DMEM, the C2C12 cells were cultured at an initial density of 5×10^3 cells/well. Two days post seeding, the cells were stained with Calcein-AM for further analysis. The adhesion area and aspect ratios of individual cells were determined from micrographs (six random positions on each hydrogel) obtained using a fluorescence microscope (BZ-9000, Keyence, Osaka, Japan) and ImageJ software (2.1.0/1.53c, NIH, USA). The aspect ratio was calculated as the ratio of the major and minor axes of the fitted ellipses. The cell circularity was calculated using the formula $4\pi \times(\text{area}/\text{perimeter}^2)$.

2.8 C2C12 cell differentiation

Cells were cultured on the hydrogels at an initial density of 1×10^5 cells/well in DMEM supplemented with 10 v/v% FBS. Upon reaching confluence, the cells were cultured in a

differentiation medium (DMEM containing 2 v/v% horse serum) following daily replenishment of the medium to support cell growth. After culturing for six days in the differentiation medium, the cells were fixed by immersion in 4% paraformaldehyde in PBS for 30 min and permeabilised with 50 mM HEPES-buffered solution containing bovine serum albumin (pH 7.4). The cells were then stained with phalloidin iFluor 647 (F-actin) and DAPI (nuclear stain). The number of cells that differentiated into multinucleated myotubes and the length of the myotubes were determined from fluorescent micrographs taken at six random positions by fluorescence microscopy using ImageJ software.

2.9 Cell sheet fabrication

Once confluence was reached, hyaluronidase was added to the medium at a final concentration of 0.1 w/v%. After 5 min, cell sheet detachment was examined using an inverted microscope (IX71; Olympus, Tokyo, Japan). The detached cell sheets were transferred to fresh 6-well plates using a pipette to assess the ability of the cell sheets to reattach to other substrates.

2.10 Statistical analysis

Microsoft Excel 2019, version 1808 (Microsoft Corp., Redmond, WA, USA) was used for data analysis. One-way analysis of variance (ANOVA) was used for statistical analyses. A post-hoc t-test was conducted using Tukey's HSD, with a p-value of <0.05 considered significantly different.

3. Results and discussion

3.1 Characterisation of the composite hydrogels

First, the mechanical properties of the composite hydrogels composed of 2 w/v% HA-Ph and 0.75 w/v% Gelatin-Ph prepared by exposure to H_2O_2-containing air for 15, 60, and 120

min was assessed. As depicted in **Fig. 5-2a**, increasing the exposure time from 15 to 60 min led to a significant increase in the Young's modulus from 0.5 ± 0.1 to 7.1 ± 0.2 kPa. However, increasing the exposure time further, from 60 to 120 min, caused a decrease in the Young's modulus from 7.1 ± 0.2 kPa to 3.9 ± 0.1 kPa. I also investigated the impact of the H_2O_2-exposure time on the hyaluronidase-mediated degradation of the hydrogels in a cell culture medium containing hyaluronidase at a final concentration of 0.1 w/v%. As shown in **Fig. 5-2b**, the 15 min-H_2O_2-exposure-hydrogels were completely degraded within 48 ± 4 min. The time required for degradation increased to 115 ± 7 min with an increase in the H_2O_2-exposure time to 60 min. A further increase in the H_2O_2-exposure time to 120 min led to a decrease in the time required for degradation of the hydrogels to 83 ± 4 min.

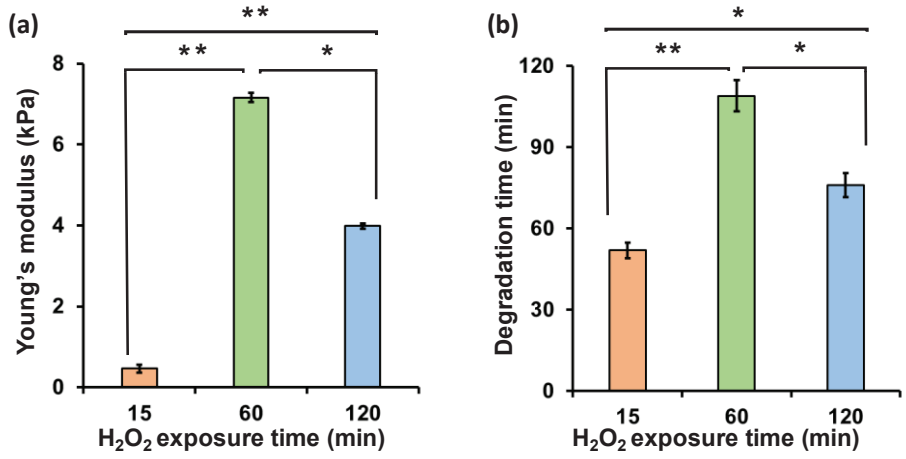

Fig. 5-2 Effect of H_2O_2 exposure time during hydrogel preparation on (a) Young's modulus of the composite hydrogels (n=3), and (b) the time until complete degradation of the composite hydrogels in medium containing 0.1 w/v% hyaluronidases (n=5). Error bars in columns: S.D. *p<0.05, **p<0.01, Tukey HSD. Reprinted from (Elvitigala et al., 2023) [50] with permission Royal Society of Chemistry.

3.2 Cell adhesion and morphology

The substrates used for the cell culture did not induce cell death. The suitability of the HA-Ph/Gelatin-Ph hydrogels for the C2C12 cells was confirmed by measuring the cell viability the

day after seeding; the viabilities of cells grown on HA-Ph/Gelatin-Ph hydrogels prepared at 15, 60, and 120 min of H_2O_2 exposure were 89%, 96%, and 95%, respectively. These results demonstrate the limited toxicity of H_2O_2 in this hydrogelation system. As shown in **Fig. 5-3a and b**, the cells cultured on the stiff hydrogel, obtained after 60 min of exposure to H_2O_2-air, showed a 2.8 and 1.5-fold increase in area compared to those cultured on the hydrogels obtained after 15 and 120 min of exposure, respectively. This was 73% of the area of those grown on cell culture dishes. In addition, cells on the hydrogel prepared with 60 min of exposure showed the highest elongation, marked by the highest aspect ratio **(Fig. 5-3c)** and the lowest circularity **(Fig. 5-3d),** compared to those on other hydrogels and culture dishes.

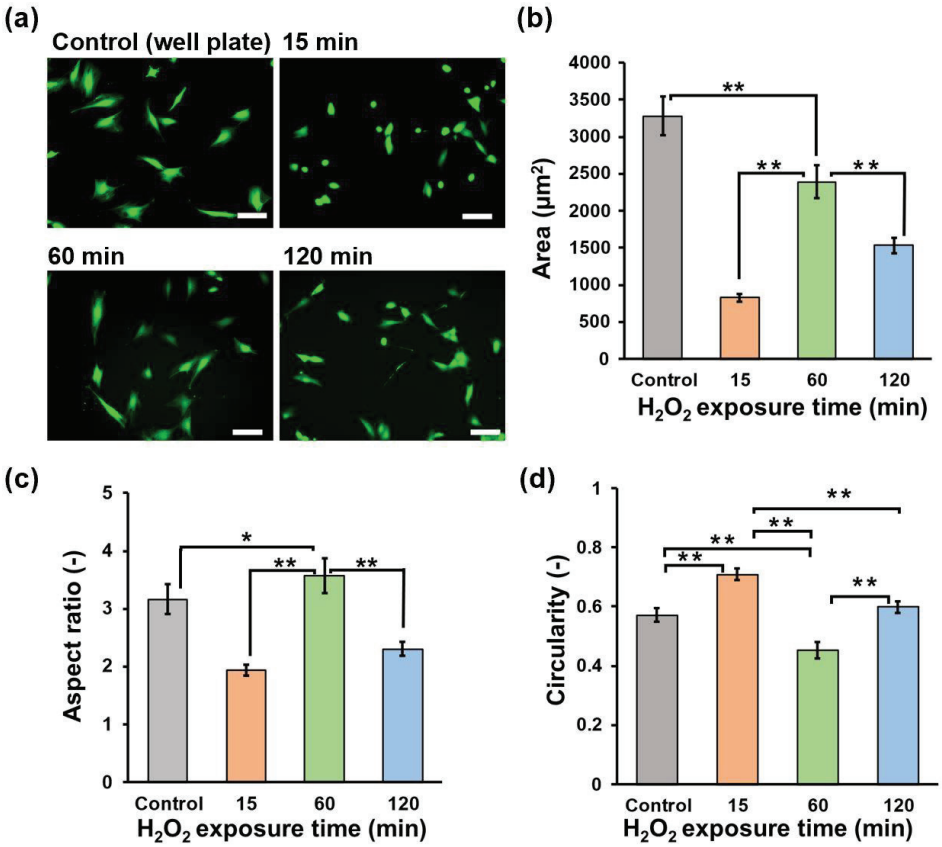

Fig. 5-3 Effect of H_2O_2 exposure time during hydrogel preparation on C2C12 cell morphology after two days of culture. (a) Fluorescence micrographs of C2C12 cells on hydrogels stained with Calcein-AM. Scale bars: 100 µm. (b) Area, (c) aspect ratio, and (d) circularity of cells on hydrogels. Error bars in columns: S.D ($n \geq 50$). (a-d) Control: On 6-well plate. *$p<0.05$, **$p<0.01$, Tukey HSD. Reprinted from (Elvitigala et al., 2023)[50] with permission from Royal Society of Chemistry

3.3 Cell differentiation on hydrogels

The myogenic differentiation of C2C12 cells on HA-Ph/Gelatin-Ph hydrogels prepared by exposure to H_2O_2 containing air for 15 to 120 min was analysed after six days of culture in differentiation medium. **Fig. 5-4a** shows cells stained with phalloidin iFluor 647 (red: F-actin) and DAPI (blue: nucleus). Comparing the density of myotubes with multinucleate in the cells, those grown on the hydrogels obtained through 60 min exposure time showed more than two times higher densities than those grown on the other hydrogels (**Fig. 5-4a, b**).

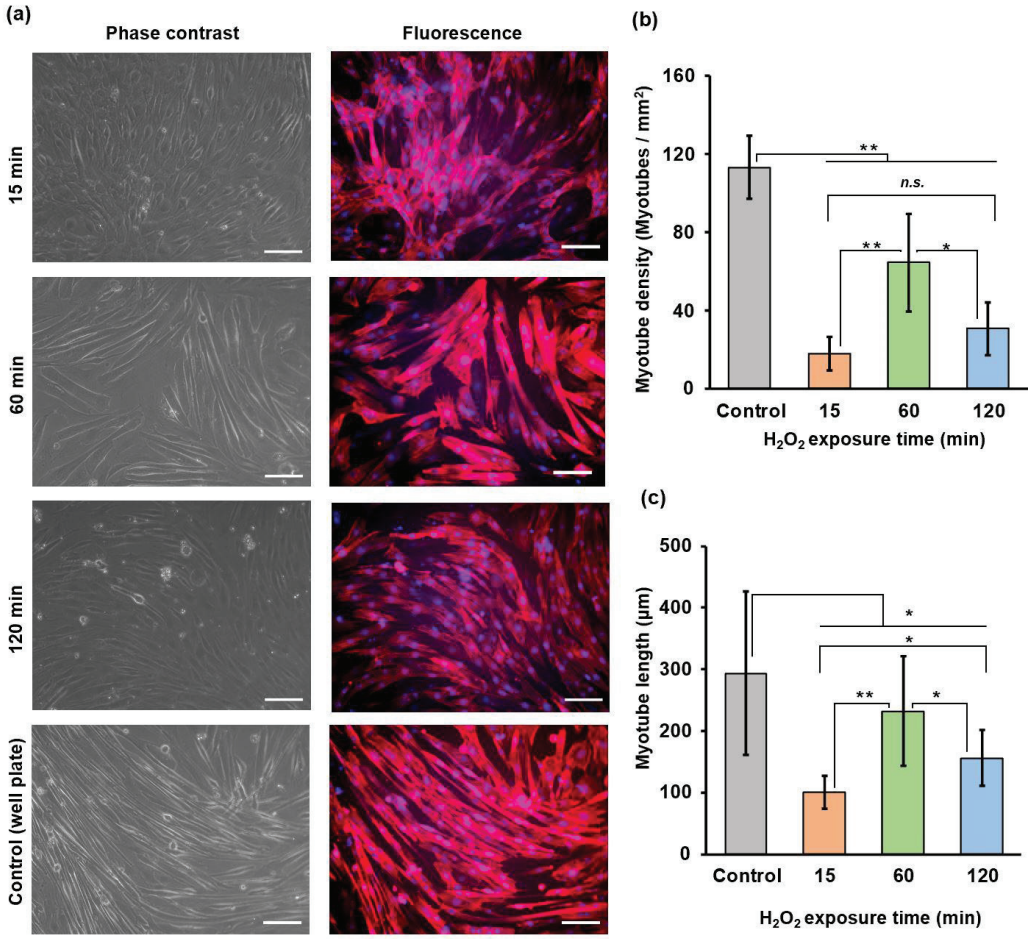

Fig. 5-4 Effect of the H_2O_2 exposure time during hydrogel preparation on myogenic differentiation of C2C12 cells. The studies were conducted after six days of culture in a differentiation medium. (a) Representative micrographs of C2C12 cells before and after staining with phalloidin iFluor 647 (red: F-actin) and DAPI (blue: nucleus), respectively. Scale bars: 100 μm. (b) The number of myotubes and (c) myotube length. Error bars in columns: S.D. ($n \geq 50$). *p<0.05, **p<0.01, *n.s.*: no significant difference, Tukey HSD. Reprinted from (Elvitigala et al., 2023) [50] with permission from Royal Society of Chemistry.

In addition, the cells on the 60 min-hydrogel had the longest myotubes (**Fig. 5-4c**). Both, myotube density and length were 1.7-fold and 2.9-fold greater in cells grown on the 60 min-hydrogel than in those cultured on cell culture dishes, respectively.

3.4 Cell sheet harvesting

To harvest the cell sheets, hyaluronidase was added to the medium at a final concentration of 0.1 w/v% after the induction of myogenic differentiation. As shown in **Fig. 5-5a-c**, the cells detached from the hydrogels after 5 min of hyaluronidase addition, while preserving cell-to-cell connections; that is, the cells detached as cell sheets. In contrast, the cells detached by collagenase treatment lost their cell-to-cell connections and broke into small pieces **(Fig. 5-5h)**.

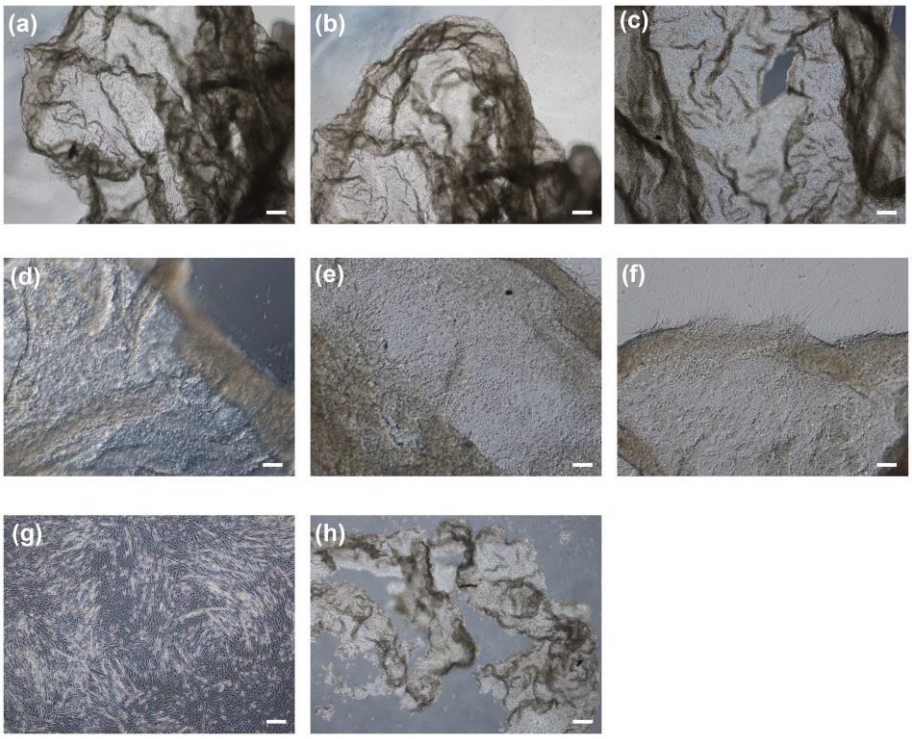

Fig. 5-5 Photomicrographs of detached cell sheets by adding 0.1 w/v% hyaluronidase to the hydrogel prepared through (a) 15, (b) 60, and (c) 120 min of exposure to air containing H_2O_2, and (d-f) re-attachment of the cell sheets to wells of a 6-well plate, respectively. Photomicrographs of the cells on hydrogel prepared from the solution containing 2 w/v% Gelatin-Ph through 60 min of exposure to air containing H2O2 after soaking in medium containing (g) 0.1 w/v% hyaluronidase, and (h) 0.1 w/v% collagenase for 5 min. Scale bars: 100 μm. Reprinted from (Elvitigala et al., 2023) [50] with permission from Royal Society of Chemistry.

In addition, the cells did not detach from the hydrogel composed solely of Gelatin-Ph upon hyaluronidase addition to the medium **(Fig. 5-5g)**. These results indicate that the detachment of cell sheets from the HA-Ph/Gelatin-Ph hydrogels was caused by the degradation of HA-Ph by hyaluronidase. All detached cell sheets were re-adhered to the cell culture dishes within 2 h **(Fig. 5-5d-f).**

3.5 Discussion

The primary objective of this study was to assess the potential of hyaluronidase degradable HA-Ph/Gelatin-Ph hydrogels as platforms for cell sheets production from myoblasts. These HA composite hydrogels present advantages over conventionally used temperature responsive PNIPAAm surfaces, such as the ability to easily control polymer content and modulate crosslinking density and degradation, which in turn influence hydrogel stiffness and interaction with cell surface receptors. The selected HA-Ph (2 w/v%) and Gelatin-Ph (0.75 w/v%) concentrations were based on preliminary solution viscosity studies to ensure ease of handling and complete hydrogel degradation by hyaluronidase. Solutions containing more than 2 w/v% HA-Ph were too viscous for pipetting and hydrogels with a Gelatin-Ph content higher than 0.75 w/v% required both hyaluronidase and protease for complete degradation. The chosen HRP concentration (1 U/mL) facilitated the investigation of the correlations between HRP-catalysed crosslink formation and polymer chain degradation by H_2O_2 [45,47,76,167].

To modulate polymer crosslinking and degradation in the hydrogels with H_2O_2, I varied the exposure times of the HA-Ph, Gelatin-Ph, and HRP mixtures to air containing 16 ppm H_2O_2. The measurement of the mechanical properties has direct implications for the contradictory effects of H_2O_2. The changes observed in the Young's modulus with increasing exposure time to H_2O_2 containing air (**Fig. 5-2a**) can be attributed to alterations in the phenol moiety crosslinking and polymer chain degradation. These trends are consistent with our previous

findings, [45,47] despite the different polymer contents of the hydrogels. The degradation of polymers by oxidative cleavage by H_2O_2 is well known [168] and H_2O_2 induced degradation of Gelatin-Ph [18,76] and HA-Ph has been reported [45,47]. Those observations were confirmed in this study. The shorter degradation time of the less-rigid hydrogels (**Fig. 5-2a, b**) may be attributed to the looser polymer network, which allows easier hyaluronidase penetration. Although here used air with 16 ppm H_2O_2, higher concentrations could potentially reduce the time required to achieve comparable crosslinking and degradation. Although not investigated in this study, the effects of H_2O_2 concentration should be carefully considered when applying the current method to adjust the hydrogel properties based on Ph-group polymers. HA-Ph, Gelatin-Ph, and HRP concentrations also affect the hydrogel properties and should be considered.

The observed trend of larger cell area and aspect ratio for C2C12 cells on stiffer HA-Ph/Gelatin-Ph composite hydrogels (**Fig. 5-3a, b**) is consistent with our previous results on C2C12 cells on Gelatin-Ph hydrogels [18]. Similar stiffness-dependent changes in myoblast morphology have been reported for other substrates [158]. Stiff substrates have been shown to facilitate actin polymerisation and assembly, leading to cell elongation and cytoskeletal tension maintenance [169]. In contrast, softer substrates hinder F-actin bundle and stress fibre formation, resulting in smaller cell area, higher circularity and aspect ratio values [45,170,171]. The effect of low molecular weight HA-Ph generated through the cleavage of the polymer chain by H_2O_2 on the morphology of C2C12 cells was assessed. It has been reported that the interaction between low molecular weight HA and CD44 and the RHAMM receptor triggered a signalling pathway cascade that alters cell behaviour [120,172].

Differences in myotube formation among C2C12 cells on hydrogels with varying stiffness can also be attributed to the hydrogel stiffness, as the highest myotube formation with the largest length was observed on the stiffest hydrogel fabricated at 60 min of H_2O_2 exposure (**Fig. 5-4**). Several studies have reported higher myoblast differentiation on stiffer hydrogels [159,173].

Stiffer substrates can better withstand the forces generated by contracting cells, thereby allowing for improved myotube formation [174]. A possible explanation for the longer myotube formation in stiffer hydrogels is that there is a correlation between stiffness and adhesion properties of myoblasts. This can be explained by the fact that ECM stiffness affects the tension and force generated by cells. On a soft substrate, cells generate less tension because of the lack of resistance, resulting in shorter myotubes. In contrast, on a stiff substrate, cells generate more tension, resulting in longer myotubes. A previous study by Bettadapur et al. showed the effect of substrate stiffness on myotube length using a gelatin hydrogel, in which longer myotubes were formed on stiffer substrates compared to softer substrates [175]. The low myotube formation observed on the hydrogel fabricated at 15 min of H_2O_2 exposure could be due to substrate deformation or collapse under cell contraction forces, inhibiting myotube formation [174]. Interestingly, compared to cells grown on the 15 min H_2O_2 exposure hydrogels, lower myotube formation was observed in cells cultured on hydrogel fabricated by 120 min of H_2O_2 exposure (**Fig. 5-4**). This phenomenon may have been caused by the presence of low molecular weight HA-Ph fragments resulting from prolonged H_2O_2 exposure. Earlier investigations have found that the molecular weight of HA has varying effects on muscle cell differentiation, with low molecular weight HA exhibiting an inhibitory effect [176]. Low molecular weight HA-Ph fragments may interact with HA cell receptors (CD44 and RHAMM), leading to the inhibition of myoblast behaviour, including myogenesis [162]. Indeed, HA binding to cells is reported to inhibit myogenesis [161]. Overall, the complex interplay between substrate stiffness and molecular weight plays a role in C2C12 differentiation.

In this study, cell sheets capable of reattaching to the substrates were successfully harvested by treatment with hyaluronidase (**Fig. 5-6**). All cell sheets detached within 5 min and there were no notable differences depending on exposure time to air containing H_2O_2 for cell detachment, despite significant differences in the time necessary for complete hydrogel

degradation (**Fig. 5-2b**). This is because cell sheet detachment resulted from the degradation of the hydrogel surface in contact with the cells, indicating that the crosslinking density of the polymers had little effect on the time required for complete degradation. There are few safety concerns for the use of hyaluronidase to harvest cell sheets for clinical applications, because hyaluronidase is already used in clinical applications, including ophthalmic and dermatologic surgery [177]. Using alginate and cellulose derivatives instead of HA-Ph is another option. Cell sheets have been obtained by treatment with alginate lyase [178,179] and cellulase [164] without using protease. However, to the best of our knowledge, these enzymes have not been applied clinically, making hyaluronidase-degradable substrates more attractive than those degradable by alginate lyase or cellulase. As shown in **Fig. 5-4**, the degree of myogenic differentiation and the cell shape within each cell sheet were not uniform. Cell sheet functionality beyond the reattachment ability was not investigated in this study. The reattached cell sheets proliferated on the new surface without detachment, demonstrating the long-term viability of the cell sheets as reported in the previous studies that obtained cell sheet using other substrate such as PNIPAAm [144]. The functions required for cell sheets vary depending on their applications in tissue regeneration, drug testing, and disease modelling. The crucial finding of this study was the potential to fabricate cell sheets from myoblasts with different qualities using solutions containing HA-Ph, Gelatin-Ph, and HRP by controlling the exposure time to air containing H_2O_2. Further studies on the detailed functionality of cell sheets will be conducted in the future, considering their applications for specific purposes.

4. Conclusion

In this chapter, the potential of HA-Ph/Gelatin-Ph hydrogels as platforms for muscle cell sheet fabrication by modulating their physicochemical properties through control of the H_2O_2 exposure time was demonstrated. Unlike the previous chapters that focused on vascular

endothelial cells, this chapter demonstrated the broader applicability of HA-Ph hydrogels beyond angiogenesis. The findings show that stiffer hydrogels facilitated a higher density of myotube formation, whereas softer and intermediately stiff hydrogels led to a lower density of myotube formation. Furthermore, I successfully harvested cell sheets with different myotube densities within 5 min of hyaluronidase addition. The harvested cell sheets maintained their morphology and were reattached to the cell culture well plates within 2 h. These results demonstrate the versatility and potential of HA-Ph/Gelatin-Ph hydrogels obtained by controlling H_2O_2-mediated crosslinking and degradation for fabricating muscle cell sheets from myoblasts. The results underscore the importance of HA-Ph degradation and hydrogel stiffness in regulating cellular behavior, consistent with the insights gained from Chapters II, III, and IV. The successful application of HA-Ph hydrogels in muscle tissue engineering opens new avenues for their use in regenerative medicine and therapeutic interventions. Continued investigation and optimisation of this platform will be crucial to unlock its full potential for advancing the fields of tissue engineering, regenerative medicine, and disease modelling.

Some portion of this thesis, including text and figures, have been previously published in the journal article “Tuning the Crosslinking and Degradation of Hyaluronic Acid/Gelatin Hydrogels Using Hydrogen Peroxide for Muscle Cell Sheet Fabrication” by Elvitigala et al., published in *Soft Matter*, 2023, 19, 5880 (Reference No. 50). These sections are reproduced here with permission from the Royal Society of Chemistry (London, United Kingdom).

General conclusions

This thesis explores the effects of degraded HA-Ph on vascular endothelial cells (VECs) behavior. Through the methodical investigation of H_2O_2-mediated (Chapter II), light irradiation-mediated (Chapter III), and sonication-mediated (Chapter IV) degradation, significant insights into how controlled degradation processes influence the angiogenic potential of VECs have been revealed. Thus, this thesis advances our understanding and application of HA-Ph in tissue engineering and regenerative medicine.

Chapter II investigates the differential effects of H_2O_2-mediated degradation on the properties of HA-based hydrogels and their subsequent influence on VECs network formation. An optimum hydrogel stiffness of 2.40 kPa, achieved after 60 min of exposure to H_2O_2, was identified as critical for promoting effective human umbilical vein endothelial cells (HUVECs) network formation. This finding not only underscores the importance of mechanical properties in the design of biomaterials but also highlights the role of controlled HA-Ph degradation in enhancing cellular responses. Through detailed experiments, this study demonstrates how degradation kinetics and the resulting hydrogel stiffness directly affect cell adhesion and the ability to form network structures, providing critical insights into the material-cell interface that guides tissue engineering applications.

In Chapter III, the focus shifts to the investigation of light irradiation-mediated crosslinking as a method to delicately control HA-Ph degradation and hydrogel formation. Using 45 min of light irradiation, this approach allows precise tuning of hydrogel properties, achieving optimal conditions for HUVEC network formation. This study reveals that intermediate light irradiation times promoted optimal hydrogel stiffness and the production of LMWHA-Ph fragments. These fragments interacted with CD44 receptors, significantly influencing F-actin fiber formation, which is crucial for HUVEC network structure.

Chapter IV focused on sonication-mediated degradation of HA-Ph, aiming to replicate the bioactive cues of naturally occurring LMWHA. By incorporating degraded HA-Ph into hydrogel scaffolds, this study confirmed the critical influence of HA-Ph molecular weight on VECs behavior, particularly network formation. This chapter demonstrates that physical degradation methods can produce bioactive materials. The study provides compelling evidence that HA-Ph degradation products, particularly those interacting with the CD44 receptor, play a pivotal role in enhancing the angiogenic potential of HUVECs. It highlights the intricate interplay between HA-Ph molecular weight, hydrogel stiffness, and VECs behavior.

Chapter V explores the use of HA-Ph hydrogels in muscle tissue engineering. Using mouse myoblast cells (C2C12), this chapter demonstrates the broader applicability of HA-Ph hydrogels beyond angiogenesis. The hydrogels were prepared using HRP-mediated crosslinking, where H_2O_2 was also used to induce polymer degradation, similar to the studies in Chapter II. The controlled degradation and mechanical properties of HA-Ph hydrogels facilitate myogenic differentiation, providing insights into their potential for muscle tissue regeneration. The results showed that varying the H_2O_2 exposure time influenced the degradation of HA-Ph in the hydrogel, which in turn affected myoblast adhesion and differentiation into myotubes. This chapter highlights the ability of HA-Ph-based hydrogels to support muscle cell sheet fabrication with high structural integrity and functionality, underscoring their potential in developing advanced biomaterials for repairing and regenerating muscle tissues.

Overall, this research provides a comprehensive understanding of how HA degradation and the mechanical properties of hydrogels influence VECs and muscle cell functions. Our findings underscore the potential of HA-Ph hydrogels as versatile biomaterials for various tissue engineering applications, offering new avenues for regenerative medicine and therapeutic interventions. This work contributes valuable insights into the design and optimization of

hydrogel-based scaffolds for promoting specific cellular responses, paving the way for future advancements in tissue engineering and regenerative therapies.

Suggestions for future works

Based on the findings of this study, future research can explore several promising directions to further advance the field of tissue engineering and regenerative medicine.

Transition from 2D to 3D culture systems: The current study has primarily focused on 2D culture systems. The next step involves transitioning to 3D culture systems using the developed HA-Ph hydrogels. 3D cultures provide a more physiologically relevant environment that better mimics in vivo conditions. This transition will enable a more accurate study of cell behavior, differentiation, and interaction within a 3D matrix, offering deeper insights into tissue engineering and regenerative medicine applications.

Co-culture with cancer cells in a 3D System: Future research should investigate the co-culture of vascular endothelial cells with cancer cells within a 3D hydrogel system. This approach can provide valuable insights into tumor angiogenesis, tumor microenvironment interactions, and the effects of the surrounding matrix on cancer cell behavior. Understanding these interactions in a 3D context is crucial for developing effective cancer therapies and studying tumor progression.

Investigation of HA-Ph interaction with other hyaluronan receptors: While this study focused on the interactions between HA-Ph and CD44 receptors, future research should consider the role of other hyaluronan receptors, such as RHAMM, in cellular functions within a 3D context. This could provide a more comprehensive understanding of how different receptors mediate cellular responses to HA-Ph, potentially unveiling new pathways for enhancing angiogenesis and tissue regeneration.

References

1. P. Rajendran, T. Rengarajan, J. Thangavel, Y. Nishigaki, D. Sakthisekaran, G. Sethi and I. Nishigaki, *Int. J. Biol. Sci.*, 2013, **9**, 1057.
2. P. Carmeliet and R. K. Jain, *Nature*, 2000, **407**, 249–257.
3. M. Bisht, D. C. Dhasmana and S. S. Bist, *Indian J. Pharmacol.*, 2010, **42**, 2.
4. D. Hanjaya-Putra, S. Saha, F. Fan, L. Alderfer, F. Graham and E. Hall, *Biomater. Sci*, 2023, **11**, 7346.
5. I. Marei, T. Abu Samaan, M. A. Al-Quradaghi, A. A. Farah, S. H. Mahmud, H. Ding and C. R. Triggle, *Front. Cardiovasc. Med.*, 2022, **9**, 847554.
6. A. Collen, P. Koolwijk, M. Kroon and V. W. M. Van Hinsbergh, *Angiogenesis*, 1998, **2**, 153–166.
7. B. Sanchez, L. Li, J. Dulong, G. Aimond, J. Lamartine, G. Liu and D. Sigaudo-Roussel, *Front. Cell Dev. Biol.*, 2019, **7**, 3389.
8. M. S. K. Chong, W. K. Ng and J. K. Y. Chan, *Stem Cells Transl. Med.*, 2016, **5**, 530.
9. K. L. DeCicco-Skinner, G. H. Henry, C. Cataisson, T. Tabib, J. Curtis Gwilliam, N. J. Watson, E. M. Bullwinkle, L. Falkenburg, R. C. O'Neill, A. Morin and J. S. Wiest, *J. Vis. Exp.*, 2014, **91**, 51312.
10. F. Tetzlaff and A. Fischer, *BIO-PROTOCOL*, 2018, **8**, 2995.
11. P. Y. Chu, H. Y. Hsieh, P. S. Chung, P. W. Wang, M. C. Wu, Y. Q. Chen, J. C. Kuo and Y. J. Fan, *iScience*, 2023, **26**, 106927.
12. C. O. Crosby and J. Zoldan, *Regen. Biomater.*, 2019, **6**, 61.
13. K. L. DeCicco-Skinner, G. H. Henry, C. Cataisson, T. Tabib, J. Curtis Gwilliam, N. J. Watson, E. M. Bullwinkle, L. Falkenburg, R. C. O'Neill, A. Morin and J. S. Wiest, *J. Vis. Exp.*, 2014, **91**, 51312.
14. S. Ullm, A. Krüger, C. Tondera, T. P. Gebauer, A. T. Neffe, A. Lendlein, F. Jung and J. Pietzsch, *Biomaterials*, 2014, **35**, 9755–9766.
15. S. Sakai and M. Nakahata, *Chem. – An Asian J.*, 2017, **12**, 3098–3109.
16. U. Blache, E. M. Ford, B. Ha, L. Rijns, O. Chaudhuri, P. Y. W. Dankers, A. M. Kloxin, J. G. Snedeker and E. Gentleman, *Nat. Rev. Methods Prim.*, 2022, **2**, 98.
17. Y. Sun, Z. Xu, M. Wang, S. Lv, H. Wu, G. Chi, L. Li and Y. Li, *Front. Bioeng. Biotechnol.*, 2020, **8**, 791.
18. W. Mubarok, K. C. M. L. Elvitigala and S. Sakai, *Gels*, 2022, **8**, 387.
19. H. S. Hwang and C. S. Lee, *Gels*, 2023, **9**, 588.
20. A. D. Doyle, S. S. Nazari and K. M. Yamada, *Phys. Biol.*, 2017, **19**, 1478.
21. C. Buckley, H. Wang, R. O'Dell, M. Del Rosario, M. Parimala Chelvi Ratnamani, M. Rome and H. Wang, *ACS Appl. Mater. Interfaces*, 2024, **16**, 18522–18533.
22. F. Briggs, D. Browne and P. Asuri, *Int. J. Mol. Sci.,* 2022, **23**, 4118.
23. F. Xing, C. Zhou, D. Hui, C. Du, L. Wu, L. Wang, W. Wang, X. Pu, L. Gu, L. Liu, Z. Xiang and X. Zhang, *Nanotechnol. Rev.*, 2020, **9**, 1059–1079.
24. D. C. West, I. N. Hampson, F. Arnold and S. Kumar, *Science*, 1985, **228**, 1324–1326.
25. K. Kouvidi, A. Berdiaki, D. Nikitovic, P. Katonis, N. Afratis, V. C. Hascall, N. K. Karamanos and G. N. Tzanakakis, *J. Biol. Chem.*, 2011, **286**, 38509–38520.
26. S. J. Kim and S. C. Owen, *Biochim. Biophys. Acta - Biomembr.*, 2020, **1862**, 183348.
27. E. Hachet, H. Van Den Berghe, E. Bayma, M. R. Block and R. Auzély-Velty, *Biomacromolecules*, 2012, **13**, 1818–1827.
28. L. Y. W. Bourguignon, *Semin. Cancer Biol.*, 2008, **18**, 251.
29. D. Nikitovic, K. Kouvidi, N. K. Karamanos and G. N. Tzanakakis, *Biomed Res. Int.*, 2013, **2013**, 12.
30. E. Dřímalová, V. Velebný, V. Sasinková, Z. Hromádková and A. Ebringerová, *Carbohydr. Polym.*, 2005, **61**, 420–426.
31. V. Bourguignon and B. Flamion, *FASEB J.*, 2016, **30**, 2108–2114.

32. A. Berdiaki, M. Neagu, I. Spyridaki, A. Kuskov, S. Perez and D. Nikitovic, *Antioxidants*, 2023, **12**, 824.
33. J. Schmidt, N. Pilbauerova, T. Soukup, T. Suchankova-Kleplova and J. Suchanek, *Biomolecules*, 2021, **11**, 1–16.
34. D. Jones, A. Tezel and M. Borrell, *Dermatologic Surg.*, 2010, **36**, 804–809.
35. A. Berdiaki, M. Neagu, I. Spyridaki, A. Kuskov, S. Perez and D. Nikitovic, *Antioxidants*, 2023, **12**, 824.
36. D. Zhang, Y. Ren, Y. He, R. Chang, S. Guo, S. Ma, F. Guan and M. Yao, *Mater. Today Bio*, 2022, **15**, 100278.
37. N. N. Mahamuni and A. B. Pandit, *Ultrason. Sonochem.*, 2006, **13**, 165–174.
38. H. Chen, J. Qin and Y. Hu, *Mol.,*2019, **24**, 617.
39. V. G. Muir and J. A. Burdick, *Chem. Rev.*, 2021, **121**, 10908.
40. C. Loebel, S. E. Szczesny, B. D. Cosgrove, M. Alini, M. Zenobi-Wong, R. L. Mauck and D. Eglin, *Biomacromolecules*, 2017, **18**, 855–864.
41. S. Khunmanee, Y. Jeong and H. Park, *J. Tissue Eng.*, 2017, 8.
42. J. Xu, Y. Liu and S. hui Hsu, *Molecules*, 2019, **24**, 3005.
43. M. Zhang, X. Chen, K. Yang, Q. Dong, H. Yang, S. Gu, W. Xu and Y. Zhou, *Carbohydr. Polym.*, 2023, **301**, 120372.
44. S. Sakai, H. Ohi, T. Hotta, H. Kamei and M. Taya, *Biopolymers*, 2019, **109**, e23080.
45. W. Mubarok, K. C. M. L. Elvitigala, M. Nakahata, M. Kojima and S. Sakai, *Cells*, 2022, **11**, 881.
46. S. L. Fenn and R. A. Oldinski, *J. Biomed. Mater. Res. B. Appl. Biomater.*, 2016, **104**, 1229.
47. K. C. M. L. Elvitigala, W. Mubarok and S. Sakai, *Polymers.*, 2022, **14** 5034.
48. K. C. M. L. Elvitigala, L. Mohan, W. Mubarok, S. Sakai, *Adv. Healthc. Mater.*, 2024, **13**, 2303787.
49. K. C. M. L. Elvitigala, W. Mubarok and S. Sakai, *Biomolecules*, 2024, **14**, 50604.
50. K. C. M. L. Elvitigala, W. Mubarok and S. Sakai, *Soft Matter*, 2023, **19**, 5880–5887.
51. N. Brassard-Jollive, C. Monnot, L. Muller and S. Germain, *Front. Cell Dev. Biol.*, 2020, **8**, 1206.
52. M. I. Bogorad, J. DeStefano, A. D. Wong and P. C. Searson, *Microcirculation*, 2017, **24**, e12360.
53. V. Coelho-Santos, A. A. Berthiaume, S. Ornelas, H. Stuhlmann and A. Y. Shih, *Proc. Natl. Acad. Sci. U. S. A.*, 2021, **118**, e2100866118.
54. R. L. Saunders and D. A. Hammer, *Cell. Mol. Bioeng.*, 2010, **3**, 60.
55. J. H. Yeon, H. R. Ryu, M. Chung, Q. P. Hu and N. L. Jeon, *Lab Chip*, 2012, **12**, 2815–2822.
56. I. Arnaoutova and H. K. Kleinman, *Nat. Protoc.*, 2010, **5**, 628–635.
57. I. Arnaoutova, J. George, H. K. Kleinman and G. Benton, *Angiogenesis*, 2009, **12**, 267–274.
58. K. Chwalek, L. J. Bray and C. Werner, *Adv. Drug Deliv. Rev.*, 2014, **79**–**80**, 30–39.
59. M. V. Tsurkan, P. V. Hauser, A. Zieris, R. Carvalhosa, B. Bussolati, U. Freudenberg, G. Camussi and C. Werner, *J. Control. Release*, 2013, **167**, 248–255.
60. M. Sun, G. Chi, P. Li, S. Lv, J. Xu, Z. Xu, Y. Xia, Y. Tan, J. Xu, L. Li and Y. Li, *Int. J. Med. Sci.*, 2018, **15**, 257.
61. Y. Ni and M. Y. M. Chiang, *Soft Matter*, 2007, **3**, 1285–1292.
62. R. Tzoneva, V. Uzunova, S. Apostolova, A. Krüger-Genge, A. T. Neffe, F. Jung and A. Lendlein, *Clin. Hemorheol. Microcirc.*, 2016, **64**, 941–949.
63. Y. Liu, L. Sun, Y. Huan, H. Zhao and J. Deng, *J. Surg. Res.*, 2006, **136**, 85–91.
64. D. Yee, D. Hanjaya-Putra, V. Bose, E. Luong and S. Gerecht, 2011, **118**, 804-15.
65. N. Monteiro, W. He, C. M. Franca, A. Athirasala and L. E. Bertassoni, *ACS Biomater. Sci. Eng.*, 2018, **4**, 2563–2570.
66. J. S. Frenkel, *Int. Wound J.*, 2014, **11**, 159–163.
67. K. L. Schwertfeger, M. K. Cowman, P. G. Telmer, E. A. Turley and J. B. McCarthy, *Front. Immunol.*, 2015, **6**, 236.
68. F. Gao, C. X. Yang, W. Mo, Y. W. Liu and Y. Q. He, *Clin. Investig. Med.*, 2008, **31**, E106–E116.
69. L. Chen, C. Fu, Q. Zhang, C. He, F. Zhang and Q. Wei, *FASEB J.*, 2020, **34**, 13125–13139.

70. L. Zhao, H. Mitomo, M. Zhai, F. Yoshii, N. Nagasawa and T. Kume, *Carbohydr. Polym.*, 2003, **53**, 439–446.
71. M. W. Sabaa, R. R. Mohamed, S. H. Eltaweel and R. S. Seoudi, *J. Appl. Polym. Sci.*, 2012, **123**, 3459–3469.
72. I. Dmitriev, I. Kuryndin, N. Bobrova and M. Smirnov, *Mater. Today Commun.*, 2015, **4**, 93–100.
73. X. Liu, Y. Jiang, H. He and W. Ping, *Food Struct.*, 2014, **2**, 41–48.
74. X. Li, A. Xu, H. Xie, W. Yu, W. Xie and X. Ma, *Carbohydr. Polym.*, 2010, **79**, 660–664.
75. W. Mubarok, K. C. M. L. Elvitigala, M. Nakahata, M. Kojima and S. Sakai, *Cells.*, 2022, **11**, 881.
76. W. Mubarok, Y. Qu and S. Sakai, *ACS Appl. Bio Mater.*, 2021, **4**, 0c01675.
77. S. Sakai, K. Hirose, K. Taguchi, Y. Ogushi and K. Kawakami, *Biomaterials*, 2009, **30**, 3371–3377.
78. I. Catelas, N. Sese, B. M. Wu, J. C. Y. Dunn, S. Helgerson and B. Tawil, *Tissue Engineering, Parts A*, 2006, **12**, 2385–2396.
79. V. Agarwal, E. S. Tjandra, K. S. Iyer, B. Humfrey, M. Fear, F. M. Wood, S. Dunlop and C. L. Raston, *Toxicol. Res.*, 2014, **3**, 223–227.
80. R. C. Savani, G. Cao, P. M. Pooler, A. Zaman, Z. Zhou and H. M. DeLisser, *J. Biol. Chem.*, 2001, **276**, 36770–36778.
81. Y. Z. Wang, M. L. Cao, Y. W. Liu, Y. Q. He, C. X. Yang and F. Gao, *Experimental Biology and Medicine*, 2011, **236**, 84–90.
82. M.-N. Sabine, G. John, K. Shant and S. Msrk, *Int. J. Oncol.*, 2009, 761.
83. D. Park, Y. Kim, H. Kim, K. Kim, Y. S. Lee, J. Choe, J. H. Hahn, H. Lee, J. Jeon, C. Choi, Y. M. Kim and D. Jeoung, *Mol. Cells*, 2012, **33**, 563.
84. J. Yang, M. Yamato, T. Shimizu, H. Sekine, K. Ohashi, M. Kanzaki, T. Ohki, K. Nishida and T. Okano, *Biomaterials*, 2007, **28**, 5033–5043.
85. J. P. Califano and C. A. Reinhart-King, *Cell. Mol. Bioeng. 2008 12*, 2008, **1**, 122–132.
86. Y. Kubota, H. K. Kleinman, G. R. Martin and T. J. Lawley, *J. Cell Biol.*, 1988, **107**, 1589–1598.
87. X. Chen, H. Zhang, J. Cui, Y. Wang, M. Li, J. Zhang, C. Wang, Z. Liu and Q. Wei, *Gels*, 2023, **9**, 155.
88. J. Zhang, Y. Wang, Q. Wei, Y. Wang, M. Li, D. Li and L. Zhang, *Int. J. Biol. Macromol.*, 2022, **219**, 1216–1226.
89. J. Zhang, Y. Wang, Q. Wei, M. Li and X. Chen, *J. Colloid Interface Sci.*, 2024, **653**, 1514–1525.
90. F. Fan, B. Su, A. Kolodychak, E. Ekwueme, L. Alderfer, S. Saha, M. J. Webber and D. Hanjaya-Putra, *ACS Appl. Mater. Interfaces*, 2023, **15**, 58195.
91. G. Camci-Unal, D. Cuttica, N. Annabi, D. Demarchi and A. Khademhosseini, *Biomacromolecules*, 2013, **14**, 1085–1092.
92. D. Jiang, J. Liang and P. W. Noble, *Annu. Rev. Cell Dev. Biol.*, 2007, **23**, 435–461.
93. S. Sakai, H. Ohi and M. Taya, *Biomol. 2019, Vol. 9, Page 342*, 2019, **9**, 342.
94. S. Sakai, S. Ito, H. Inagaki, K. Hirose, T. Matsuyama, M. Taya and K. Kawakami, *Biomicrofluidics, 2011*, **5**, 013402.
95. S. woo Lee, J. Kim, M. Do, E. Namkoong, H. Lee, J. H. Ryu and K. Park, *Acta Biomater.*, 2020, **115**, 275–287.
96. K. N. Meadows, P. Bryant and K. Pumiglia, *Journal of biological chem.*, 2001, **276,** 49289.
97. T. Roy, B. D. James and J. B. Allen, *Macromol. Biosci.*, 2021, **21**, 2000337.
98. D. Hanjaya-Putra, V. Bose, Y. I. Shen, J. Yee, S. Khetan, K. Fox-Talbot, C. Steenbergen, J. A. Burdick and S. Gerecht, *Blood*, 2011, **118**, 804–815.
99. S. Gerecht, J. A. Burdick, L. S. Ferreira, S. A. Townsend, R. Langer and G. Vunjak-Novakovic, *Proc. Natl. Acad. Sci.*, 2007, **104**, 11298–11303.
100. M. Frye, A. Taddei, C. Dierkes, I. Martinez-Corral, M. Fielden, H. Ortsäter, J. Kazenwadel, D. P. Calado, P. Ostergaard, M. Salminen, L. He, N. L. Harvey, F. Kiefer and T. Mäkinen, *Nat. Commun.*, 2018, **9**, 1–16.

101. E. Nyman, F. Huss, T. Nyman, J. Junker and G. Kratz, *J. Plast. Surg. Hand Surg.*, 2013, **47**, 89–92.
102. C. C. Termeer, J. Hennies, U. Voith, T. Ahrens, J. M. Weiss, P. Prehm and J. C. Simon, *J. Immunol.*, 2000, **165**, 1863–1870.
103. X. Pang, W. Li, L. Chang, J. E. Gautrot, W. Wang and H. S. Azevedo, *ACS Appl. Mater. Interfaces*, 2021, **13**, 25792–25804.
104. W. Mubarok, K. C. M. L. Elvitigala, M. Nakahata, M. Kojima and S. Sakai, *Cells*, 2022, **11**, 881.
105. W. Mubarok, K. C. M. L. Elvitigala, T. Kotani and S. Sakai, *Carbohydr. Polym.*, 2023, **316**, 121026.
106. M. Khanmohammadi, S. Sakai and M. Taya, *Int. J. Biol. Macromol.*, 2017, **97**, 308–316.
107. M. Hidaka, M. Kojima, M. Nakahata and S. Sakai, *Polymers.*, 2021, **13**, 1382.
108. H. Chen, J. Qin and Y. Hu, *Mol.*, 2019, **24**, 617.
109. J. Xu, M. Sun, Y. Tan, H. Wang, H. Wang, P. Li, Z. Xu, Y. Xia, L. Li and Y. Li, *Differentiation*, 2017, **96**, 30–39.
110. M. Sun, G. Chi, P. Li, S. Lv, J. Xu, Z. Xu, Y. Xia, Y. Tan, J. Xu, L. Li and Y. Li, *Int. J. Med. Sci.*, 2018, **15**, 257–268.
111. Y. T. Yeh, S. S. Hur, J. Chang, K. C. Wang, J. J. Chiu, Y. S. Li and S. Chien, *PLoS One*, 2012, **7**, 1–13.
112. I. Caon, B. Bartolini, A. Parnigoni, E. Caravà, P. Moretto, M. Viola, E. Karousou, D. Vigetti and A. Passi, *Semin. Cancer Biol.*, 2020, **62**, 9–19.
113. H. Jariyal, C. Gupta and A. Srivastava, *Int. J. Biol. Macromol.*, 2020, **160**, 1078–1089.
114. L. Alderfer, E. Russo, A. Archilla, B. Coe and D. Hanjaya-Putra, *FASEB J.*, 2021, **35,** e21498.
115. D. Hanjaya-Putra, J. Yee, D. Ceci, R. Truitt, D. Yee and S. Gerecht, *J. Cell. Mol. Med.*, 2010, **14**, 2436–2447.
116. D. Cheresh, G. Editor and D. E. Ingber, *Circ. Res.*, 2002, **91**, 877–887.
117. D. K. Choi, Y. K. Kim, S. W. Park, H. Lee, S. Lee, S. A. Kim, S. J. Kim, J. Lee, W. Kim, S. H. Min and J. H. Yu, *Sci. Reports 2020 101*, 2020, **10**, 1–11.
118. L. Y. W. Bourguignon, H. Zhu, L. Shao and Y. W. Chen, *J. Biol. Chem.*, 2001, **276**, 7327–7336.
119. A. G. Tavianatou, I. Caon, M. Franchi, Z. Piperigkou, D. Galesso and N. K. Karamanos, *FEBS J.*, 2019, **286**, 2883–2908.
120. S. Misra, V. C. Hascall, R. R. Markwald and S. Ghatak, *Front. Immunol.*, 2015,**6,** 201.
121. H. Harada and M. Takahashi, *J. Biol. Chem.*, 2007, **282**, 5597–5607.
122. H. Chen, J. Qin and Y. Hu, *Mol.*, 2019, **24**, 617.
123. S. Sakai, S. Yamaguchi, T. Takei and K. Kawakami, *Biomacromolecules*, 2008, **9**, 2036–2041.
124. X. Z. Shu, Y. Liu, F. Palumbo and G. D. Prestwich, *Biomaterials*, 2003, **24**, 3825–3834.
125. G. Camci-Unal, D. Cuttica, N. Annabi, D. Demarchi and A. Khademhosseini, *Biomacromolecules*, 2013, **14**, 1085–1092.
126. J. Berlan, F. Trabelsi, H. Delmas, A. M. Wilhelm and J. F. Petrignani, *Ultrason. Sonochem.*, 1994, **1**, S97–S102.
127. A. P. Tabatabai, B. P. Partlow, N. R. Raia, D. L. Kaplan and D. L. Blair, *Langmuir*, 2018, **34**, 15383–15387.
128. S. Sakai, Y. Yamada, T. Zenke and K. Kawakami, *J. Mater. Chem.*, 2008, **19**, 230–235.
129. S. Sakai, H. Ohi and M. Taya, *Biomol.*, 2019, **9**, 342.
130. M. Slevin, S. Kumar and J. Gaffney, *J. Biol. Chem.*, 2002, **277**, 41046–41059.
131. A. Sattar, P. Rooney, S. Kumar, D. Pye, D. West and P. Ledger, 1994, **103**, 576.
132. S. Ibrahim and A. Ramamurthi, *J. Tissue Eng. Regen. Med.*, 2008, **2**, 22–32.
133. S. Ibrahim and A. Ramamurthi, *J. Tissue Eng. Regen. Med.*, 2010, **5**, 122–132.
134. B. Duan, L. A. Hockaday, E. Kapetanovic, K. H. Kang and J. T. Butcher, *Acta Biomater.*, 2013, **9**, 7640–7650.
135. J. F. Murphy, F. Lennon, C. Steele, D. Kelleher, D. Fitzgerald and A. Long, *FASEB J.*, 2005, **19**, 1–17.
136. M. Graupera and M. Potente, *Exp. Cell Res.*, 2013, **319**, 1348–1355.

137. K. D. Puri, T. A. Doggett, C. Y. Huang, J. Douangpanya, J. S. Hayflick, M. Turner, J. Penninger and T. G. Diacovo, *Blood*, 2005, **106**, 150–157.
138. K. Yoshioka, K. Yoshida, H. Cui, T. Wakayama, N. Takuwa, Y. Okamoto, W. Du, X. Qi, K. Asanuma, K. Sugihara, S. Aki, H. Miyazawa, K. Biswas, C. Nagakura, M. Ueno, S. Iseki, R. J. Schwartz, H. Okamoto, T. Sasaki, O. Matsui, M. Asano, R. H. Adams, N. Takakura and Y. Takuwa, *Nat. Med.,* 2012, **18**, 1560–1569.
139. K. Nishida, M. Yamato, Y. Hayashida, K. Watanabe, K. Yamamoto, E. Adachi, S. Nagai, A. Kikuchi, N. Maeda, H. Watanabe, T. Okano and Y. Tano, *N Engl J Med*, 2004, **351**, 1187.
140. Y. Sawa, Y. Yoshikawa, K. Toda, S. Fukushima, K. Yamazaki, M. Ono, Y. Sakata, N. Hagiwara, K. Kinugawa and S. Miyagawa, *Circ. J.*, 2015, **79**, 991–999.
141. M. Sato, M. Yamato, K. Hamahashi, T. Okano and J. Mochida, *Anat. Rec.*, 2014, **297**, 36–43.
142. P. Thummarati and M. Kino-oka, *Front. Bioeng. Biotechnol.*, 2020, **8**, 578140.
143. J. Lee, D. Shin and J. L. Roh, *Theranostics*, 2018, **8**, 3964–3973.
144. Z. Tang, Y. Akiyama and T. Okano, *J. Polym. Sci. Part B Polym. Phys.*, 2014, **52**, 917–926.
145. N. Yamada, T. Okano, H. Sakai, F. Karikusa, Y. Sawasaki and Y. Sakurai, *Die Makromol. Chemie, Rapid Commun.*, 1990, **11**, 571–576.
146. Y. Arisaka, J. Kobayashi, K. Ohashi, K. Tatsumi, K. Kim, Y. Akiyama, M. Yamato and T. Okano, *Regen. Ther.*, 2016, **3**, 97–106.
147. K. Kieswetter, Z. Schwartz, D. D. Dean and B. D. Boyan, *Crit. Rev. Oral Biol. Med.*, 1996, **7**, 329–345.
148. S. Sakai, Y. Liu, T. Matsuyama, K. Kawakami and M. Taya, *J. Mater. Chem.*, 2012, **22**, 1944–1949.
149. S. Sakai, Y. Yamamoto, G. Enkhtuul, K. Ueda, K. Arai, M. Taya and M. Nakamura, *Macromol. Biosci.*, 2017, **17**, 1600416.
150. X. Chen, H. Zhang, J. Cui, Y. Wang, M. Li, J. Zhang, C. Wang, Z. Liu and Q. Wei, *Gels*, 2023, **9**, 155.
151. M. Li, D. Sun, J. Zhang, Y. Wang, Q. Wei and Y. Wang, *Biomater. Sci.*, 2022, **10**, 5430–5458.
152. P. Zhao, Z. Guo, H. Wang, B. Zhou, F. Huang, S. Dong, J. Yang, B. Li and X. Wang, *Biomater. Adv.*, 2023, **152**, 213481.
153. H. Cao, L. Duan, Y. Zhang, J. Cao and K. Zhang, *Signal Transduct. Target. Ther.,* 2021, **6**, 1–31.
154. Y. Yang, K. Shi, K. Yu, F. Xing, H. Lai, Y. Zhou, P. Xiao, Y. Yang, K. Yu, F. Xing, H. Lai, K. Shi, Y. Zhou and P. Xiao, *Adv. Healthc. Mater.*, 2022, **11**, 2101504.
155. J. Ciriza, A. Rodríguez-Romano, I. Nogueroles, G. Gallego-Ferrer, R. M. Cabezuelo, J. L. Pedraz and P. Rico, *Mater. Sci. Eng. C. Mater. Biol. Appl.*, 2021, 112003.
156. K. Vats and D. S. W. Benoit, *Tissue Engineering, Part B.*, 2013, **19**, 455–469.
157. F. Brandl, F. Sommer and A. Goepferich, *Biomaterials*, 2007, **28**, 134–146.
158. A. J. Engler, M. A. Griffin, S. Sen, C. G. Bönnemann, H. L. Sweeney and D. E. Discher, *J. Cell Biol.*, 2004, **166**, 877–887.
159. J. Tomasch, B. Maleiner, P. Heher, M. Rufin, O. G. Andriotis, P. J. Thurner, H. Redl, C. Fuchs and A. H. Teuschl-Woller, *Front. Bioeng. Biotechnol.*, 2022, **20**, 836520.
160. J. M. Silva Garcia, A. Panitch and S. Calve, *Acta Biomater.*, 2019, **84**, 169–179.
161. M. J. Kujawa, D. G. Pechak, M. Y. Fiszman and A. I. Caplan, *Dev. Biol.*, 1986, **113**, 10–16.
162. Y. Leng, A. Abdullah, M. K. Wendt and S. Calve, *Matrix Biol.*, 2019, **78**–**79**, 236.
163. H. Tian, L. Lin, J. Chen, X. Chen, T. G. Park and A. Maruyama, *J. Control. Release*, 2011, **155**, 47–53.
164. S. Sakai, Y. Ogushi and K. Kawakami, *Acta Biomater.*, 2009, **5**, 554–559.
165. L. T. Denes, L. A. Riley, J. R. Mijares, J. D. Arboleda, K. McKee, K. A. Esser and E. T. Wang, *Skelet. Muscle*, 2019, **9**, 17.
166. M. Kodaka, Z. Yang, K. Nakagawa, J. Maruyama, X. Xu, A. Sarkar, A. Ichimura, Y. Nasu, T. Ozawa, H. Iwasa, M. Ishigami-Yuasa, S. Ito, H. Kagechika and Y. Hata, *Exp. Cell Res.*, 2015, **336**, 171–181.
167. W. Mubarok, K. C. M. L. Elvitigala and S. Sakai, *Gels*, 2022, **8**, 387.
168. Z. Ma, Y. Wu, Y. He and T. Wu, *RSC Adv.*, 2013, **3**, 12049–12051.
169. S. Walcott and S. X. Sun, *Proc. Natl. Acad. Sci.*, 2010, **107**, 7757–7762.

170. J. T. Parsons, A. R. Horwitz and M. A. Schwartz, *Nat. Rev. Mol. Cell Biol.*, 2010, **11**, 633–643.
171. T. Iskratsch, H. Wolfenson and M. P. Sheetz, *Nat. Rev. Mol. Cell Biol. 2014 1512*, 2014, **15**, 825–833.
172. K. J. Kim, O. H. Lee and B. Y. Lee, *Br. J. Nutr.*, 2011, **106**, 1836–1844.
173. K. J. M. Boonen, K. Y. Rosaria-Chak, F. P. T. Baaijens, D. W. J. Van Der Schaft and M. J. Post, *Am. J. Physiol. - Cell Physiol.*, 2009, **296**, 1338–1345.
174. M. Levy-Mishali, J. Zoldan and S. Levenberg, *Tissue Eng. - Part A*, 2009, **15**, 935–944.
175. A. Bettadapur, G. C. Suh, N. A. Geisse, E. R. Wang, C. Hua, H. A. Huber, A. A. Viscio, J. Y. Kim, J. B. Strickland and M. L. McCain, *Sci. Reports,* 2016, **6**, 1–14.
176. L. C. Hunt, C. Gorman, C. Kintakas, D. R. Mcculloch, E. J. Mackie and J. D. White, *J. Biol. Chem.*, 2013, **288**, 13006–13021.
177. B. A. Buhren, H. Schrumpf, N. P. Hoff, E. Bölke, S. Hilton and P. A. Gerber, *Eur. J. Med. Res.*, 2016, **21**, 5.
178. S. Sakai, T. Matsuyama, K. Hirose and K. Kawakami, *Biomacromolecules*, 2010, **11**, 1370–1375.
179. Y. Liu, S. Sakai and M. Taya, *Acta Biomater.*, 2013, **9**, 6616–6623.

List of publications

Papers:

1. Kelum Chamara Manoj Lakmal Elvitigala, Wildan Mubarok, Shinji Sakai. Human Umbilical Vein Endothelial Cells Form a Network on a Hyaluronic Acid/Gelatin Composite Hydrogel Moderately Crosslinked and Degraded by Hydrogen Peroxide. *Polymers*, 2022, *14*, 5034.

2. Kelum Chamara Manoj Lakmal Elvitigala, Wildan Mubarok, Shinji Sakai. Tuning the Crosslinking and Degradation of Hyaluronic Acid/Gelatin Hydrogels Using Hydrogen Peroxide for Muscle Cell Sheet Fabrication. *Soft Matter*, 2023,*19*, 5880. (Inside Cover)

3. Kelum Chamara Manoj Lakmal Elvitigala, Lakshmi Mohan, Wildan Mubarok, Shinji Sakai. Phototuning of Hyaluronic-Acid-Based Hydrogel Properties to Control Network Formation in Human Vascular Endothelial Cells. *Advanced Healthcare Materials*, 2024, *13*, 2303787.

4. Kelum Chamara Manoj Lakmal Elvitigala, Wildan Mubarok, Shinji Sakai. Hydrogels with Ultrasound-Treated Hyaluronic Acid Regulate CD44-Mediated Angiogenic Potential of Human Vascular Endothelial Cells In vitro. *Biomolecules*, 2024, *14*, 604.

Related Papers:

1. Wildan Mubarok, Kelum Chamara Manoj Lakmal Elvitigala (equal contribution with first author), Shinji Sakai. Modulation of Cell-Cycle Progression by Hydrogen Peroxide-Mediated Crosslinking and Degradation of Cell-Adhesive Hydrogels, *Cells*, 2022, *11*, 881.

2. Wildan Mubarok, Kelum Chamara Manoj Lakmal Elvitigala, Shinji Sakai. Tuning Myogenesis by Controlling Gelatin Hydrogel Properties through Hydrogen Peroxide-Mediated Crosslinking and Degradation. *Gels*, 2022, *8*, 387.

3. Wildan Mubarok, Kelum Chamara Manoj Lakmal Elvitigala, Kotani Takahashi, Shinji Sakai. Visible light photocrosslinking of sugar beet pectin for 3D bioprinting applications. *Carbohydrate Polymers*, 2023, *316*, 121026.

4. Kotoko Furuno, Kelum Chamara Manoj Lakmal Elvitigala, Suzuki Keiichiro, Shinji Sakai. Local delivery of adeno-associated viral vectors with electrospun gelatin nanofiber mats. *Journal of Biomedical Materials Research, Part B,* 2023, *210*, 112960.

5. Shinji Sakai, Shota Yamamoto, Ryo Hirami, Mitsuyuki Hidaka, Kelum Chamara Manoj Lakmal Elvitigala. Enzymatically gellable chitosan inks with enhanced printability by chitosan nanofibers for 3D printing of wound dressings. *European Polymer Journal,* 2024 *112*, e35345.

International Conference/Symposium:

1. Kelum Chamara Manoj Lakmal Elvitigala, Wildan Mubarok, Masaki Nakahata, Masaru Kojima, Shinji Sakai, Influence of Hydrogen Peroxide-Mediated Crosslinking and Degradation on Cell-Adhesive Gelatin Hydrogels, *26th Symposium of Young Asian Biological Engineering Community*, Kobe, Japan, November (2021).

2. Kelum Chamara Manoj Lakmal Elvitigala, Wildan Mubarok, Ikki Horiguchi, Masaru Kojima, Shinji Sakai, C2C12 behavior on composite hydrogels obtained via enzymatic crosslinking and degradation, *Society of Chemical Engineering Japan (SCEJ) 53rd Autumn Meeting*, Nagano, Japan, September (2022).

3. Kelum Chamara Manoj Lakmal Elvitigala, Wildan Mubarok, Ikki Horiguchi, Masaru Kojima, Shinji Sakai, Human Umbilical Vein Endothelial Cell Behavior on Gelatin-Ph/HA-Ph hydrogel obtained via Hydrogen Peroxide-Mediated Crosslinking and Degradation, SBJ *74th Annual Meeting*, Osaka, Japan, October (2022).

4. Kelum Chamara Manoj Lakmal Elvitigala, Wildan Mubarok, Ikki Horiguchi, Masaru Kojima, Shinji Sakai, Effect of hyaluronic acid molecular weight on HUVEC network

formation on composite hydrogel, *Society of Chemical Engineering Japan (SCEJ) 88th Annual Meeting*, Tokyo, Japan, March (2023).

5. Kelum Chamara Manoj Lakmal Elvitigala, Wildan Mubarok, Ikki Horiguchi, Masaru Kojima, Shinji Sakai, The Effect of Oxidative Degradation of Phenolated Hyaluronic Acid on HUVEC Network Formation, *Society of Chemical Engineering Japan (SCEJ) 54th Autumn Meeting*, Fukuoka, Japan, September (2023).

6. Kelum Chamara Manoj Lakmal Elvitigala, Wildan Mubarok, Ikki Horiguchi, Masaru Kojima, Shinji Sakai, Human Umbilical Vein Endothelial Cells Behaviour on Hyaluronic Acid-based Hydrogel Obtained via Hydrogen Peroxide-Mediated Crosslinking and Degradation, *8th International Symposium on Biomedical Engineering (ISBE)*, Bali, Indonesia, October (2023).

7. Kelum Chamara Manoj Lakmal Elvitigala, Ikki Horiguchi, Masaru Kojima, Shinji Sakai, The Impact of Tyramine-Modified Hyaluronic Acid on Human Umbilical Vein Endothelial Cell Network Formation, *Society of Chemical Engineering Japan (SCEJ) 89th Annual Meeting*, Osaka, Japan, March (2024).

Acknowledgements

The author is deeply grateful to Professor Shinji Sakai (Graduate School of Engineering Science, Osaka University) for his constant guidance, helpful advice, and encouragement throughout this study. The author would like to offer one's special thanks to Associate Professor Masaru Kojima (Graduate School of Engineering Science, Osaka University), Assistant Professor Ikki Horiguchi (Graduate School of Engineering Science, Osaka University), and Assistant Professor Masaki Nakahata (Graduate School of Science, Osaka University) or their valuable guidance and support during this work.

The author is also grateful to Professor Yasunori Okano (Graduate School of Engineering Science, Osaka University) and Professor Shinji Deguchi (Graduate School of Engineering Science, Osaka University) as advisors for their valuable advice and comments to this dissertation.

The author is thankful to Ms. Hanako Nakajima (Graduate Students Section), Ms. Emiko Tasaka, Ms. Hiromi Ishikawa, and Naoko Nakanishi (Σ Advisement Room for International Students) and Ms. Masako Karita and Ms. Mariko Shibukawa for their support in daily life in Japan. The author would like to thank all the members of Sakai Laboratory for their experimental collaboration and friendship.

The author would like to express the deepest appreciation to his family, Ms. Zhou YI, for her understanding and continuous encouragement throughout his student life in Japan for the past 3 years.

The author gratefully acknowledges the financial support of this study from Rotary Yoneyama Scholarship foundation and Japanese Government Scholarship.